UNIVERSITÀ
DEGLI STUDI
DI PADOVA

Sede Amministrativa: **Università degli Studi di Padova**

Dipartimento Territorio e Sistemi Agro-Forestali (TeSAF)

SCUOLA DI DOTTORATO DI RICERCA IN: **Territorio, Ambiente, Risorse e Salute**

CICLO: **XXVIII**

TITOLO TESI

SEDIMENT DYNAMICS IN HIGH GRADIENT STREAMS: BEDLOAD INVESTIGATION IN TWO STUDY AREAS LOCATED IN ALPINE AND ANDINE ENVIRONMENTS

Direttore della Scuola: Ch.mo Prof. Mario Aristide Lenzi

Supervisore: Ch.mo Prof. Mario Aristide Lenzi

Co-Supervisore: Prof. Luca Mao

Dottorando: Riccardo Rainato

CONTENTS

LIST OF FIGURES

LIST OF TABLES

ABSTRACT

The major part of mountain drainage networks is formed by high gradient channels and their nature and dynamics affect the features of sediment delivered to downstream channels, determining the quantity, timing and size of material transported by lowland rivers. Bedload is the transport process that regards the coarser particles, that are mobilized by rolling, sliding and saltating on the channel bed. In mountain environments, the analysis and quantification of bedload transport is of fundamental importance for hazard assessment, understanding the morphodynamics of higher order channels, planning and designing reservoir sedimentation. The importance of this phenomenon contrasts with the fact that it is difficult and impractical to monitor, especially in small, steep mountain basins, due to its high-energy and impulsive nature. Moreover, in mountain streams the particle motion is strongly affected by the bed structures as well as by the highly heterogeneous channel-bed material, acting especially through the hiding/exposure, consolidation and embedding effects. These issues are reflected in the use of bedload equations that, being calibrated on data from laboratory flume experiments or from specific study areas, generally show low performances. Different direct and indirect methods can be used to monitor the bedload in the field but generally require either expensive structures (i.e. permanent monitoring stations) or extensive and perilous surveys (i.e. tracers, bedload traps). Consequently, field bedload data are relatively scarce, and monitoring programs maintained continuously over long-term periods are particularly rare. Thanks to the assumption that bedload transport may be understood as the result of random individual particle displacements, the sediment tracing method was widely employed in the last years. Such method allow to obtain precious data concerning sediment dynamic in mountain streams, improving the results obtainable by samplers, traps and permanent monitoring stations. This thesis aims to investigate the sediment dynamics in two study areas: the Rio Cordon (Alps) and Estero Morales (Andes), focusing particularly on the bedload. The Rio Cordon (northeast Italy) is a typical alpine channel characterized by step-pool and riffle-pool morphology and by a mean slope equal to 13%. The catchment extended 5 km^2 exhibits a nivo-pluvial runoff regime. The second study site is the Estero Morales, a high-gradient stream located in the Metropolitan Region (central Chile). The channel bed exhibits boulder-cascade, step-pool and plane bed morphologies while the average slope is of about 9.5%. The basin (27 km^2) hosts the San Francisco glacier (1.8 km^2) that strongly affects the hydrological regime. In particular during the melt period (December-March) the glacier ensures daily discharge fluctuations with highly variable associated bedload transport rates. These study areas were investigated because different in terms of extent, geology, morphology, altitude,

vegetation, climate, precipitation and flow regime. This dissimilarity allowed to carry out a comparative analysis.

First, nearly 30 years of monitoring of sediment fluxes in the Rio Cordon instrumented basin were analyzed. The collected bedload and suspended sediment transport data allows sediment dynamics to be analyzed at different time scales, ranging from short- (single event) to long-term (three decades). The Rio Cordon monitoring station has been operating since 1986, continuously recording water discharge, bedload and suspended load (at 1 hr intervals, and 5 min intervals during floods). At the flood event scale, a good relationship was found between peak (Q_{peak}) and sediment load. The annual trend of sediment fluxes was analyzed as well as the single floods contribution to the total sediment yield. The annual suspended load contribution ranges from 10 to 2524 t y^{-1}, while the bedload varies from 0 to 1543 t y^{-1}. The higher annual yields were recorded in the years when large floods occurred, highlighting that the sediment budget in the Rio Cordon is strongly controlled by the occurrence of high magnitude events. Investigation of the seasonal suspended load contribution demonstrated that from 1986 to 1993 most sediments were transported during the snowmelt/summer seasons, whilst autumn and snowmelt were the dominant seasons contributing to sediment yield in the periods 1994-2004 and 2004-2014, respectively. The mean annual sediment yield from 1986 to 2014 is equal to 103 t km^{-2} y^{-1}, and overall, bedload accounts for 21% of the total sediment yield. The ratio between the amount of sediment transported by the floods and the effective runoff of the events allowed the temporal trends of transport efficiency to be inferred, highlighting the existence of periods characterized by different sediment availability. In particular, a period with high transport efficiency appears to have occurred after an exceptional event registered in September 1994 (RI > 100 years). The 1994 flood affected the sediment availability at the basin and channel bed scales, and provided a legacy influencing the sediment dynamics in the basin over the long-term by increasing the transport efficiency for approximately a decade. The achieved results update the sediment budget assessed in the Rio Cordon, shedding further light on the long-term and recent behavior of sediment dynamics in a high gradient mountain basin.

Once assessed the quantity and timing of sediment yield, the sediment entrainment conditions were investigated. For this purpose, the tracing method was used in either study areas. Specifically, on the channel bed of Rio Cordon and Estero Morales creeks were seeded 250 and 429 PITs (i.e Passive Integrated Transponder), respectively. In the Rio Cordon, the tracers are monitored since the 2010, analyzing the displacement over a study reach 320 m long. The Estero Morales creek was equipped with tracers since the austral summer 2014, and the

displacements over a reach of approximately 700 m were monitored. Overall, 25 PIT surveys were performed in the two study areas, using a mobile antenna to detect the position of the tracers. In the Estero Morales and Rio Cordon the average recovery rate was 50% and 70%, respectively. These values are in line with the recoveries obtained by similar works concerning the tracing of bedload using PIT tracers. In terms of peak of water discharge (Q_{peak}), in the Alpine channel the monitored floods range between 0.44 $m^3 s^{-1}$ to 2.10 $m^3 s^{-1}$, while in the Andean stream Q_{peak} varies among 3.44 $m^3 s^{-1}$ and 4.68 $m^3 s^{-1}$. In either study cases, the influence of particle size and hydraulic forcing conditions on the sediment entrainment were investigated. In both channels, the size-selective transport appears the prevalent transport dynamic during the relative low-moderate magnitude floods while equal mobility conditions were triggered by the higher magnitude events. Notwithstanding the similar dynamics, the relationship between the grain size distribution of tracers mobilized and Q_{peak} seems to suggest that in the Rio Cordon the sediment entrainment is strongly affected by particle size, while in the Estero Morales such relationship is poorly defined. In order to compare the hydraulic forcing conditions, the unit stream power (ω) is derived from discharge measurement. Additionally for each displacement, the flow duration curve was realized and consequently the 25^{th} (ω_{25}), 50^{th} (ω_{50}) and 75^{th} (ω_{75}) percentiles of unit stream power were calculated. These significant percentiles, with the ω_{peak}, are used in order to test their capacity to explain the relationship among hydraulic forcing and tracers displacement. In both study areas, the mean transport distances are better correlated with the ω_{peak} of individual transport events, which appears the most relevant descriptor as regards the sediment entrainment. In this sense, the Estero Morales showed a persistent high transport capacity, while the Rio Cordon exhibited similar conditions only above a threshold (~ 400 W m^{-2}). Over such threshold the Alpine stream exhibits higher transport efficiency compared to the Andean channel.

This thesis benefited by two monitoring programs. First, the long-lasting monitoring program undertaken on the Rio Cordon thanks to the experimental station active since 1986, that permitted to produce long-term data series, very precious in order to analyze the sediment dynamics over long-term. Secondly, the use of PIT tracers in the Estero Morales and Rio Cordon creeks allowed to obtain interesting results concerning the sediment entrainment in this two study areas, permitting to perform a comparative analysis. In this sense, the PIT tracers have proved to be a very fitting method to monitoring the bedload without disturbing the channel bed and avoiding empirical assumptions regarding the sediment transport.

RIASSUNTO

La maggior parte della rete idrografica montana è costituita da collettori ad elevata pendenza (torrenti montani). La natura e la dinamica di tali collettori influenzano le caratteristiche del materiale solido rilasciato a valle, determinando aspetti quali quantità, temporalità e caratteristiche fisiche del sedimento trasportato ai fiumi pedemontani e vallivi. Col termine trasporto di fondo (*bedload*) si definisce la mobilitazione del materiale grossolano presente in un collettore, materiale che viene mobilitato lungo il letto tramite rotolamento, strisciamento e saltazione. In ambiente montano, l'analisi e la quantificazione del trasporto di fondo è di fondamentale importanza per diversi aspetti, come ad esempio poter meglio comprendere le condizioni morfo-dinamiche dei collettori montani, valutare il pericolo connesso al trasporto solido, pianificare e progettare opere di trattenuta. L'importanza di questo fenomeno contrasta però col fatto che esso è di difficile monitoraggio, soprattutto nei piccoli bacini montani, a causa della sua natura puramente impulsiva. Inoltre, nei torrenti montani la mobilità del sedimento è fortemente influenzata dalla presenza di forme di fondo e dal materiale altamente eterogeneo costituente il letto del collettore, aspetti che si traducono negli effetti di nascondimento/esposizione (*hiding/exposure*), consolidamento (*consolidation*) e incorporamento (*embedding*). Tali condizioni rendono difficile la valutazione del trasporto di fondo e si riflettono, ad esempio, nelle equazioni predittive. Esse, infatti, sono perlopiù sviluppate tramite esperimenti di laboratorio (*flume*) o calibrate in specifiche aree studio, e quindi forniscono generalmente basse performance se applicate ad altri siti di studio. Diversi metodi diretti ed indiretti possono essere utilizzati in campo al fine di monitorare il trasporto di fondo. Generalmente tali metodi richiedono la realizzazione di dispendiose strutture (es. stazioni di monitoraggio permanenti) o estese e perigliose indagini di campo (es. *tracers*, *bedload traps*). Come conseguenza, i dati di campo riguardanti il trasporto di fondo sono relativamente scarsi, ed in particolare i programmi di monitoraggio mantenuti nel lungo periodo sono particolarmente rari. Grazie all'assunzione che il trasporto di fondo può essere inteso come il risultato di singoli movimenti casuali di particelle, negli ultimi anni il metodo dei traccianti (*tracers*) è stato largamente impiegato in campo. Tale metodologia consente di ottenere preziosi dati riguardanti le dinamiche di trasporto solido, affinando i risultati ottenibili tramite *samplers*, *traps* e stazioni di monitoraggio permanenti.

L'obiettivo principale del lavoro di tesi è stato quello esaminare le dinamiche di trasporto solido in due aree studio, il Rio Cordon (Alpi) e l'Estero Morales (Ande), focalizzandomi in particolare nell'indagine del trasporto solido di fondo. Il Rio Cordon (NE Italia) è un tipico torrente alpino, caratterizzato da una prevalente configurazione *step-pool*/*riffle-pool* e da un

pendenza media pari al 13%. Il bacino esteso 5 km^2 mostra un regime dei deflussi dominato da scioglimento nivale e da precipitazione piovose. In questo bacino è in funzione dal 1986 una stazione di monitoraggio, realizzata al fine di registrare in continuo le portate liquide ed il trasporto solido (di fondo e in sospensione). Il secondo sito è l'Estero Morales, torrente montano situato nella Región Metropolitana de Santiago (Cile centrale). Il collettore presenta una morfologia mista, in cui prevalgono le configurazioni a *boulder-cascade*, *step-pool* e *plane bed*, mentre la pendenza media è pari al 9.5%. Questo bacino andino ospita il ghiacciaio San Francisco (1.8 km^2), il quale influenza notevolmente il regime idrologico dell'area studio. Durante il periodo di scioglimento (Dicembre-Marzo), il ghiacciaio assicura fluttuazioni giornaliere nelle portata idriche con un ampio variabilità nei tassi di trasporto solido. Queste aree studio sono state esaminate in quanto diverse in termini di geologia, morfologia, vegetazione, clima, precipitazioni e regime delle portate. Tale diversità ha permesso di poter eseguire un'analisi comparativa tra le due aree studio.

Grazie ai dati prodotti dalla stazione di monitoraggio situata nel Rio Cordon, sono stati analizzati i flussi di sedimento registrati dal 1986 ad oggi. I dati raccolti riguardanti sia il trasporto solido di fondo che in sospensione hanno permesso di analizzare le dinamiche di trasporto solido a diverse scale temporali, spaziando dal breve (eventi di piena) al lungo periodo (tre decenni). A scala di evento, una buona relazione è stata trovata tra picco di portata (Q_{peak}) e le quantità di sedimento trasportate. Il trend annuale nei flussi di sedimento è stato esaminato così come il contributo dei singoli eventi alla produzione totale di sedimento da parte del bacino. In questo senso, il contributo annuale in sospensione varia tra 10 e 2524 t y^{-1} mentre il trasporto di fondo varia tra 0 e1543 t y^{-1}. In termini di quantità trasportate, i maggiori apporti annuali sono stati registrati negli anni in cui si sono verificati eventi ad elevata magnitudo, evidenziando come il budget di sedimento nel Rio Cordon sia controllato dal verificarsi di tali fenomeni. L'analisi del trasporto in sospensione stagionale ha dimostrato che tra il 1986 e il 1993 la maggior parte del materiale fine è stato mobilitato durante lo scioglimento nivale e durante la stagione estiva. L'autunno ed il periodo di scioglimento nivale sono stati invece le stagioni che hanno principalmente contribuito nei periodi 1994-2004 e 2004-2014, rispettivamente. Il bacino del Rio Cordon, nel periodo 1986-2014, è stato caratterizzato da una produzione media annuale di sedimento pari a 103 t km^{-2} y^{-1}, con il trasporto di fondo che ha contributo per il 21% al totale trasportato. Il rapporto tra la quantità di sedimento trasportato da ciascun evento ed il volume d'idrogramma che ha contribuito a tale evento di trasporto, ha permesso di ottenere un trend temporale riguardante l'efficienza di trasporto. Tale trend ha evidenziato l'esistenza di periodi caratterizzati da una diversa

disponibilità di sedimento. In particolare, un periodo ad elevata efficienza di trasporto sembra essersi verificato successivamente ad un evento eccezionale registrato nel Settembre 1994 (RI > 100 years). Tale evento ha influenzato le disponibilità di sedimento sia a scala di bacino che di collettore, e la sua magnitudo ha influenzato le dinamiche di trasporto solido nel lungo periodo, incrementandone l'efficienza per circa un decennio. I risultati ottenuti aggiornano il budget di sedimento riguardante il Rio Cordon, facendo inoltre luce sulle quelle che possono essere nel lungo periodo le dinamiche di trasporto in un bacino alpino.

Una volta affrontata la questione della quantità e la temporalità con cui un collettore montano può trasportare sedimento, la tesi si è focalizzata nell'esaminare le condizioni di mobilità che caratterizzano il trasporto di fondo. A questo scopo, il metodo dei traccianti e stato utilizzato in entrambi i siti di studio. Nello specifico 250 PITs (*Passive Integrated Transponders*) sono stati installati nel Rio Cordon, mentre 429 sono stati posizionati nell'Estero Morales. Nel collettore alpino i *tracers* sono stati monitorati a partire dal 2010, indagandone gli spostamenti lungo un tratto di studio esteso 320 m. L'Estero Morales è stato equipaggiato con i traccianti a partire dall'estate australe 2014 ed utilizzando un tratto di studio esteso circa 700 m. Complessivamente nelle aree di studio sono stati eseguiti 25 monitoraggi PIT, avvalendosi di un'antenna mobile per determinare la posizione dei traccianti. Nelle campagne di misura effettuate nell'Estero Morales e nel Rio Cordon sono stati raggiunti dei tassi di recupero dei traccianti pari al 50% e 70%, rispettivamente. Tali valori sono in linea con i tassi ottenuti da lavori simili riguardanti il monitoraggio tramite *tracers*. In termini di portata al picco, nel Rio Cordon sono stati monitorati eventi compresi tra 0.44 $m^3 s^{-1}$ e 2.10 $m^3 s^{-1}$, mentre nell'Estero Morales Q_{PEAK} varia tra 3.44 $m^3 s^{-1}$ e 4.68 $m^3 s^{-1}$. In entrambi i siti, è stata esaminata l'influenza sia della dimensione del sedimento sia delle condizioni idrologiche sulle distanze di trasporto. In entrambi i casi, il trasporto selettivo appare la dinamica di trasporto prevalente durante gli eventi a bassa e media magnitudo; mentre condizioni di equimobilità sono state innescate dagli eventi ad elevata magnitudo. Nonostante queste dinamiche simili, la relazione tra granulometria dei traccianti mobilitati e Q_{peak} sembra suggerire che nel Rio Cordon il trasporto è fortemente influenzato dalle dimensioni della particella, mentre nell'Estero Morales tale relazione appare alquanto debole. Al fine di confrontare i casi studio, lo stream power (ω) è stato utilizzato in entrambi i siti per descrivere le condizioni idrologiche. Per ciascun movimento PIT, è stata realizzata la relativa curva di durata potendo così calcolare anche il 25° (ω_{25}), 50° (ω_{50}) e 75° (ω_{75}) percentile di unit stream power a cui è stato sottoposto ciascun tracciante. In entrambi i siti la distanza media è positivamente correlata con ω_{peak}, il quale appare il descrittore più rilevante per quanto riguarda la mobilità dei traccianti. In

questo senso, nell'Estero Morales è stata riscontrata durante l'intero periodo di studio una elevata capacità di trasporto. Nel Rio Cordon condizioni comparabili sono state osservate solo oltre una specifica soglia (~ 400 W m^{-2}), oltre cui il collettore alpino mostra capacità di trasporto superiori rispetto a quanto osservato nel torrente andino.

Questa tesi beneficia di due programmi di monitoraggio dedicati al trasporto di fondo. Il primo è rappresentato dal monitoraggio a lungo termine in corso nel Rio Cordon e svolto dal 1986 dalla stazione sperimentale. Tale programma ha prodotto una serie di dati estesa quasi tre decenni, permettendo di analizzare le dinamiche di trasporto solido nel lungo periodo. Oltre a ciò, il monitoraggio intrapreso nell'Estero Morales e nel Rio Cordon tramite l'uso di traccianti PIT ha consentito di ottenere interessanti risultati riguardanti la mobilità del sedimento in queste due aree studio, permettendo di effettuare un analisi comparativa. In questo senso, i traccianti PIT si sono dimostrati un metodo particolarmente adatto al monitoraggio del trasporto di fondo, il quale non causa disturbi al letto del collettore ed evita di doversi avvalere di assunzioni empiriche riguardanti un fenomeno così complesso come il trasporto solido.

1. CHAPTER ONE – BACKGROUND

1.1. State of the art

1.1.1. The sediment transport in mountain fluvial systems

In a fluvial system, the sediment transport, i.e. the motion of sediments that occurs along a specific stream, can occur by different ways (Fig. 1). The molecules and ions (nutrient, metals, silt), or generally the very fine particles, are mainly transported by dissolved load while, the under-flotation transport prevails when the density of sediment is lower respect to water density. In mountain fluvial systems the transport processes may occur mainly as floods with suspended and bedload transport but also as debris and mud flows, depending on connectivity with source areas (Cavalli et al., 2013), type and degree of activity of sediment supply (Lenzi, 2004; Recking, 2012), hydraulic conditions (Lenzi et al., 2006a; Recking et al., 2012a), grain size distribution of transported and bed material (Mao et al., 2008; Yager et al., 2012), presence of in-channel wood (Wilcox and Wohl, 2006) and channel morphology (Mao et al., 2009).

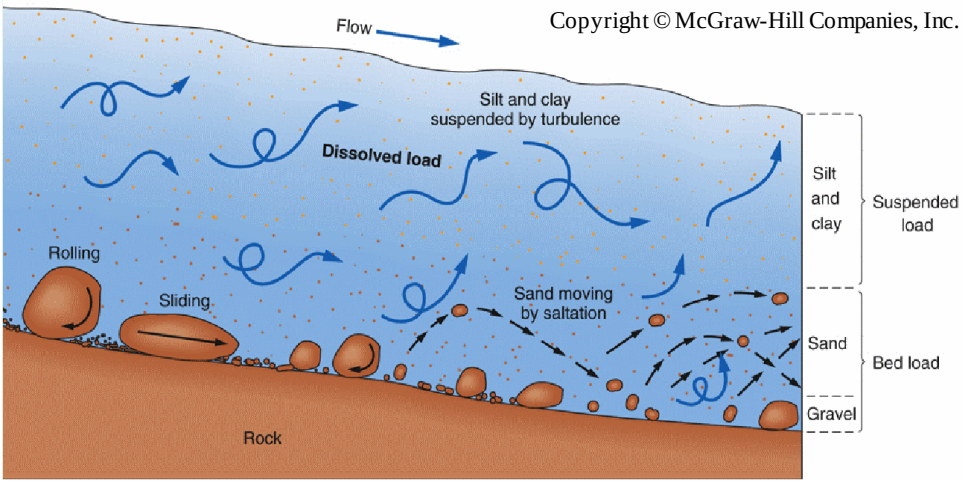

Figure 1: Sediment transport processes

Suspended sediment transport is the mobilization of finer particles suspended in the water columns. It can influence the channel morphology (Wohl, 2000) and its assessment is important for the study of water quality, reservoir sedimentation, and for surveying erosion processes on hillslopes (Lenzi et al., 2003; Soler et al., 2008). The total suspended concentration consists mostly of material eroded from the hillslopes or streambank, but also of sediment already present in the riverbed that becomes re-suspended when flow increases

(Eder et al., 2010). Suspended transport depends upon the catchment size, stability of the coarse surface layer of the channel, the amount, duration, intensity and spatial extent of precipitation and soil moisture, among other parameters (Klein, 1984; DeBoer and Campbell, 1989; Lenzi et al., 2003; Seeger et al., 2004; Soler et al., 2008). In high-gradient streams, suspended load can exceed bedload. Indeed, the contribution of the suspended sediment fraction to the total sediment load in these environments can range from 10 to 100% (Bathurst et al., 1987; Barsch et al., 1994; Billi et al., 1998; Lenzi and Mao, 2003; Mao, 2004). Suspended load seems to be more important than bedload in the Pitzbach basin (Austrian Alps), where it accounts for at least 75% of total sediment transport (Turowsky et al., 2010). Analyzing the sediment yield in 21 small catchments within the Dora Baltea mountain basin (western Italian Alps), Vezzoli (2004) estimated a suspended load fraction equal to 0.41. In addition, Lenzi and Marchi (2000) examining the partitioning in flood events between 1987 and 2002 in the Rio Cordon, reported that suspended fractions ranged from 0.16 to 1.00 depending on the range of flood magnitude. The suspended sediment yield frequently shows seasonal behavior (Collins, 1990; Bogen, 1995; Lenzi et al., 2003). An assessment of the seasonal relationship between water discharge (Q) and suspended sediment concentration (SSC) can be helpful in order to calculate suspended sediment delivery, to predict transport loads or to estimate SSC in similar basins with no available data. Campbell and Bauder (1940) proposed the following power-law sediment-discharge relationship, since used by many authors (e.g. Asselman, 2000):

$$SSC = a\,Q^{b} \qquad \text{Eq.1}$$

where a and b are the empirical fitting parameters. Due to the heterogeneous distribution of sediment sources within the catchment area as well as the spatial and temporal variability of controlling factors, the relationship between SSC and Q varies not only between seasons but also from event to event as well as during a single flood (Lenzi and Marchi, 2000; Schmith and Morche, 2006; Gao and Josefson, 2012; Aich et al., 2014) and seasonally (e.g. Iida et al., 2012). The parameters a and b often describe a hysteretic loop (Williams, 1989) that makes it difficult to predict the magnitude of suspended sediment production in relation to precipitation (Banasik and Bley, 1994) or to snowmelt runoff (Lenzi et al., 2004; Mao, 2004). This aspect may be improved especially through the continuous monitoring of water discharge and suspended sediment transport, allowing the suspended sediment load to be

assessed in relation to the different determining factors as well as its role in the total sediment load.

Coarser particles are transported as bedload, rolling, sliding or saltating on the channel bed. In mountain environments, the analysis and quantification of bedload transport is of fundamental importance for hazard assessment, understanding the morphodynamics of higher order channels, planning and designing reservoir sedimentation (Rickenmann, 1999; Nitsche et al., 2011). The importance of this phenomenon contrasts with the fact that it is difficult and impractical to monitor, especially in small, steep mountain basins, due to its high-energy and impulsive nature. These issues are reflected in the use of bedload equations that, being calibrated on data from laboratory flume experiments or from specific study areas, generally show low performances (D'Agostino and Lenzi, 1999; Barry et al., 2004; Yager et al., 2015). Different direct and indirect methods can be used to monitor the bedload in the field but generally require either expensive structures (i.e. permanent monitoring stations) or extensive and perilous surveys (i.e. tracers, bedload traps). Consequently, field bedload data are relatively scarce, and monitoring programs maintained continuously over long-term periods are particularly rare.

1.1.2. Sediment supply

Contrary to the large lowland rivers, in headwater streams the sediment transport is strongly dependent by the local sediment availability. Specifically, in high gradient channels the sediment entrainment appears strictly affected by the material supplied by the source areas, i.e. hillslope processes, bank and channel-bed erosions (Recking, 2012). The sediment supply plays a key role also regarding the channel stability. Overall, a mountain fluvial system exhibits a condition of equilibrium when its topography is stable, with no significant geomorphic changes. Such condition occurs when the sediment supply is balanced with the transport capacity. If one of this two factors prevails, the state of equilibrium disappears in favor to "unstable" conditions. The prevalence of the sediment supply triggers deposition along the channel and, thus aggradation of the bed. On the other hand, when transport capacity > sediment supply, the stream is characterized by a deficit of material transportable and the excess of stream power causes the predominance of erosion processes. In the mountain streams, the sediment supply affects also the grain size characteristics (Nelson et al., 2009), influencing in turn the ecological status (Buffington et al., 2004). An appropriate assessment of the sediment supply that characterize a study area permits to evaluate the stability of the study reaches, allowing to control the sedimentation hazard (Yager et al.,

2012). Recently, a classification of the mountain streams based on the sediment supply conditions was proposed by Recking (2012), analyzing 13 study areas. The author identify:

- Low sediment supply: limited supply of pebble and gravel, that are stored in channel below cobble and boulders. The motion take place only locally. The stream characterized by such condition typically exhibits a step-pool configuration with no lateral sediment input.
- Moderate sediment supply: this typology represents channels seasonally fed by coarse and heterogeneous colluviums material. This sediment reaches the channel bed and is arranged in loose manner, easily transportable.
- High sediment supply: streams characterized by a continuous availability of loose material, derived from hillslope processes or from bank erosions. Also, the channel bed can become a significant source area, in particular subsequently to an extraordinary flood event that modifies the bed-forms, removing the eventual armour layer.

1.1.3. Sediment yield

The erosional denudation of mountain ranges plays a key role with respect to global cycles of weathering and sediment supply to lowland and oceans. In this sense, the rivers are the most important agents of downstream sediment delivery (Hinderer et al., 2013). Specifically, the major part of mountain drainage networks is formed by steep channels and their nature and dynamics affect the features of sediment delivered to downstream channels, determining the quantity, timing and size of material transported by lowland rivers (Yager et al., 2012). Due to the complex and changeable hydraulic and morphological conditions of the mountain environment, a wide range of sediment delivery may be expected in catchments similar in size but subject to different dominant processes (e.g. Mao et al., 2008). Reviewing the data present in literature, Hinderer et al. (2013) assessed the sediment yield of several mountain ranges. The data show that highest sediment delivery was observed in the eastern coastal ranges of Taiwan (1900 – 65000 t km^{-2} y^{-1}) and in the glaciated southeastern Alaskan mountains (15000 – 120000 t km^{-2} y^{-1}). Alps (50 – 5000 t km^{-2} y^{-1}) and Andes (50 – 1300 t km^{-2} y^{-1}) exhibit comparable magnitude of sediment yield, while Himalayas ranges are slightly higher (250 – 5000 t km^{-2} y^{-1}). Moreover, the magnitude of sediment fluxes in the same basin may strongly vary from event to event, as from year to year (Lenzi et al., 2003; Turowski et al., 2010). An accurate evaluation of the total sediment load as well as its partitioning (bedload vs. suspended load) is crucial in mountain basins due to the effects on water quality, fish habitat, geomorphic changes, channel stability and evolution, reservoir

management, infrastructure design and hazard assessment. The large variability observable in sediment delivery can be noted also as regards the bedload/suspended load contributions to the total sediment load. Turowski et al. (2010) collecting the data available in literature regarding sand-bed and gravel-bed rivers, detected long-term bedload fraction between 0.1 to 1.0 with a general decrease of fraction with increasing the drainage area. If performed at both the short- (single flood event) and long-term (year or decade) scales, this kind of analysis may be a valuable support for land-use decision makers and managers (Turowski et al., 2010). A short-term analysis can allow the sediment dynamics during flood events to be investigated, providing useful information for applications such as hazards assessment and infrastructure design, while in the long-term it can offer an average assessment about the sediment fluxes magnitude that is a key factor for applications such as reservoir management, environmental engineering, and planning for climate or land-use changes.

1.1.4. Channel morphology

In mountain environment the channel morphology is strongly dominated by the sediment transport. In this environment the channel configuration is the result of many geological, climatic, hydrological and hydraulic factors, that affect the stream from a long time (Lenzi, 2001). Montgomery and Buffington (1997) taking into account features such as bed material, bedform pattern, dominant roughness elements, dominant sediment sources, sediment storage elements, confinement and slope, identified five different morphological typologies that can occur in mountain streams (Fig. 2). The authors defined these morphology as: cascade, step-pool, plane bed, pool riffle and dune ripple.

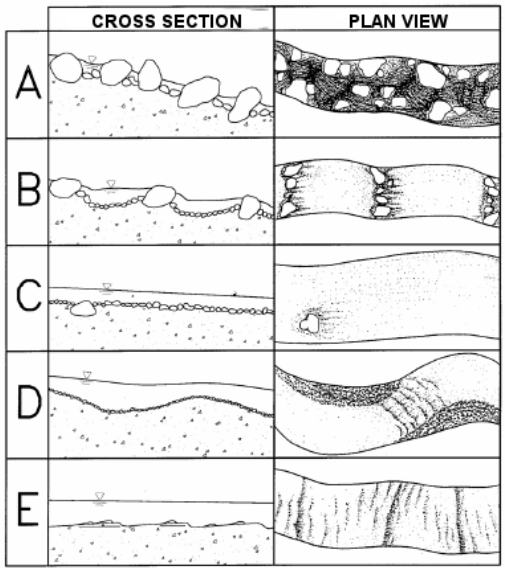

Figure 2: The Montgomery and Buffington (1997) classification which identifies: cascade (A), step-pool (B), plane bed (C), pool riffle (D) and dune ripple (E).

While pool riffle (Fig. 3) and dune ripple are more common with moderate slopes, the cascade, step-pool and plane bed configurations are the principal morphologies detectable in the high gradient channels. Due to the complex morphological conditions that characterized the mountain environment, along a certain stream, the above mentioned configurations are frequently mixed between them.

Figure 3: Pool riffle segment (Estero Morales, January 2014)

The cascade configuration (Fig. 4) is characterized by disorganized bed material, in which prevails cobbles and large boulders. This morphology exhibits high stability, with the larger elements mobilized only by flood events characterized by recurrence interval (RI) > 50-100 years (Montgomery and Buffington, 1997). The main sources of roughness are the grains and banks, whilst the sediment entrainment consists in smaller gravel that moves over larger bed elements.

Figure 4: Cascade morphology (Estero Morales, February 2014).

The step-pool sequence (Fig. 5) is the most common configuration when the channel gradient exceeds the ~ 2% – 3% (Grant et al., 1990), especially with slope between 3% – 30% (Lenzi, 2001). In this configuration, a well structured fluvial organization appears with vertical oscillation in the flow. Specifically, the morphology features a staircase-like developed along the longitudinal profile, with the alternation of pools (containing finer material) delimited by cobbles and boulders positioned transverse to the channel (Recking et al., 2012b). The channel bed material is dominated by boulders, cobbles and coarse pebbles. In addition to the already mentioned slope parameter, some authors identified other factors that support the development of step-pool systems, as a heterogeneous bed characterized by largest material immobile expect under step forming conditions (D'Agostino and Lenzi, 1997) and low sediment transport rate and low sediment supply condition (Grant et al., 1990). In this sense, the flume-analysis performed by Whittaker (1987) and the field investigation carried out in the Rio Cordon creek by Lenzi (2001), highlighted that step-pool morphology represents a stable structure regarding the floods characterized by RI < 30-40 years, while for larger events such configuration can collapse. Thus, the step-pool sequence represents a very stable morphology that can be modified only by high magnitude floods. In terms of sediment mobility, under ordinary hydraulic forcing conditions the sediment transport is affected by the upstream-sediment supply (i.e. hillslope processes), whilst the channel bed not represent an active source area because characterized by large individual elements forming the stable steps, which in turn control the stability of whole system (Lenzi, 2004). Several authors highlighted that the presence of bed irregularities and bedforms (i.e. step-pool, cascade, large boulders) cause a significant additional factor of form resistance to the flow and, furthermore, to the incipient motion.

Figure 5: Step-pool morphology (Rio Cordon, June 2013)

Contrary to the just described configurations, in the plane-bed morphology (Fig. 6) a lack of well-developed bedforms is observable. The grain size of channel-bed material ranges among sand to gravel, with the predominance of cobbles, pebbles and fine gravel. Similarly to the cascade, the main sources of roughness are the grains and banks (Montgomery and Buffington, 1997). Frequently, the plane-bed reaches exhibit armoured bed surfaces that require near-bankfull threshold for the entrainment of sediment.

Figure 6: Plane-bed morphology (Rio Cordon, July 2014)

1.1.5. Bedload in mountain streams

Bedload is the transport process that regards the coarser clasts, which are mobilized along the channel bed by rolling, sliding and saltation. As said, in mountain streams the analysis and quantification of bedload transport is of fundamental importance for many applications and, furthermore, the bedload volumes represent the primary source of concern, more than flood water volumes (Lenzi et al., 2004). Especially in the context of EU framework, an accurate assessment of sediment transport is required by flood risk mapping and management. From ecological point of view, in many mountain regions the spawning habitats of fish species (e.g. salmon) are strongly affected by bedload (Vazquez-Tarrio and Menendez-Duarte, 2014). Especially in the steep channels, the importance of this phenomenon contrasts with the fact that its monitoring is problematic. The high-energy and impulsive nature that characterize the bedload combined with factors as longitudinal channel slope, particle size interactions, hiding-protrusion effects, bedforms and armour layer strongly affect the investigation and assessment of bedload dynamics. The hiding/exposure effect due to highly heterogeneity in bed structures causes that the smaller particles are more difficult to

mobilize than if they were in a bed with uniform sized material, whilst the larger sizes appear easier to entrain (MacFarlane and Wohl, 2003; Bathurst, 2013). In terms of impulsive nature, the bedload events that occur during storms affect both geomorphic change and natural hazard in mountain regions. During such event the transport rate is function of the width and depth of bed scouring, as well as of transport distances of the sediment grains (Schneider et al., 2014). Analysis performed in laboratory or in gravel bed rivers (Einstein, 1937; Hassan et al., 1991; Wilcock, 1997; Wilcock and McArdell, 1997) highlighted conflicting results as regards a possible relationship between grain size and travel displacement. Several authors (Andrews, 1983; Ashworth and Ferguson, 1989; Wilcock, 1998) on the basis of field measurement suggested the existence of different phases regarding the bedload transport:

- Phase 1: occurring when fine sediments, mainly sand, moving over a stable bed.
- Phase 2: due to moderate discharge, in this phase occurs a size-selective motion and also the coarser material is locally entrained.
- Phase 3: takes place in the case of highest flows that cause the entrainment of the sediment under equal mobility conditions.

According to these results, "partial transport" is defined the condition in which only a fraction of exposed sediment, within a specific size range and a specific study period, is entrained (Wilcock and McArdell, 1997).

In light of the complex conditions that characterize the bedload transport, in unmeasured streams the assessment of volume mobilized is frequently relied on empirical equations. Such equations are normally derived from laboratory flume experiments or from specific study areas, and thus, exhibit high uncertainties (Schneider et al., 2014).

1.1.6. Incipient motion

The just mentioned longitudinal channel slope, particle size interactions, hiding-protrusion effects, bedforms and armour layer caused an increase in the dimensionless critical shear stress, that is most used term to express the threshold of sediment incipient motion. In order to assess incipient motion conditions, Shields (1936) carried out flume-laboratory experiments, relating the dimensionless shear stress (τ^*) to the Reynolds number (Re^*). Such terms are obtainable by the following equations:

$$\tau^* = \frac{R\gamma i}{(\gamma_s - \gamma)D} \qquad \text{Eq.2}$$

$$Re^* = \frac{u_* \cdot D}{v} \quad \text{Eq.3}$$

the dimensionless shear stress is a function of the hydraulic radius (R), water specific weight (γ), channel-bed slope (i), sediment specific weight (γ_s) and grain size characteristics of analyzed stream D. In equation 2, u_* is the friction velocity and v is the kinematic viscosity. Therefore, $Re^*$is a ratio between the inertial and viscous forces and allows to quantifies their relative importance for given flow conditions. Shields considering the median grain size (D_{50}), highlighted as the dimensionless critical shear stress (τ_c^*) that represents the condition in which occurs the incipient motion, is constant and equal to 0.056 for Reynolds number > 400, or rather in the case of turbulent flow conditions. Integrating the results obtained by the various relations between Re^* and τ^*, Shields created a graph, also known as Shields abacus (Fig. 7).

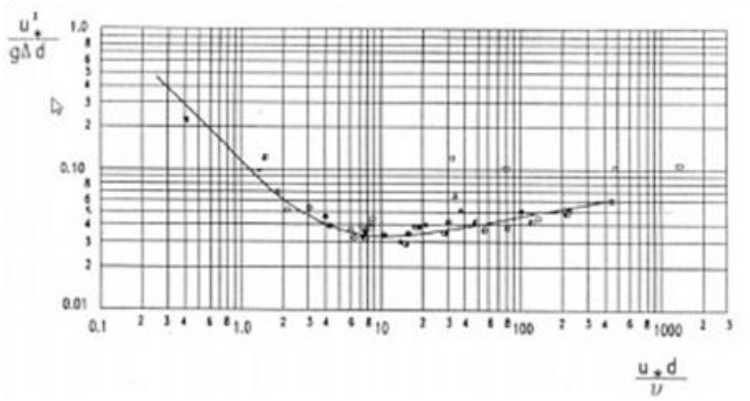

Figure 7: Shields abacus

In terms of sediment motion, the graph shows the curve representing the state of equilibrium. Along this curve $\tau^* = \tau_c^*$, while below the line $\tau^* < \tau_c^*$ and then there are no conditions for the grains motion. Under such conditions the deposition is favored. Above the curve $\tau^* > \tau_c^*$ and, therefore, conditions for sediment transport occur. The research carried out by Shields is a milestone that allows to better understand the sediment transport processes. However, it is a theoretical treatment of the phenomenon. In fact, in a real fluvial environment the assessment of sediment motion conditions appears more complicated. The Shields approach was developed using an artificial flume characterized by low slope and homogeneous grain size distribution. Such conditions are rarely observed in fluvial systems, especially in gravel bed rivers and mountain streams where the slope may exhibit very high values and the grain size distribution is highly heterogeneous. Additionally, factors as grain sorting (Hammond et al.,

1984), particle size interactions and hiding-protrusion effects (Fig. 8) (Ashworth and Ferguson, 1989), relative roughness D_{50}/h (Bathurst et al., 1983) and longitudinal channel slope strongly influence the evaluation of the threshold of incipient motion.

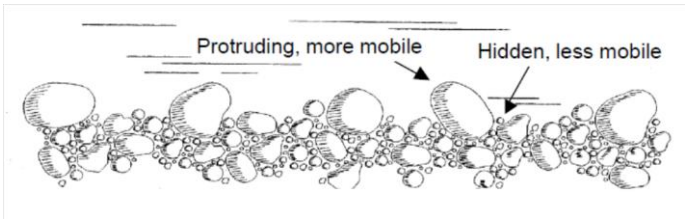

Figure 8: Hiding-protrusion effects in a channel-bed characterized by heterogeneous grain size distribution.

The mountain streams are mainly characterized by heterogeneous channel-bed material. Under these conditions the stability of a particle is affected by the ratio of its size to a reference size (Bathurst, 2013). Particles larger respect the reference size are relatively easier to entrain than the same particles in a uniform bed material because they protrude above the smaller clasts and, thus, experience a higher drag force (Fenton and Abbott, 1977). On the other hand, the smaller particles are relatively more difficult to move than if they were in a uniform channel-bed because hidden below larger clasts. Bathurst (2013), focusing on the entrainment conditions in heterogeneous channel-bed material, identified the embedding, consolidation and exposed patches as components that may affect the motion. If the channel-bed is composed by coarser particles protruded into the bed, it exhibits a smooth bed surface with a full embedding (Fig. 9). Due to the absence of hiding/exposure effect the smaller particles are mobilized by size-selective transport, whilst the coarse sediment require additional hydraulic forcing to be extracted from the channel-bed and entrained.

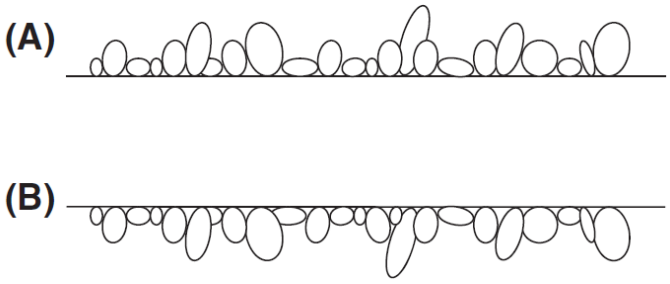

Figure 9: Conceptual example of zero embedding (A) and maximum embedding (B) conditions (Bathurst, 2013).

The consolidation effect is particularly evident in the basins where long periods among bedload events occur. In this sense, the consolidation of channel-bed material can be

commonly observed in the nivo-pluvial catchments, in which the bedload events are mainly concentrated during the snowmelt season or triggered by significant storms. In addition, the occurrence of recurrent floods capable to disturb but not entrain the bed material enhances the consolidation of channel-bed, increasing its stability (Bathurst, 2013).

The spatial distribution of exposed patches along the channel-bed can alter the entrainment of the particles. The co-presence of fine material deposited both in loose manner and hidden under coarser clasts causes that it can be mobilized by different discharges, showing altered dynamics (Bathurst, 2013).

In the light of the influence of bed irregularities and bedforms on the assessment of incipient motion, several approaches were presented following the example of Shields (1936). Bagnold (1966) proposed the use of the stream power (ω) defined as the rate of energy (W m^{-2}), expense by water flow per unit area of the channel bed (Mao et al., 2008). The ω is expressed by the equation:

$$\omega = \rho g Q S / B \qquad \text{Eq.4}$$

where Q (m^3 s^{-1}) is the water discharge, S is the channel bed slope (m m^{-1}), B the channel width (m).

The stream power evaluated as function of slope, discharge and width is easy to define also by field surveys (Petit et al., 2005). The influence of bedforms resistance on the critical stream power (ω_c) was investigated by several authors. The work carried out by (Petit et al., 2005) on 14 different study areas in the Belgian Ardennes highlighted as the value of ω_c was higher in low order streams, in particularly where the channel was characterized by highly developed bedforms. Ferguson (2005), reviewing the Bagnold (1966) approach, showed that the presence of form resistance in addition to grain roughness not affects the calculation of ω. In the recent years the Ferguson's hypothesis was largely accepted and the stream power approach was applied in several works concerning fluvial processes, e.g. the assessment of fluvial system forms and process attributes (Fonstad, 2003), influence of sediment supply on bedload (Recking, 2012), assessment of predicting equations (Vazquez-Tarrio and Menendez-Duarte, 2015) and bedload tracing (Mao et al., 2008; Schneider et al., 2014).

Currently, the comprehension concerning the incipient motion conditions appears strongly affected by a lack of field data, that are mostly derived by specific study areas. In this sense, Bathurst (2013) suggests as key points to be investigated:

- the difference among the critical conditions in streams with uniform or heterogeneous bed material;
- the rate of change regarding the largest particle size mobilized with the applied flow condition;
- the roles that bedforms and monitoring methods play in determining the rate of such change.

1.1.7. Monitoring of bedload

An accurate monitoring and quantification of bedload appears crucial, especially in light of its importance on the fluvial processes. Notoriously, the assessment of bedload in mountain streams is difficult, and such limitation is reflected in the scarce performances exhibited by the existing formulas. For these reasons, there is a increasing requirement of monitoring the bedload through field survey and if possible through long-term series of data. For this purpose, several monitoring methods were developed in the recent years. Each technique features own assumptions and, thus, appears particularly fitting to specific aspects of sediment transport (Vazquez-Tarrio and Menendez-Duarte, 2014). The methods can be classified in direct methods, i.e. systems capable to measure the volume or the weight of the material transported in a defined time period, or indirect methods, that permit to minimize the disturbance of the transport process (Rickenmann et al., 2012) but require a previous calibration phase through the direct methods.

1.1.7.1. Direct methods

The morphological method take origin from the assumption that geomorphic changes are related to the sediment transport processes. This method is applied on great spatial scales and on long-time series of data, using mainly multi-temporal cross sections, aerial photographs and digital elevation models (DEMs). The aim is the evaluation of the historical evidence of the channel variations.

The Vortex tube sampler consists in a horizontal element (Fig. 10a) below a channel with an intake slot along its longitudinal axis. Such device, capturing the sediment transported by the flow, allows the continuous measure of the bedload transport. The material is accumulated in the tube and then a periodical emptying operation is required. The collected samples allow grain size distribution (GSD) to be analyzed. The vortex sampler can be affected by water circulation within the trap. Moreover, the gravel particles during high magnitude floods may over passing the top. Since the capturing efficiency is due to tube diameter, the use of vortex

sampler is more suitable for the gravel bed rivers where the grain sizes are generally smaller respect to the mountain streams.

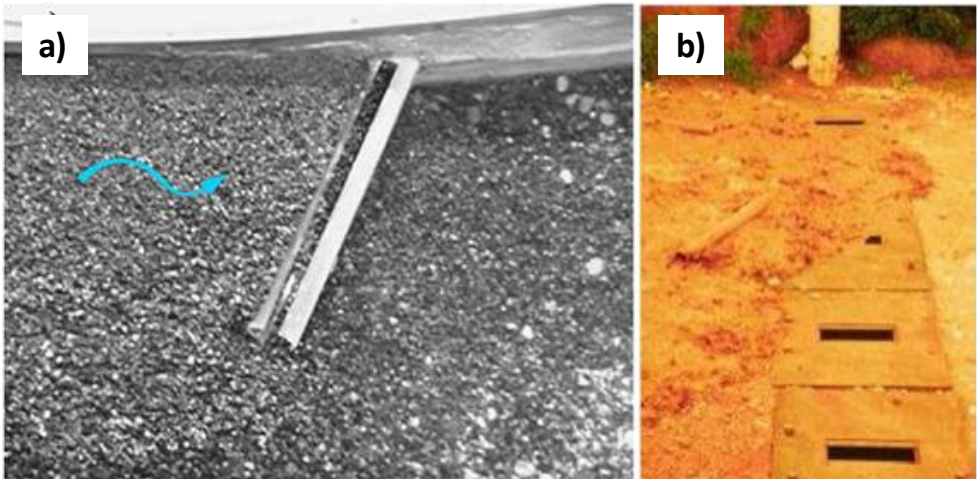

Figure 10: Vortex sampler (a) and Reid sampler (b).

The Reid sampler is a method similar to the just mentioned Vortex tubes sampler. In this case the trap is a stainless steel box with a concrete liner (Fig. 10b). In the upper part (channel bed) is equipped with a removable steel lid that permits to adjust the dimension of slot while at the bottom are located water-filled pressure pillow and pressure transmitters. The Reid sampler allows bedload transport rate and its fluctuations to be evaluated. Similarly to Vortex sampler, the trapping efficiency is due to relationship between the slot dimension and particle size. Moreover, the storage volume is limited and thus, requires a periodically emptying. Also in this case the GSD of the transported material can be evaluated. The Reid sampler is mainly employed in gravel bed rivers.

The Helley-Smith sampler is a portable trap that can be used from bridge, boat, ford, footbridge, allowing to evaluate the transport rate e grain size of transported material. The device is characterized by an iron intake with a 1.9 m^2 polyester mesh sample bag attached to the nozzle. The most used intake dimensions are 76 x 76 mm and 152 x 152 mm, respectively. If employed in mountain streams is preferably to use the Helley-Smith sampler from footbridge. Due to the wide temporal and spatial variability of bedload, is recommended to carrying out various surveys along the cross section investigated. The efficiency of the sampler decreases with progressive filling of the trap and, thus, decreases for long-lasting monitoring. The trapping efficiency may be influenced also by the superficial grain size and presence of obstructions. The blockage of the intake and the perching of sampler's intake are the two main sources of interference with the collection of bedload using the Helley-Smith

device (Mao et al., 2008). Comparing the results obtained by 76-mm Helley-Smith and pit trap, Sterling and Church (2002) noticed that the portable trap underestimated the largest particle size entrained. Similar results were achieved by Ashiq and Bathurst (1999) that in data acquired by 152-mm Helley-Smith observed an underestimation concerning the largest grains mobilized respect those detected by tracers. Promising results were obtained by Lenzi et al. (2006) and Mao et al. (2008) that noticed a good order of magnitude but not exact agreement between tracer displacements and 152-mm Helley–Smith data.

The Bunte sampler (Fig. 11) consists of a 0.3 x 0.2 m aluminum frame with a plastic net approximately 0.9 m long attached. Such net, characterized by a 3.9 mm mesh width, has the aim of collect the sediment transported by the flow. The Bunte sampler allows to assess the bedload transport for a longer temporal scale respect to the device above mentioned and may work without user. Due to the its characteristics, the Bunte sampler appears more fitting to the mountain streams monitoring. This device, as the Vortex and Reid sampler, requires a periodic emptying from the material accumulated in the inner basket. In this sense, the sediment captured represents the bedload sample for all flows occurred from the last removal phase. The Bunte sampler can be affected by water circulation within the trap as the Vortex and Reid devices. A comparison between Bunte and 76-mm Helley–Smith sampler was carried out by Bunte et al. (2008). Investigating the bedload in eight study areas, the authors noticed significant differences in the relationship largest particle captured/water discharge resulted by the two monitoring methods. The authors suggested that, under low hydraulic forcing, the accidental pick-up of clasts during the sampler installation can increase the largest particle collected, while the sampler nozzle size limits the maximum particle that can be captured during high hydraulic forcing.

Figure 11: Bunte sampler in Estero Morales (on the left), and phase of retreat of the samplers (on the right).

The tracers method consists in individual particles that are collected, dried, painted and replaced into the channel (Fraley, 2004). The use of tracers appears particularly adapted to the stochastic nature of the bedload transport that can be view as a random processes of individual particle displacements (Liebault et al., 2012). The tracers allow to analyze the dynamic of particles characterized by different dimensions, investigating the mobility triggered by specific and measured hydraulic forcing conditions. Different approaches can be used to mark the particles, i.e. boulders and large cobbles can be individually numbered or painted, whilst sample areas entirely colored can be realized. Overall, this method is cheap and relatively easy, while the main limit is its limitation to narrow channel (< 20 m) (Vazquez-Tarrio and Menendez-Duarte, 2014). In wide rivers the safety conditions not allow an accurate channel inspection. In turn, the tracers detected on the total population installed (i.e. recovery rate) abruptly decrease, affecting the statistical significance. Frequently, the use of the marked grains is associated to the flow competence approach, that relates the flow magnitude to the largest particle transported (Andrews, 1983). Such approach is called flood competence when the maximum transported particle can be related to the corresponding peak of water discharge (Mao et al., 2008). Generally, the tracers method permits to investigate the gravel mobility in rivers, complementing what can be learned using bedload samplers or fixed traps (Ferguson, 2005). Moreover, the bedload tracing can permit to obtain information about sediment travel distances (Hassan et al., 1991), bedload transport rates (Haschenburger and Church, 1998), incipient conditions (Church and Hassan, 2002) and estimation of bedload volumes during flood events (Liébault and Laronne, 2008; Schneider et al., 2014). In the recent years, new sophisticated methods to mark the grains were developed. The application of the radiofrequency identification technology (RFID) to the sediment tracing allowed to detect the tracers once buried, increasing the recovery rates (Fig. 12a). Specifically, the insertion of passive integrated transponders (PIT-tags) in fluvial sediment was initially used to monitoring the salmonid population behavior (Prentice et al., 1990). Subsequently, the method was introduced also in studies concerning the fluvial dynamic (Ergenzinger et al., 1989; Chacho et al., 1994; Lamarre et al., 2005). The main advantages of PITs employ is that are small, no expensive and allow long-lasting monitoring. Moreover, this typology of transponders can be programmable with a unique identification code (ID), permitting to continuously identify the clast. Significant is also the range of detection, in fact a PIT tags can be identified down to a depth of 0.6 m and the signal is not affected by water, rock, wood or mud (Schneider et al., 2014). The disposition of the tracers along specific cross section can be both organized or distributed in random manner. During each tracers inventory, the PITs are recovered and the

travel distance from the starting point is measured. This monitoring can be performed by an operator that scans the river channel using a mobile antenna or by a system of fixed antennas. Currently, the tracers were infrequently used to analyze the bedload in steep mountain streams. Lenzi (2004) carried out a research in the Rio Cordon, an alpine basin extended about 5 km^2 with an estimated bankfull discharge equal to 2.30 m^3 s^-1. Thanks to the use of 430 natural pebbles, cobbles and boulders (*b* axis between 32 and 512 mm) placed across 2 sections and analyzing several flood events, the author highlighted different relationship among distance of movement, particle size and flow magnitude. In case of high magnitude floods ($Q > 4.0$ m^3 s^{-1}) the marked particles showed a similar travel distance for the major part of the grain size classes. Specifically, discharge > 4.30 m^3 s^{-1} triggered equal mobility conditions to large part of the tracers population. The occurrence of an exceptional flood (Q_{peak} = 10.40 m^3 s^{-1}, R.I. > 100 years), allowed the author to evaluate the tracers entrainment particles during such conditions. During this event the high peak flow caused the mobilization of the most part of the material located along the streambed. The finer grain size showed higher travel distance that decreases, with the increasing *b* axis. Overall, the results suggested that during the extraordinary flood a size-selective entrainment affected the boulder elements in which the displacement rapidly decreased with grain size. On the other hand, equal mobility occurred in cobbles and pebbles grain size, in which the travel distance was detected independent to the grain size. It is worth to noticing that such transport dynamic was triggered by an exceptional flood capable also to remove both the armour layer and step-pool configuration of the Rio Cordon creek. Under near-bankfull conditions (Q_{peak} ~ 2 m^3 s^{-1}) the sediment entrainment appears strongly influenced by the trapping action performed by the bedforms. These results suggests that, in such study area, a size-selective transport occurs during ordinary events (R.I. < 5 years) while equal mobility conditions take place only for high magnitude/low frequency flood events (R.I. > 50 years) (Mao et al., 2008).

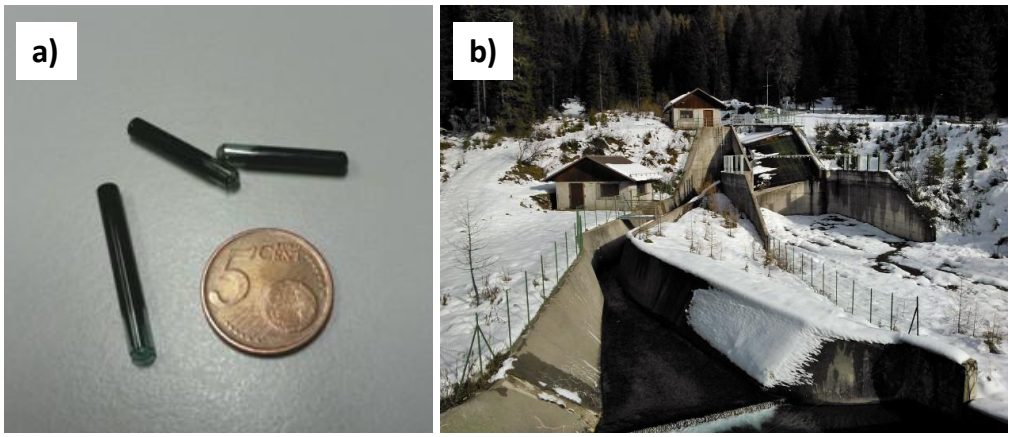

Figure 12: Passive Integrated Transponders (a), the Rio Cordon monitoring station (b).

The permanent monitoring stations (Fig. 12b) are very expensive structures but**,** if properly equipped, allow the continuous monitoring of the sediment fluxes. Such structures permit to accurately investigate the short- and long-term sediment dynamics. Sediment volumes transported by single floods, transport rate (kg/h or m^3/h), threshold of incipient motion, grain size distribution of the deposited material but also long-term dynamic of sediment transport are some of the data that can be produced by a monitoring station. For these reasons the existing experimental sites represent precious tools for the scientific community as well as for the institutions that deal with mountain streams and land use planning (Di Stefano et al., 2008). In particular, these monitoring sites become of extreme value when long-term series of data are eventually produced, thus allowing statistical analysis and experience-based predictions (Mao et al., 2006).

1.1.7.2. Indirect methods

Overall, the indirect methods show some advantages respect to the direct approaches. They are robust, not expensive, easily to install on existing structures, not invasive and permit long-lasting monitoring. Moreover, if properly equipped such devices continuously record data, permitting to investigate the spatial and temporal variability of bedload. On the other hand, the disadvantages consist in: necessity of structures where install the devices, exists a lower threshold as regards the detectable grain size and a preliminary local calibration phase is required, that is not yet errors-free. However, also without calibration, the indirect methods allow to obtain data about: incipient motion, number of pulses vs. water discharge and sediment dynamics at different temporal scale.

The Swiss geophone consists in a sensor, placed in or near the streambed, which records the noise generated by impact of the particles on a metallic grid (Fig. 13a). It is a no-invasive method and therefore the water and sediment flow are not disturbed. The noise increases with augmenting the transport rates while, its frequency is inversely proportional to the sediment sizes. Also without calibration phase the Swiss geophone allows to investigate the incipient motion and number of impulse vs. water discharge.

Figure 13: Swiss (a) and Japanese (b) geophones.

The Japanese geophone (Fig. 13b) is an acoustic sensor connected to a empty metallic tube, that records the noise originated by impacts of the transported sediment. It is a multi-frequency sensor and therefore the calibration depends from the sensibility of microphone and from the grain size characteristics of mobilized particles.

The Swedish geophone consists in a multi-frequency sensor installed under a metallic grid extended 50x50 cm. This type of geophone requires a preliminary calibration phase to carried out in laboratory. Also in this case the grain size strongly influences the data resulted.

Recently, portable bedload impact plates (Fig. 14) were used to monitoring the bedload transport. These devices generally consist in a slightly convex stainless steel plate with a steel cylinder enclosing an accelerometer installed on a side. The number of impacts is recorded by a data logger connected to the accelerometer (Mao et al., 2015). Contrary to the above mentioned devices, the portable impact plate is supplied by rechargeable batteries and, thus, not require a fixed electrical system.

Figure 14: Impact plate

1.2. Aims

This thesis aims to investigate the dynamics of sediment transport in steep mountain channels, focusing particularly on the bedload. The major part of mountain drainage networks is formed by high gradient channels and their nature and dynamics affect the features of sediment delivered to downstream channels, determining the quantity, timing and size of material transported by lowland rivers. In this sense, the monitoring and assessment of bedload allow precious field-data to be obtained, improving the knowledge about the fluvial systems. In this sense, the thesis aims to investigate the bedload process in two study areas: the Rio Cordon (Alps) and Estero Morales (Andes) These study areas were investigated because different in terms of extent, geology, morphology, altitude, vegetation, climate, precipitation and flow regime. Specifically, the Rio Cordon basin is characterized by a nivo-pluvial runoff regime with low sediment supply conditions, while the creek shows a strongly armoured step-pool configuration. On the other hand, the Estero Morales is a glacierized basin characterized by high sediment supply. The stream exhibits a step-pool morphology, whilst in the channel-bed prevails the incoherent and loose material, not armoured. This dissimilarity allowed a comparative analysis to be carried out.

In terms of analysis, first, nearly 30 years of monitoring of sediment fluxes in the Rio Cordon instrumented basin were analyzed at different time scales, ranging from short- (single event) to long-term (three decades). The results obtained permitted to investigate the quantity and timing of sediment delivered by a mountain channel. Once assessed the quantity and timing of sediment yield, the sediment entrainment conditions were investigated. For this purpose the tracing method was used in either study areas. Specifically, on the channel bed of Rio Cordon and Estero Morales creeks were seeded 250 and 429 PITs (i.e Passive Integrated Transponder), respectively.

Overall, only few field dataset are available in literature on which both the bedload volumes and the transport distance of tracers were investigated in steep streams (e.g. Lenzi, 2004; Liébault and Laronne, 2008; Houbrechts et al., 2012). Understanding how bedload volumes and transport distances scale with flood magnitude can be essential to predicting large transport events and the relating dynamics (Schneider et al., 2014).

2. CHAPTER TWO – MATERIAL AND METHODS

2.1. Study areas

2.1.1. Rio Cordon

The Rio Cordon basin (Fig. 15) is located in the eastern Italian Alps (Dolomites). The basin drains a surface of 5 km^2, and elevations range from 1763 to 2763 m a.s.l. The basin is characterized by typical Alpine climatic conditions with an average annual precipitation of 1100 mm that occurs mainly as snowfall between November and April and as storms in the summer season. The runoff therefore exhibits a nivo-pluvial regime dominated by snowmelt between May and June and with significant floods that are recorded in summer and early autumn due to persistent rainfall. The upper part of the basin geology is dominated by dolomites, limestones volcaniclastic conglomerates and tuff sandstones (Wengen group). The lower part of the catchment is characterized by the presence of calcareous, calcareous–marly and arenaceous rocky outcrops. Quaternary moraine and scree deposits are very common throughout. In this regard, the basin is located in the lithotectonic zone called Southern Calcareous Alps (Hinderer et al., 2013).

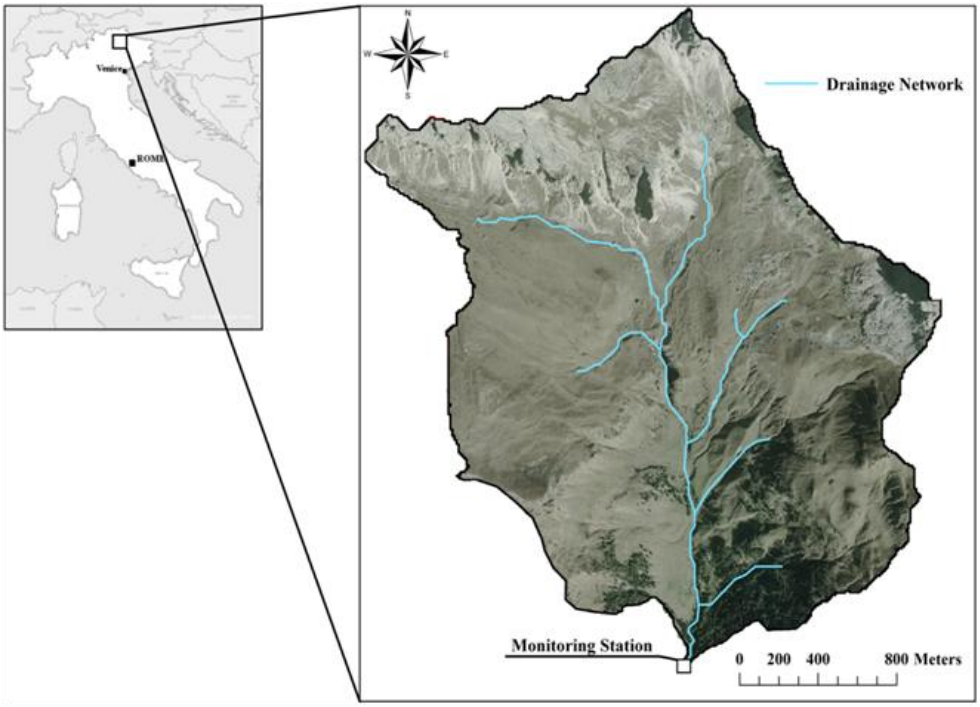

Figure 15: The Rio Cordon study basin.

In the catchment forests cover just 7% of the total basin (*Picea abies* and *Larix decidua*) and only in the lower part of the area. The major part of the catchment features Alpine grasslands (61%) and shrubs (18%). The remaining 14% of the basin extension is bare land. The sediment source areas (Fig. 16) cover 5.2% of the basin and are formed mainly by talus slopes, shallow landslides, eroded stream banks and debris flow channels (Lenzi et al., 2003).

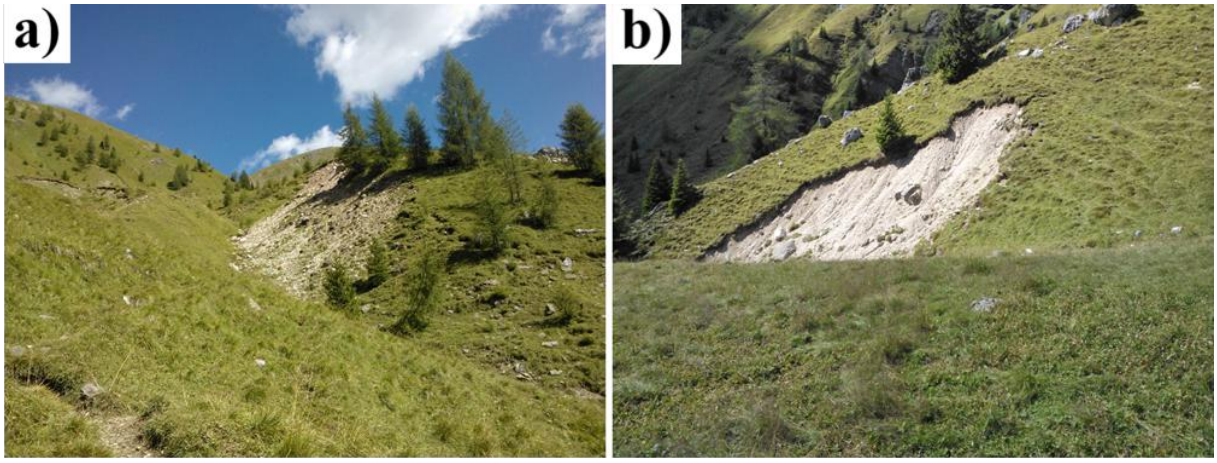

Figure 16: Source areas detected in July 2013 in medial (a) and upper part (b) of the basin

About 50% of source areas is located upstream of a median, low gradient belt (Fig. 17) where sediment deposition takes place. Consequently, the basin headwaters provide a minor contribution to the total sediment yield, independently from the local intensity of erosion processes (Dalla Fontana and Marchi, 2003). Scree deposits on talus slopes are usually distant and disconnected from the main channel, and the stream normally has low to moderate sediment supply conditions (Mao et al., 2009).

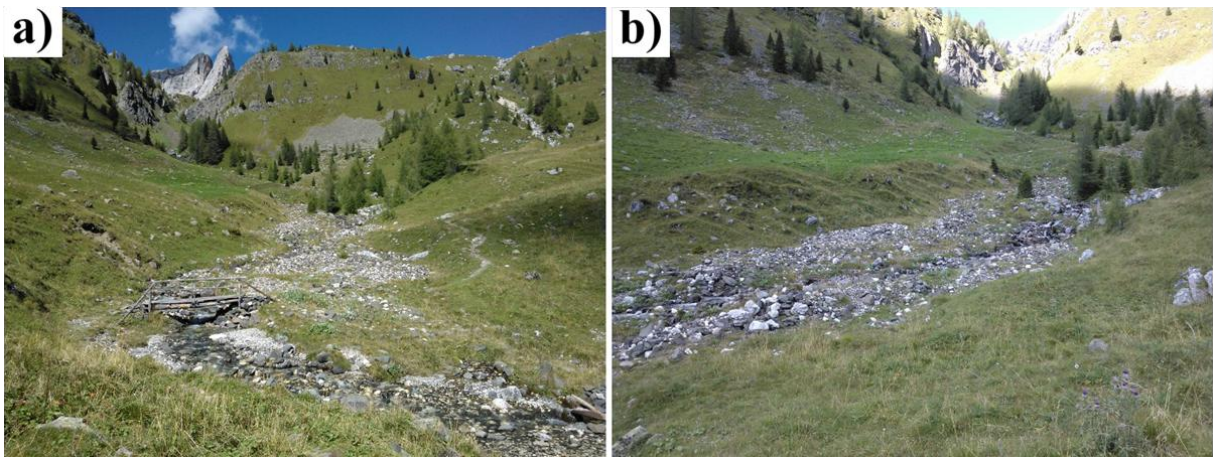

Figure 17: The low gradient belt located in the median part of Rio Cordon basin (images related to July 2013), photos from downstream (a) and left side (b).

The Rio Cordon creek (Fig. 18) has developed its main channel mainly over quaternary moraine and scree deposits. The average slope of the stream is about 17% and in its lower portion features a rough channel bed with a step-pool morphology and large boulders. In August 2014 the grain size distribution (GSD) of the channel bed surface was studied collecting 326 particles and using the grid by number approach. The results show that the GSD is characterized by D_{16} equal to 29 mm, D_{50}=114 mm and D_{84}=358 mm. Such results are in line with the GSD (D_{16}=37 mm; D_{50}=119 mm; D_{84}=357 mm) obtained by Mao (2004) and confirm that the surface GSD is larger than the subsurface GSD (D_{50ss}= 38 mm/D_{84ss}= 125 mm) (Mao et al., 2010), demonstrating the persistence of a strong degree of bed armouring (D_{50}/D_{50ss} = 3).

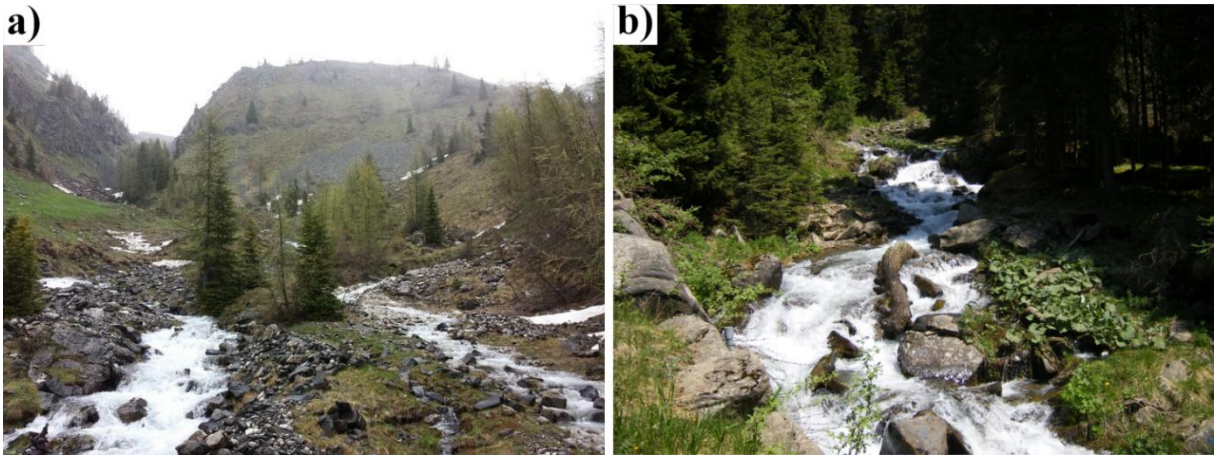

Figure 18: The upper reach of the Rio Cordon during snowmelt period (a), and the lower reach during summer season (b).

2.1.1.1. Monitoring station

The outlet of the catchment is equipped with a permanent monitoring station set up in 1986 by Veneto Region – Experimental Centre of Arabba and actually managed by ARPA Veneto (Fig. 19). Specifically the station is located at an altitude of 1763 m a.s.l., just below the upper limit of the forest. The numerous devices installed for monitoring water discharge, bedload transport and suspended sediment concentration, among other parameters, have been described in detail in previous papers (e.g. Fattorelli et al., 1988; Lenzi et al.,1990; Rickenmann et al., 1998; Lenzi et al, 1999; Mao et al., 2010).

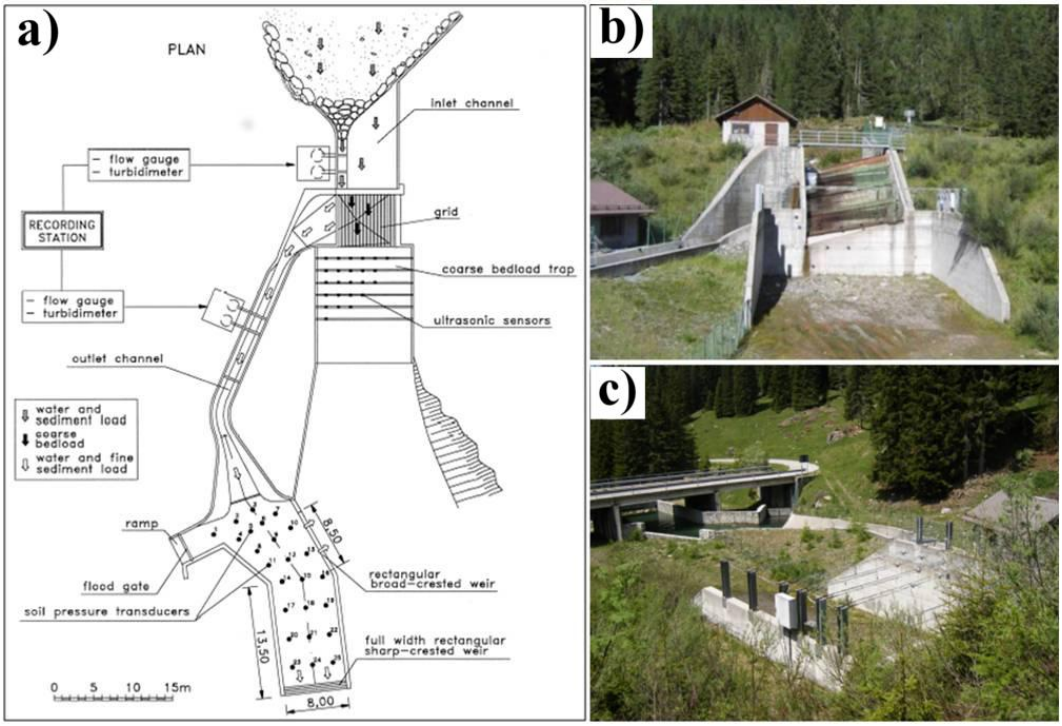

Figure 19: The Rio Cordon monitoring station: plan (a), photos from downstream (b) and upstream (c).

The structure is also equipped with a meteorological station that allows data concerning precipitation, air temperature, atmospheric pressure, relative humidity and solar radiation to be acquired. An additional ARPAV meteorological station, equipped with air temperature sensors and rain gauges, is located at an altitude of 2130 m a.s.l, in the locality of Mondeval di Sora (BL). The station mainly consists of an inlet flume, an inclined grid, a storage area for bedload material, an outlet flume and a settling basin for the suspended load material. The inlet flume is characterized by a longitudinal slope equal to 3% and by a cross section that, thanks to the particular design, allows an accurate measurement of water discharge both in case of ordinary and exceptional floods. The inclined grid (longitudinal and transversal slope equal to 60% and 27%, respectively) enables the coarse sediment (> 20 mm) to be separated

from water and fine material. Once separated, the coarse material is deposited in the storage area where 24 ultrasonic sensors on a fixed frame continuously measure the increasing volume of accumulated sediments during flood events. Once separated from the coarse sediment, the flow runs through a flume that directs it into a settling basin (area of about 205 m^2 and depth of 3.5 m) where the sediment < 20 mm is stored. The liquid discharge is continuously measured (at 1 hr intervals, 5 min during floods) through 2 water level gauges and 1 sharp-crested weir, installed at 3 different locations. One is in the inlet channel, the second along the flume situated downstream from the inclined grid while the last one is at the outlet of the settling basin. A Partech SDM-10 light absorption turbidimeter is installed in the outlet flume while a light-scatter turbidimeter type Hach SS6 is connected to the inlet flume. Both are installed in correspondence to the water level gauges in order to simultaneously measure the water level and suspended sediment concentration (SSC). Several papers have been published thanks to the data produced by the Rio Cordon monitoring station (D'Agostino et al., 1994; Lenzi et al., 1997, 1999, 2003, 2004; Lenzi and Marchi, 2000; Lenzi and Mao, 2003; Mao, 2004; Mao et al., 2008; Picco et al., 2012; Rainato et al., 2013). Indeed, the presence of the station enabled analysis of every flood event, characterized by bedload and suspended sediment transport, that occurred from 1986 to 2014 (Tab. 1). The monitoring station is currently managed by ARPA Veneto, Regional Department for Land Safety. Notwithstanding the experimental station, in the Rio Cordon the bedload was investigated also using tracers and Helley-Smith (Lenzi, 2004; Lenzi et al., 2006b; Mao and Lenzi, 2007; Mao et al., 2008). Using marked particles, Lenzi (2004) assessed the critical discharge that defining the initiation of motion equal to of 0.65 $m^3 s^{-1}$.

2.1.1.2. Recorded events

The most severe flood ever recorded at the Rio Cordon monitoring station occurred on September 14, 1994. The flood was originated by extremely heavy rainfall with maximum rates of 7.2 mm for 5 min, 16.4 mm for 15 min and 25.3 mm for 30 min (Lenzi and Marchi, 2000), which caused the highest discharge ever recorded at the station: 10.42 $m^3 s^{-1}$, with a recurrence interval (RI) greater than 100 years (Tab. 1). This discharge destroyed the bed armour layer formed over years, and as a consequence, the channel bed became the main source of sediment, creating unlimited supply conditions. In addition, many old sediment sources were reactivated and new ones formed due to the high discharge (Lenzi et al., 2004). The event caused the transport of over 1500 t of coarse material to the station and a significant

alteration in the channel geometry (Lenzi, 2001) as well as in the sediment supply characteristics of the basin (Lenzi et al., 2004).

Moderate but persistent autumn rainfall of 101 mm in 24 hours (Mao, 2004) triggered the event that occurred on October 7, 1998. More than 900 t of fine and coarse sediment were transported by the moderate magnitude flood that took place (Tab. 1). After the event, Lenzi (2000) observed a limited number of active sediment source areas in the basin, suggesting that the material could have been supplied by the destabilized channel-bed.

There was another significant flood on May 11, 2001. In this case, there was a quasi-unlimited sediment supply as a consequence of a mud flow that occurred during snowmelt. The soil saturation mobilized a shallow landslide that moved along a small tributary (Lenzi et al., 2004). The debris fan (4176 m^3) formed on the Rio Cordon main channel provided fine sediment easily transportable downstream. These conditions led to the transport of about 137 t of bedload and more than 1000 t of fine material (Tab. 1).

The most recent events were the floods in 2012 and 2014. In 2012, a flood occurred in November due to heavy and persistent rainfall. The peak water discharge reached 2.10 $m^3 s^{-1}$, a value similar to the estimated bankfull discharge of 2.30 $m^3 s^{-1}$ (Lenzi et al., 2006a). The bedload and suspended load were 24.4 t and 60.8 t, respectively (Tab. 1). Field evidence suggested that a debris flow channel located just upstream of the monitoring station was the main sediment source area. Indeed, traces of mud were detected along the banks of that channel during a post-flood survey, confirming the occurrence of a small debris flow. A mixed snowmelt-rainfall event occurred in June 2014 with a flood peak of 2.06 $m^3 s^{-1}$. About 113 t of coarse material was transported by this flood (Tab. 1). In terms of bedload volume, the flood in June 2014 was the sixth most important recorded event. Also in this case a debris flow channel, located in the median part of the basin was identified as the main source area. The material provided by debris flow reached the channel bed approximately 1300 m upstream of the station. In this paper floods are grouped in three categories: “ordinary” events that feature peak discharges with a recurrence interval < 5 years; “large” floods that have a RI > 5 years, while the term “exceptional” (Lenzi et al., 1999) is used here only for the September 1994 event (RI > 100 y).

Table 1: Characteristics of the floods recorded by the Rio Cordon monitoring station, since 1986: Q_{peak} is the peak of water discharge ($m^3 s^{-1}$); RI the recurrence interval (years); BL the bedload (tons); SSL is the suspended sediment load (tons); TL the total load amount (tons), BL_f is the bedload fraction on the total load transported; Re is the effective runoff volume ($10^3 m^3$); D_{16}, D_{50} and D_{84} are the percentiles of the grain size distribution concerning the bedload.

	Q_{peak} ($m^3 s^{-1}$)	RI (years)	BL (t)	SSL (t)	TL (t)	BL_f (fraction)	Re ($10^3 m^3$)	D_{16} (mm)	D_{50} (mm)	D_{84} (mm)
11 October 1987	5.15	11.5	85.6	131.7	217.3	0.39	79.9	—	—	—
15 July 1988	2.43	2.0	—	—	—	—	—	—	—	—
3 July 1989	4.39	7.1	145.6	223.9	369.5	0.39	103.4	54	103	207
22 May 1990	0.85	1.0	—	—	—	—	—	—	—	—
17 June 1991	4.00	5.5	67.2	68.1	135.3	0.50	57.9	30	51	100
5 October 1992	2.91	2.7	15.5	4.8	20.3	0.76	21.5	22	43	111
2 October 1993	4.28	6.6	17.2	41.1	58.3	0.30	30.7	29	61	135
18 May 1994	1.79	1.4	1.7	2.7	4.4	0.39	5.4	21	33	52
14 September 1994	10.42	>100	1541.7	2435.1	3976.8	0.39	26.6	65	116	226
13 August 1995	2.72	2.4	10.3	98.3	108.6	0.09	1.8	—	—	—
16 October 1996	2.96	2.8	94.7	294.4	389.1	0.24	22.0	40	79	143
27 June 1997	1.46	1.2	—	—	—	—	—	—	—	—
7 October 1998	4.73	8.8	516.8	393.5	910.3	0.57	91.8	40	78	157
20 September 1999	3.65	4.4	32.7	50.9	83.6	0.39	10.4	32	54	98
13 October 2000	3.28	3.5	92.2	142.0	234.2	0.39	110.6	39	61	111
11 May 2001	1.46	1.2	137.8	1017.6	1155.4	0.12	8.5	33	48	69
20 July 2001	1.98	1.6	36.0	119.8	155.8	0.23	15.0	—	—	—
04 May 2002	2.29	1.8	47.2	123.0	170.2	0.28	29.4	39	59	99
16 November 2002	2.35	2.0	17.2	54.3	71.5	0.24	18.9	—	—	—
27 November 2002	2.77	2.5	119.0	373.7	492.7	0.24	70.3	26	44	78
03 May 2003	1.02	1.1	1.7	0.2	1.9	0.89	1.0	—	—	—
01 November 2004	2.05	1.6	7.9	7.6	15.5	0.51	—	25	38	62
6 October 2005	1.68	1.4	1.6	1.2	2.8	0.59	3.3	18	30	55
19 May 2006	1.28	1.1	1.2	5.1	6.3	0.19	1.0	—	—	—
24 May 2009	1.67	1.3	3.1	19.3	22.4	0.14	5.2	—	—	—
5 May 2010	1.82	1.5	1.4	14.2	15.6	0.09	3.7	—	—	—
8 June 2011	1.15	1.1	0.9	0.6	1.5	0.64	0.8	—	—	—
11 November 2012	2.10	1.7	24.4	60.8	85.4	0.29	4.6	23	38	70
17 May 2013	1.96	1.5	3.8	13.7	17.5	0.22	10.2	33	44	90
9 June 2014	2.06	1.7	113.0	76.8	189.8	0.60	16.6	24	41	64
5 November 2014	2.06	1.7	4.6	84.3	88.9	0.05	33.3	25	38	62

2.1.2. Estero Morales

The Estero Morales (Fig. 20) is a 27 km^2 basin located within the Maipo River catchment, in the Metropolitan Region (central Chile). From administrative point of view, the area is part of San José de Maipo village, Provincia de Cordillera about 90 km from Santiago de Chile. The catchment is entirely part of a protected CONAF (Corporación Nacional Forestal) reserve. It ranges between 1850 to 3815 m a.s.l, closing at the injunction with the rio Volcàn.

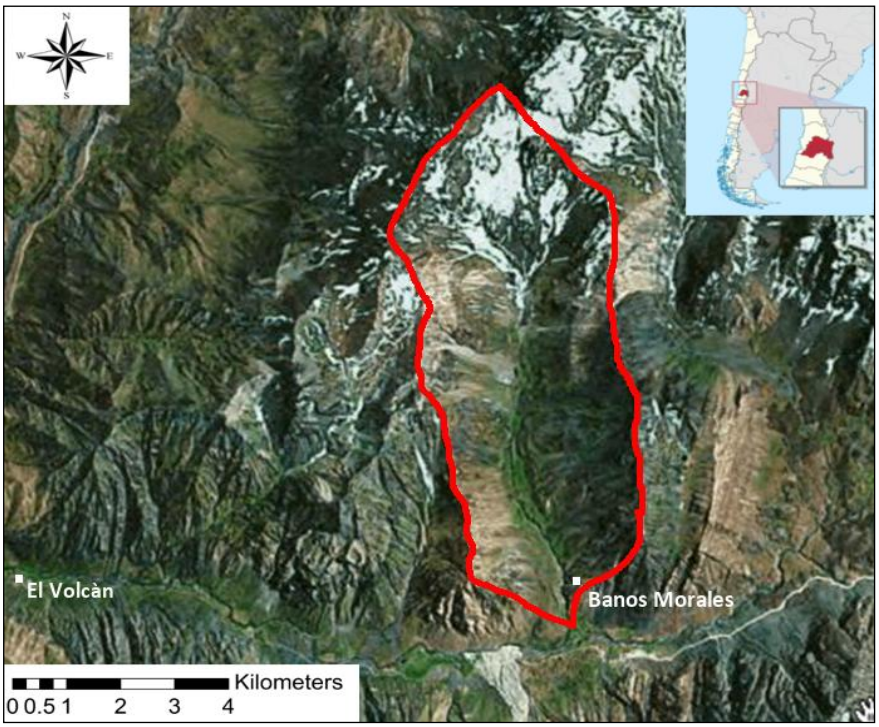

Figure 20: Estero Morales basin

The basin hosts the San Francisco glacier, currently extended 1.8 km^2 (Fig. 23). Due to the glacier, the runoff regime is mainly dominated by snow and glacier-melt in summer, while rainfall events prevail in late spring. Particularly during the melt period (December-March) the San Francisco glacier ensures daily discharge fluctuations (Fig. 21 and Fig. 22) with different bedload transport rates associated. Such condition represents the ideal scenario to monitoring bedload transport under a wide range of discharge and for a long-term period.

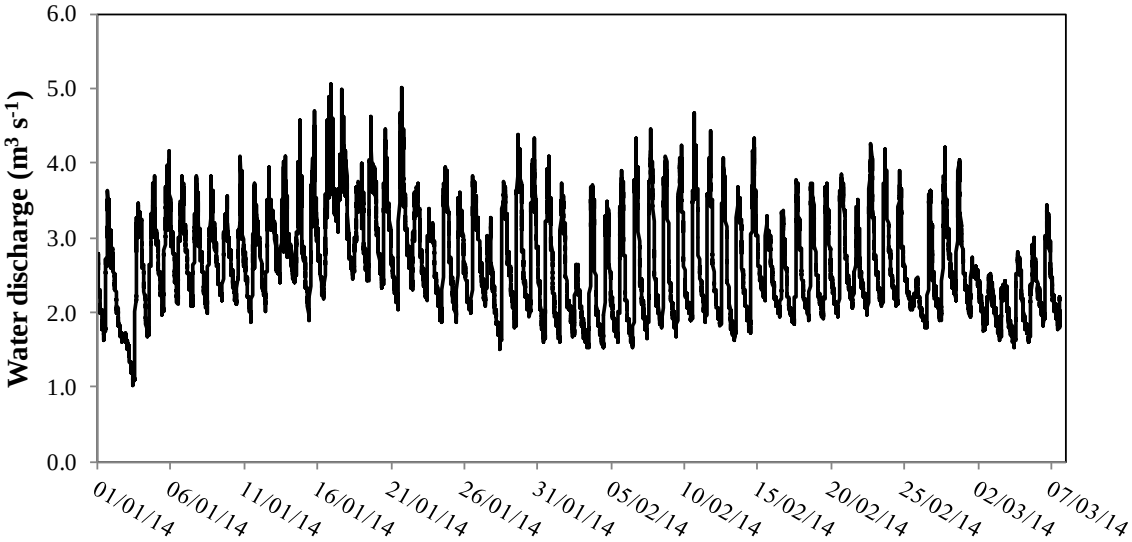

Figure 21: Hydrograph regarding the discharges occurred in the Estero Morales between January 2014 and March 2014. The daily fluctuations due to glacier-melt phase are evident.

Figure 22: Discharge fluctuations in Estero Morales creek, the water flow at 07.00am (a) and at 02.00pm (b).

The geology of the basin mainly consists in sandstones (Colimapu group), marine limestone (Lo Valdes group) and pyroclastic rocks (Abanico group). Moreover, quaternary moraines and fluvio-glacial deposits are very common along the entire catchment. The catchment exhibits typical Andean climatic conditions: average annual precipitation that ranges between 1000-2000 mm and with a predominance of snowfall respect to the rainfall (Infante Fabres, 2009). Due to the climatic conditions, large parts of the basin are completely covered by snow for about 6 months/year. In this sense, two morphoclimatic zones can be detected in the Estero Morales basin (Fig. 23). The upper part of the basin, where are located several surfaces covered by layers of permanent ice, including the large San Francisco glacier. The second zone consists in the lower part of basin, where the periglacial conditions prevail. The vegetation in the catchment consists mainly in the Andean steppe, i.e. predominance of herbaceous coverage and shrubs. The vegetation appears sparse and mainly located in the periglacial zones.

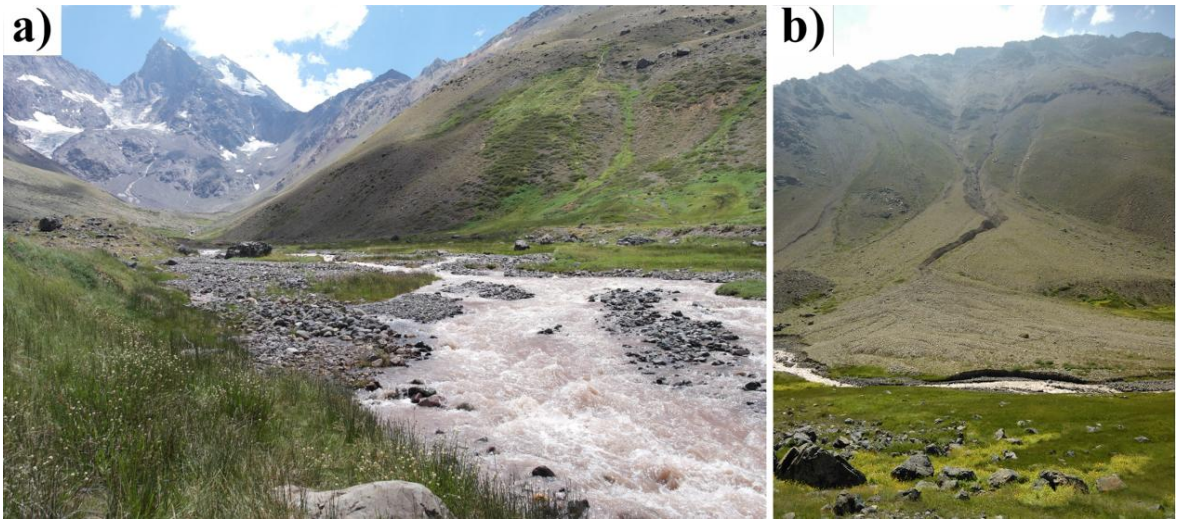

Figure 23: The upper reach of Estero Morales basin (a) with on background the San Francisco glacier; and example of source area (b) situated in the basin (debris flow).

Overall, the basin can be classified as a dynamic catchment. The combination of all processes related to the presence of glacier, ice, snow, melting water and seismic, causes that a large supply of material from the hillslopes reach the drainage network (Infante Fabres, 2009). Along the entire basin, the stream is continuously supply with incoherent material, derived especially from gravitational hillslope processes (landslides, debris flows) and talus slopes (Fig. 23). For these reasons the stream appears characterized by high sediment supply condition. The Estero Morales creek is a typical high-gradient stream with prevalent boulder-cascade, step-pool and plane bed morphologies and with an average slope equal to 9.5%. Along the entire longitudinal profile a sequence of steep reaches followed by low gradient zones can be observed. Thanks to field surveys carried out in January 2014, the grain size distribution (Fig. 24) was evaluated. In the Estero Morales, the percentile D_{16} is equal to 20 mm, D_{50}=59 mm while the D_{84}=317 mm.

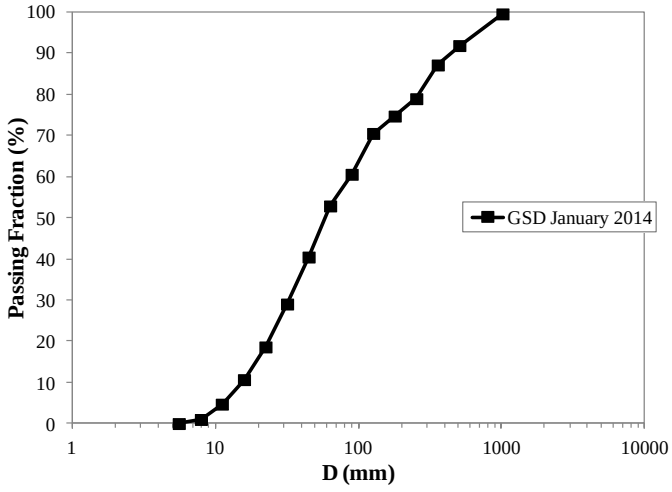

Figure 24: Grain size distribution of surface sediments in the Estero Morales.

2.2. Research methodology

2.2.1. Rio Cordon: the monitoring station data

The collaboration with the Regional Land Safety Department of ARPAV agency allowed the data produced by the monitoring station to be used and analyzed. First, the data were controlled and filtered to obtain a reliable datasets. Subsequently, the data were analyzed. In terms of water discharge measure, the data of the three water level gauges are available. In this thesis, the data produced by the upstream device (i.e. water level gauge situated in the inlet channel) were primarily used. This choice was made in order to use the more reliable device, indeed the other two water gauges suffer some calibration and maintenance issues. Moreover using the upstream sensor, the analyses appear consistent with the previous works carried out in Rio Cordon basin (Lenzi et al., 2006b; Mao et al., 2009).
First, the 60-minutes data were organized and elaborated, permitting to identify the flood events (Fig. 25). Once determined the days in which the flood took place, the 5-minutes data were isolated and analyzed. The assessment of the water discharge (Q) measured every 5 minutes allows to better evaluate the hydrograph of floods, permitting to estimate the peak discharge (Q_{peak}) as well as the duration of the event. In case of bedload transport, also the effective runoff (Re, 10^3 m^3) was estimated for each flood. The effective runoff is defined here as the portion of the hydrograph volume that contributes to the transport, exceeding the detected threshold discharges. In the Rio Cordon the determination of thresholds was possible thanks to the data produced by the ultrasonic sensors and turbidimeters.

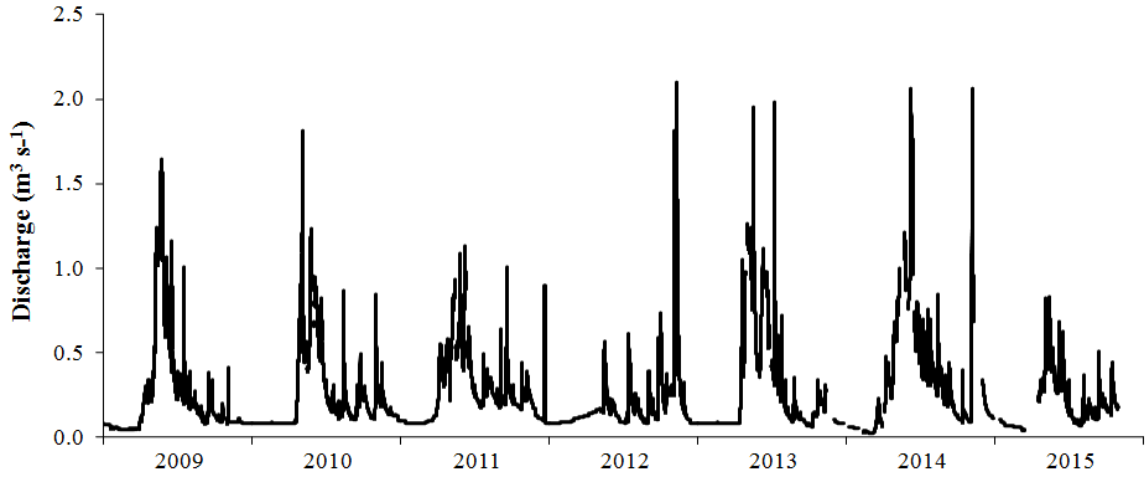

Figure 25: Hydrograph regarding the water discharge occurred in the Rio Cordon between January 2009 and December 2015.

The bedload (BL) transported to the monitoring station by the flood events was estimated from data provided by the ultrasonic sensors installed above the storage area. Unfortunately, these devices stopped working properly in 2012. For this reason, a Terrestrial Laser Scanner (TLS) was used to survey the coarse sediment volume deposited in the storage area by each bedload event occurring from 2012 to the present (Rainato et al., 2013). The point clouds produced were used to create a Digital Elevation Model (DEM) of bedload volumes. In all cases a cell size of 2 cm was obtained, while the ArcGIS® tool called Surface Volume was used to estimate the volume. Once obtained, such volumetric data was converted in weight values using a sediment relative density of 2.65 t m^{-3} and a coarse material porosity of 35%.

Also, the grain size distribution (GSD) of the coarse transported material was evaluated. First, the largest particle transported (D_{max}) was identified. This step allows to determine the flood competence of the event, i.e. the largest grain size transported by a single flood event (Andrews, 1983) to relate to the corresponding Q_{peak} (Mao et al., 2008). In order to evaluate the GSD, the grid by number approach was used as sample method. This approach consists to collect the particles using a regular grid characterized by an inter-distance equal to 2 D_{max}, avoiding to count two times the larger particles. During the field surveys, metric tapes were used for design the sample grid while calipers were used to measure the particle diameters.

Subsequently the bedload events, field surveys were carried out to identify the sources that provided coarse material. Once, identified the source areas were mapped. For this purpose a differential Global Position System (DGPS) device, with an average vertical quality equal to 2 cm, was used.

The suspended sediment load (SSL) was evaluated using the data recorded by the turbidimeters installed in the monitoring station. These data were converted from the original turbidity values (NTU, Nephelometric Turbidity Units) into SSC (g l^{-1}). For this purpose, the formulas established by Lenzi et al. (2003) for Rio Cordon were used. The turbidity-SSC transformation was based on laboratory tests and had already been used in previous works concerning the budgeting of Rio Cordon basin (Lenzi et al., 2003; Mao, 2004).

In order to evaluate the suspended sediment loads also in the periods when the turbidimeters were not recording or in the case of unreliable data (i.e. $Q<0.30$ m^3s^{-1}), an empirical SSC-water discharge relationship was developed. This approach had been proposed by Mao (2004), who inferred different relationships according to the season. According to the previous budgeting of the Rio Cordon (Lenzi et al., 2003; Mao, 2004) and taking into account the climatic features as well as the runoff regime of the study area, the snowmelt period is defined as the time interval between April, 1 and June, 15. In this period, snowmelt dominates

the runoff processes. Summer is understood to be between June, 16 and August, 31 while autumn between September, 1 and November, 30. During these periods the runoff is dominated by rainfall. Snow permanently covers the basin from December to the last days of March.

2.2.2. In-channel field activities

2.2.2.1. Characterization of hydrological conditions in the PIT-study reach

In the Rio Cordon, large part of the PIT-study reach is situated upstream of a small ephemeral tributary. To correct the possible differences between the discharge here occurred and the discharge recorded by monitoring station, along the study reach 4 PVC pipes (diameter 0.09 m) equipped with 4 capacitive piezometers (TruTrack® transducers) were installed. Therefore, such devices were installed to obtain a reliable characterization of the hydraulic forcing conditions. The capacitive piezometers were programmed to record the water stage every 15 minutes (Fig. 26b). Such time resolution required the download the data every 70 days. Once, downloaded the data were filtered and analyzed. Since 2014, to produce a stage-discharge relationship, 29 water discharge measures were carried out in correspondence to the capacitive piezometers. For this purpose, the salt dilution method (Moore, 2004) was used, employing a WTW® conductivity meter (Fig. 26c).

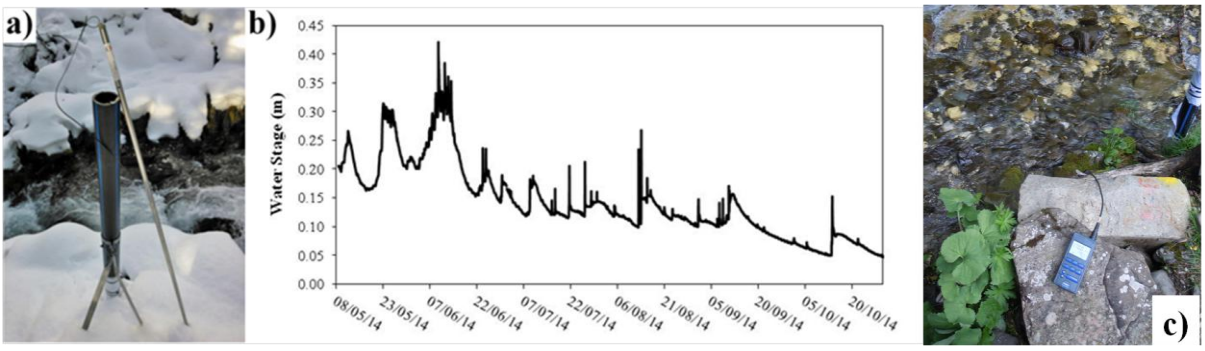

Figure 26: TruTrack® transducer installed in PVC pipe (a), water stages recorded by such device between May 2014 and November 2014 (b) and conductivity meter during a discharge measure (c).

2.2.2.2. Rio Cordon: grain size distribution analysis

In August 2014 the grain size distribution of the channel-bed material was assessed. Such analysis was performed along a representative reach of the main course, i.e. a reach characterized by the prevalent morphologies of the whole Rio Cordon channel. In this sense, carrying out a GSD analysis along a reach that shows a prevalent configuration, can

represent a significant source of uncertainty. This is due to the grain size features that clearly distinguish morphologies as step-pool, plane-bed or boulder-cascade. Coherently to the GSD performed on the bedload deposited into monitoring station, also for the channel-bed material the grid by number approach was used. The previous analysis concerning the grain size distribution of Rio Cordon creek is 2004 dated (Mao, 2004). An appropriate GSD estimation is fundamental to analyze the sediment dynamic. Mao (2004) focused the analysis on 5 different sample areas, distributed along the main channel. In August 2014, the particles were mainly collected by lower part of the stream, where the tracers were installed. The sample area (~ 65 m) is characterized by a prevalent step-pool morphology interrupted by boulder-cascade and plane-bed configurations, therefore representing a representative segment of entire Rio Cordon creek. Overall, 326 particles were collected and measured. The GSD obtained (Fig. 27) shows a percentile D_{16} equal to 29 mm, D_{50}= 114 mm, D_{84} is 358 mm, while the percentile D_{90} is equal to 455 mm.

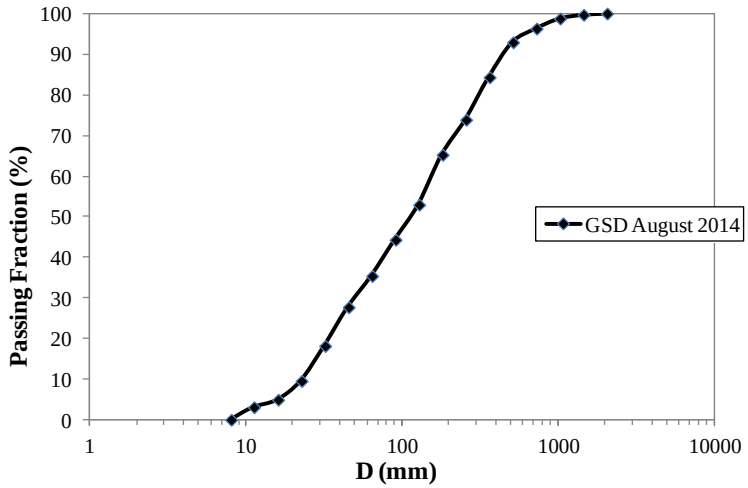

Figure 27: The grain size distribution of Rio Cordon channel-bed (August 2014).

Such percentiles appear roughly consistent with the GSD evaluated by Mao (2004). A reduction equal to 26.1% and 4.6% can be observed in D_{16} and D_{50}, respectively. Lower percentage difference can be observed in D_{84} and D_{90}, with reductions equal to 0.4% and 0.9% (Tab. 2).

Table 2. The grain size distribution estimated by Mao (2004) compared with the GSD estimated in August 2014. *N* is the number of particles collected and measured while D_{16}, D_{50}, D_{84} and D_{90} are the 16th, 50th, 84th and 90th percentiles of GSD. Δ is the percentage difference.

	N	**D_{16}**	**D_{50}**	**D_{84}**	**D_{90}**
GSD 2004	999	37	119	357	451
GSD 2014	326	29	114	358	455
Δ (%)	-	-26.1	-4.6	0.4	0.9

2.2.3. PIT tracers monitoring

In this work, PIT-tags were used both in Rio Cordon and Estero Morales creeks. Here, the terms "PIT" or "tracers" are used to identify the clasts equipped with passive integrated transponders. Additionally, the terms "survey" and "inventories" are used to describe the field-phase in which the PITs were monitored. In either cases, transponders 23 mm long with a diameter equal to 3.85 mm were employed (Fig. 28). Once installed into the particles, the tracers were seeded along line transverse respect the main flow direction. Once placed over the channel-bed, clasts were crushed with the heel of boat. Such operation allows the natural arrangement of gravel clasts on the channel-bed to be recreated (Vazquez-Tarrio and Menendez-Duarte, 2014). A poor placement of tracers, i.e. tracers simply placed on top of channel-bed, causes that they can be moved more easily respect the bed material. In turn, such mistake causes an underestimation of the incipient motion conditions (Bathurst, 2013). To monitoring the tracers displacement, a mobile antenna based on the Radio Frequency Identification (RFID) technology was used. Such device is produced by Aquartis Accueil® (Fig. 28) and consists in a control module (kept in a backpack), an LCD display panel (where read the PITs ID) and a transponder detection antenna characterized by a 0.53 m diameter. All powered through 12 VDC battery. In addition to the just mentioned device, a laser rangefinder was used to measure the distances traveled by each PIT, once found. This device is the Impulse 200R model, produced by LaserTech® and is characterized by a horizontal accuracy equal to 0.01 m. During the field surveys, the operator equipped with the antenna scans the channel bed surface. When a PIT is detected, vertical and horizontal distance were measured from a reference point by means of the laser rangefinder. In either study areas, the study reaches were organized with several cross sections. These sections, that subdivide the reaches in straight segments, were used as reference points from which the PITs displacements were measured. The use of the cross sections avoids to measure distances along curvilinear reaches, improving the field survey phase.

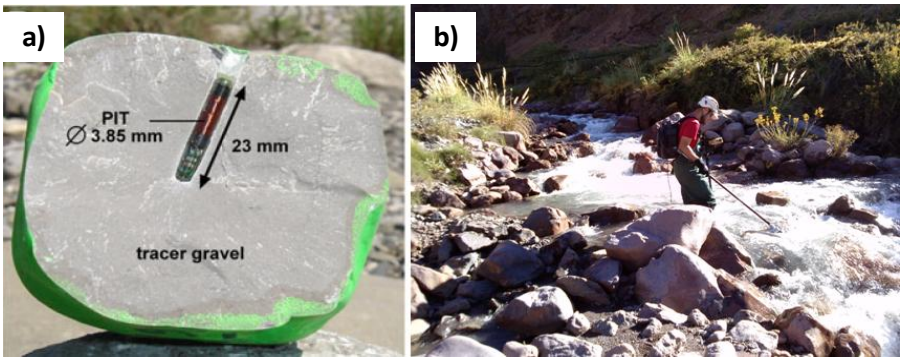

Figure 28: Clast marked with a PIT tag (a) (Liebault et al., 2012), and phase of PITs monitoring along the Estero Morales creek using the Aquartis Accueil® mobile antenna (b).

2.2.3.1. PIT in Rio Cordon creek

In the Rio Cordon between 2009 and 2012, 250 PIT-tags were installed. The particles selected for the insertion of passive transponders (*b-axis* between 40 and 190 mm) are a representative sample of the grain size distribution that characterize the channel-bed material. In this sense, the GSD of the 250 PITs exhibits a D_{16} = 47.2 mm, D_{50} equal to 66.7 mm, D_{84} = 106.6 while D_{90} is 121.6 mm (Tab. 3; Fig. 29).

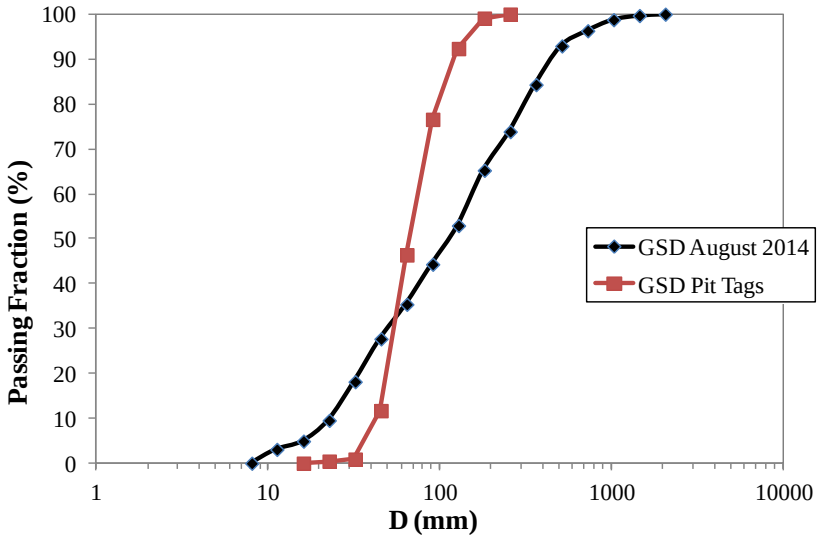

Figure 29: The grain size distribution of PIT tags (GSD Pit Tags) compared to the GSD of Rio Cordon bed material (GSD August 2014).

Table 3: Grain size distribution of PITs installed in the Rio Cordon. Number of PITs (*N*) and 16th, 50th, 84th and 90th percentiles of GSD.

N	D_{16} (mm)	D_{50} (mm)	D_{84} (mm)	D_{90} (mm)
250	47.2	66.7	106.6	121.6

The marked particles were installed 318 m upstream to the monitoring station, along a plane bed segment of main course. In order to enhance the analysis of the PITs behavior, the longitudinal profile of the study reach was surveyed (Fig. 30). For such purpose a laser rangefinder in conjunction with a topographic prism were used. Overall, 360 points were acquired along the thalweg of channel bed, producing a longitudinal profile 353 m long (1.02 point m^{-1}). The profile covers the entire study reach where the PITs tags were installed, continuing upstream for 35 m. The longitudinal profile showed as the average slope along the study reach is equal to 12.5%, i.e. lower respect to the average slope concerning the entire Rio Cordon stream (17%).

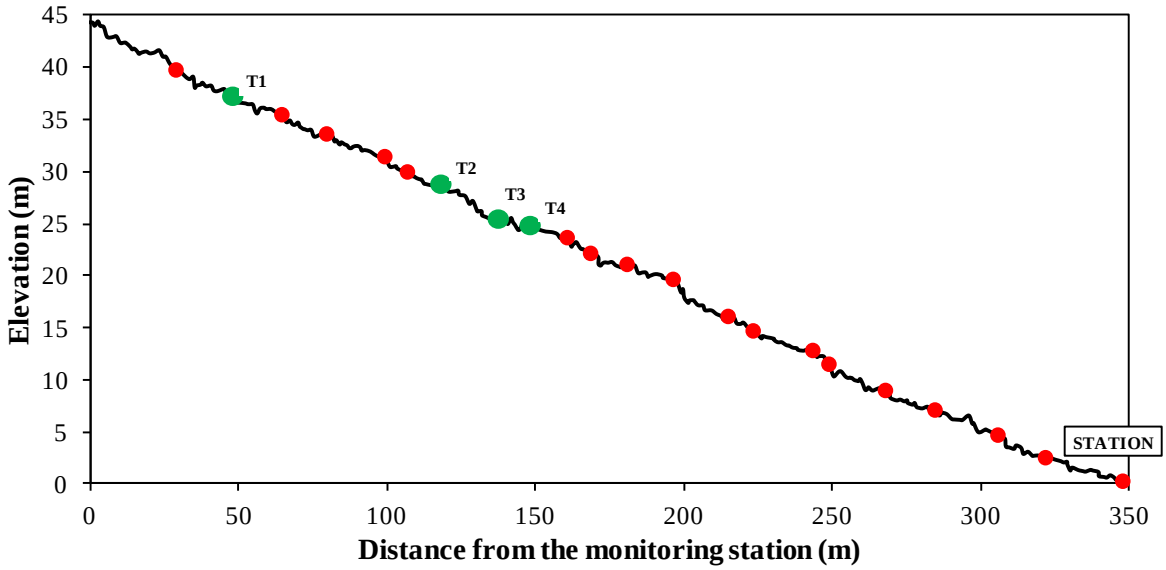

Figure 30: Longitudinal profile of PITs study reach. The red points represent the cross sections used to measuring the PITs displacements while the green points represent the capacitive piezometers installed.

As said, to improve the displacements evaluation the study sites were organized in straight segments. For this purpose, 21 cross sections were set up in the Rio Cordon and used as reference sections for measuring the tracer displacements (Fig. 31).

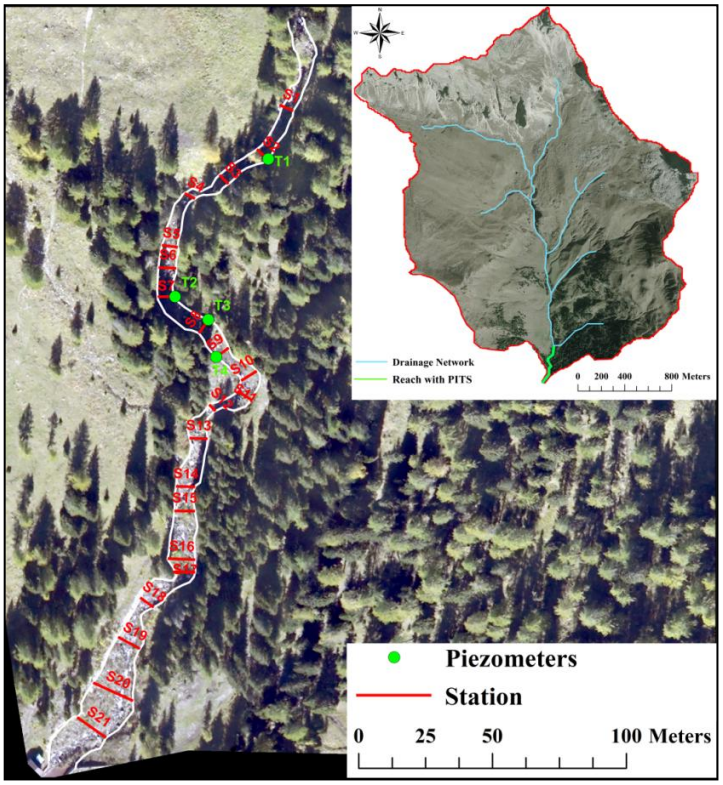

Figure 31: Localization of the PITs study reach, in red are shown the reference sections used to measuring the displacement while in green are shown the position of the 4 capacitive piezometers.

As above mentioned, in the study reach, an ephemeral tributary is located. In terms of hydrological features, its presence causes that the discharge measured at the monitoring

station (i.e. end of the study reach) may be different respect to the real discharge that flow in the site investigated. In particular, was expected that the discharge measured by the monitoring station (Q_{STAT}) could be higher respect to the discharge actually occurred in the PIT-study reach (Q_{PIT}), due to the contribution provided by the tributary. Supposedly, such contribution should be higher during the floods (ephemeral character of tributary). To a correct characterization of the hydrological condition, 4 piezometers in addition to the salt dilution method were used (Fig. 26). Overall, 29 discharge measures were performed between 2014-2015. The water stage investigated range among 0.049 m and 0.409 m, while the discharge varies between 0.09 m^3 s^{-1} to 1.86 m^3 s^{-1}. Initially, the Q_{PIT} was measured in correspondence of two different piezometers (T2 and T4), to obviate to possible instrumental malfunctions. Once observed the equivalence between these discharges; since 2015, the salt dilution measures were focused in correspondence to the piezometer located downstream (T4, upstream to the tributary). In that point, 17 discharge measures were overall performed, obtaining a good stage-discharge relationship (R^2 = 0.974). Moreover, it was noted that the Q_{PIT} - Q_{STAT} relationship clearly scale linearly (coefficient = 1.001), with an R^2 (0.987) higher respect to the stage-discharge relationship obtained (Fig. 32). Thus, the investigation highlighted that the Q_{PIT} were continuously in line with the Q_{STAT} simultaneously recorded by the monitoring station. Such evidences demonstrated that, during the study period and under the range of flood magnitude analyzed, the contribute provided by the tributary has not altered Q_{PIT} respect Q_{STAT}. In light of such result, Q_{STAT} was used to the subsequent analyses concerning the PIT tracing.

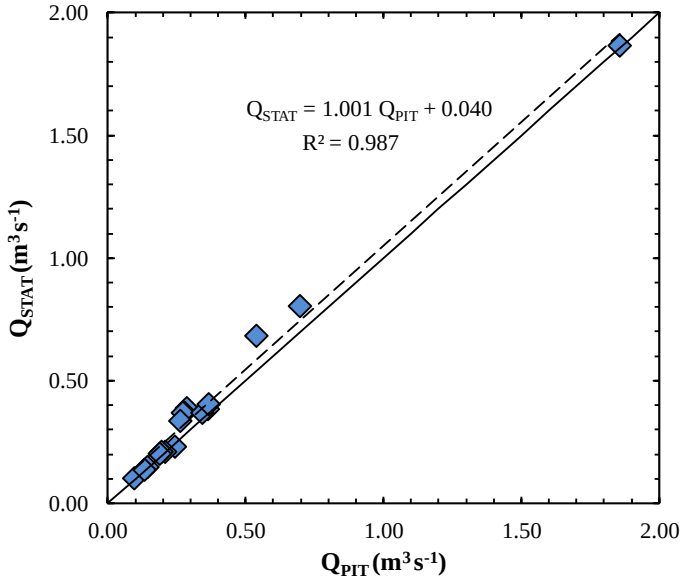

Figure 32: Relationship between the discharges measured along the PIT-study reach (Q_{PIT}) and the discharges recorded by the monitoring station (Q_{STAT}). The black line shows the ratio 1:1, while the dotted line is the regression line obtained.

2.2.3.2. PIT in Estero Morales creek

In the Estero Morales, the employment of PIT-tags is more recent respect to the Rio Cordon, indeed the bedload tracing started in 2014. In this case, the activities were focused on the PITs preparation, release, monitoring and recovery. The installation of tracers in field required a preparatory stage, that involved the collection of clasts from the study area and further laboratory activities. The preparation of PITs consisted of drilling clasts with a standing rotary drill, in the Hydraulic Engineering Laboratories of Pontificia Universidad Católica de Chile, in Santiago de Chile. Once the transponder inserted and sealed the hole, the particles were coloured with acrylic paint to enhance their visibility in the river. Each transponder was programmed with an identification code (ID) such ID was written also on the surface of each marked grain. The mass of the clast was weighted and the dimension of the three axis was measured with a caliber. This preparatory stage was replied directly in field for the particles with mass > 10 kg. Overall, 429 PIT-tags (*b-axis* between 27 - 420 mm) were prepared (Tab. 4, Fig. 33), and released by 28th January 2014.

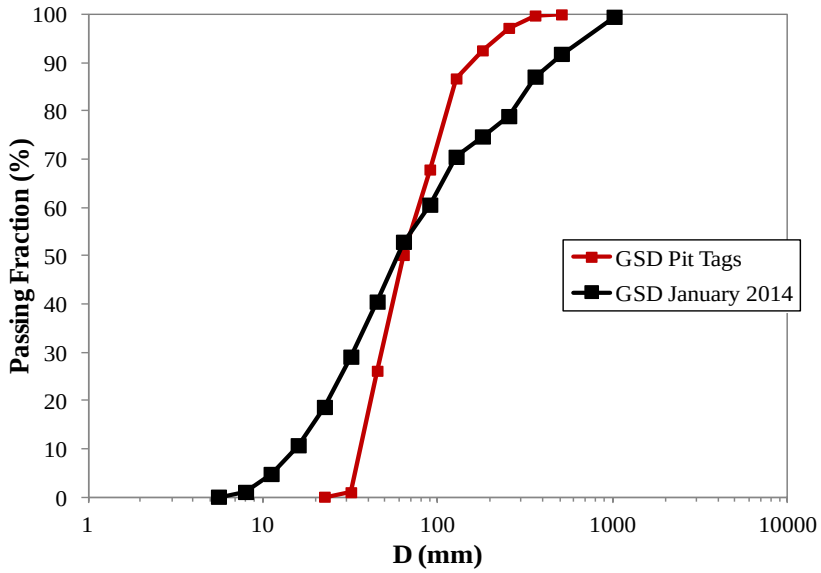

Figure 33: The grain size distribution of PIT tags (GSD Pit Tags) compared to the GSD of Estero Morales bed material (GSD January 2014).

Table 4: Grain size distribution of PITs installed in the Estero Morales creek. Number of PITs (*N*) and 16th, 50th, 84th and 90th percentiles of GSD.

N	D_{16} (mm)	D_{50} (mm)	D_{84} (mm)	D_{90} (mm)
429	39.4	63.9	121.8	155.6

The PITs was mainly released during low flow conditions, i.e. between 7.00am and 10.30am, to avoid potential perilous conditions for the operators. Different grain sizes were randomly placed in the channel-bed and on river banks. The release phase was carried out in the same days in which the monitoring were performed. The study reach extends over a length of 744 m and is characterized by a vertical gradient equal to 101 meters. Overall, 35 cross sections were created and used as references for the evaluation of PIT displacements. The tracers were released from the sections 1, 2 and 3 (i.e. upstream) and their transport was monitored until the section 35, which represents the confluence with Rio El Volcàn. Section 1 is located at the outlet of a bedrock incised canyon. This section is characterized by limited or no talus deposits on the hydrographic right, and rock walls on the left flank. Channel morphology is plane bed/step-pool, approximately 7.2 m wide. Section 2 is approximately 23 m downstream from section 1. The width of the valley is larger than in previous section, and talus deposits are present on both river side. In this point the channel morphology exhibits an abrupt change: a step-pool sequence begins downstream a boulder-cascade reach that spans over the majority of the length between the first and the second section. Section 3 is approximately 30 m downstream section 2. Channel configuration is characterized by a step-pool sequence, in which the pool width is approximately 6 m and the depth is about 2 m. Here, the cross section is highly asymmetric due to the presence of cemented alluvial deposits on the left bank, while on the right unconsolidated alluvial deposits are found. Due to the typical flow regime of the Estero Morales (glacier-melt), the channel inspections (i.e. PIT monitoring) were performed between the 7.00am and the 2.00pm, i.e. in conjunction with low-mid water stages (Fig. 21). Specifically the field works started on 29th January 2014 and ended on March, 7, requiring an intense in-channel work, performed by two operators. Overall, 15 PITs monitoring were performed. In addition to the monitoring, in the last three days of field survey the traceable PIT-tags were recovered. Such activity allowed 109 tracers to be recovered.

Contrary to the Rio Cordon, along the PIT-study reach investigated in the Estero Morales none tributary is situated. In light of that, to characterize the hydrological conditions, the discharge obtained by a level sensor placed in correspondence of the Puente Esfuerzo (i.e. in the middle of the study reach) was considered and used to the subsequent analyses (Fig. 34).

Figure 34: Water level sensor (red arrow) placed in correspondence of the Puente Esfuerzo.

2.2.3.3. Estimation of unit stream power (ω)

In both study sites, the results obtained by the bedload tracing were related to the hydrological conditions occurred (i.e. hydraulic forcing). To compare results obtained in two different study areas, these conditions were described by dimensionless terms, using the stream power approach. As above mentioned (see section 1.1.6), the stream power is an approach proposed by Bagnold (1966) e is defined as the rate of energy dissipated by water flow per unit area (unit stream power, in W m^{-2}). As can be observe in Eq.4, the site-specific values S (channel bed slope, in m m^{-1}) and B (channel width, in m) appear in the equation. Based on the results obtained by the topographic investigations, the mean slope and mean width were defined in either study cases. Specifically, in the Rio Cordon and Estero Morales was assessed a mean channel width equal to 5.7 m and 5.0 m, respectively (Tab. 5). As concerns the channel bed slope, the mean value in the Rio Cordon is 0.125 m m^{-1}, while in the Estero Morales 0.095 m m^{-1} (Tab. 5).

Table 5: Characteristics of the Rio Cordon and Estero Morales used to estimate ω

	Mean width (m)	Mean slope (m/m)
Rio Cordon	5.7	0.125
Estero Morales	5.0	0.095

3. CHAPTER THREE – RESULTS

3.1. Rio Cordon: Sediment fluxes since 1986 to the present

3.1.1. Recent bedload events (2009-2015)

3.1.1.1. Bedload event on 24th May 2009

The first bedload event analyzed is the flood that took place on 24th May 2009. The event took place during the snowmelt phase. As is possible to observe in the hydrograph (Fig. 35) during the snowmelt the water discharge show typical daily fluctuations due to the higher melt in the daytime hours. Other feature that characterize the snowmelt period is the discharge, continuously higher than 1 $m^3 s^{-1}$. In this context the bedload transport took place on May, 24 during an event with a peak of water discharge equal to 1.67 $m^3 s^{-1}$. From hydrological point of view, the May 2009 event is characterized by a low-moderate magnitude with a recurrence interval (RI) approximately of 1.3 years. Notwithstanding the magnitude, 3.1 t of coarse material was transported in the storage area (Tab. 6). Thanks to the monitoring station devices, the assessment of the bedload threshold was possible, or rather the hydrological condition in which occurred the start and the end of the transport. In this case, the transport started at a discharge equal to 1.5 $m^3 s^{-1}$ (24/05/2009 3.40pm) and ended after 13 hours (25/05/2009 4.55am) with the same discharge but during the recession limb of the hydrograph. Due to such conditions the Effective Runoff (Re) was calculated equal to 5.2 10^3 m^3 while the transport rate (BL_r) is very low, equal to 0.1 $m^3 h^{-1}$. Unfortunately the grain size distribution of the bedload material as well as the source area were not determined.

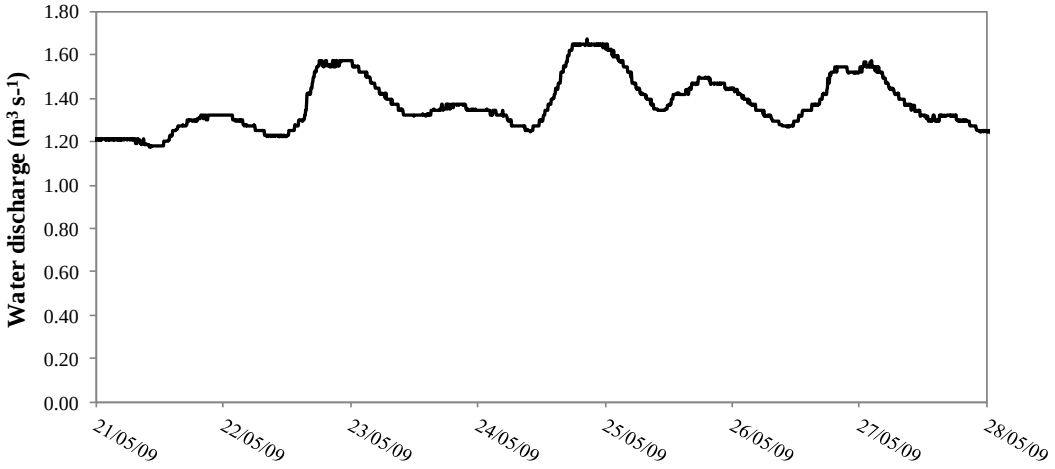

Figure 35: The hydrograph of the flood event occurred on 24th May 2009.

Table 6: Characteristics of the floods occurred on 24th May 2009. Q_{peak} is the peak of water discharge ($m^3 s^{-1}$); RI the recurrence interval (years); BL the bedload volume (m^3); Q_{START} is the discharge in correspondence of which was started the bedload; Q_{END} is the discharge in correspondence of which the bedload ended; T_{BL} is the bedload duration; Blr is the mean bedload intensity ($m^3 h^{-1}$); Re is the Effective Runoff volume ($10^3 m^3$).

Q_{peak} ($m^3 s^{-1}$)	RI years	BL (t)	Q_{START} ($m^3 s^{-1}$)	Q_{END} ($m^3 s^{-1}$)	T_{BL} (h:m)	BLr ($m^3 h^{-1}$)	Re ($10^3 m^3$)
1.67	1.3	3.1	1.5	1.5	13:00	0.1	5.2

3.1.1.2. Bedload event on 5th May 2010

In the 2010 a bedload event took place on 5th May 2010 (Fig. 36). Also in this case, the event occurred during the snowmelt season. In this case, in addition to the high discharge due to the melt of snow coverage it was added the contribution of intense rainfall that caused a peak equal to 1.82 m^3 s^{-1}, at the 10.15pm. In the hydrograph that regards the event of May 2011 the daily fluctuations of 2010 event are not observable. In this case, the flood occurred in the first days of May when the snowmelt was not yet in intensive phase, then the flood of May 2011 take origin from a mixed rainfall-snowmelt event. These conditions led to a bedload transport 11 hours long, from 5.40pm on May 5 to 5.00am on May 6. On the whole was transported downstream 1.4 t of coarse material with a transport intensity equal to 0.1 m^3 h^{-1} (Tab. 7). As a consequence of these conditions the Effective Runoff of the event is equal to 3.7 10^3 m^3. Also in this case the grain size distribution of the bedload material as well as the source area were not determined.

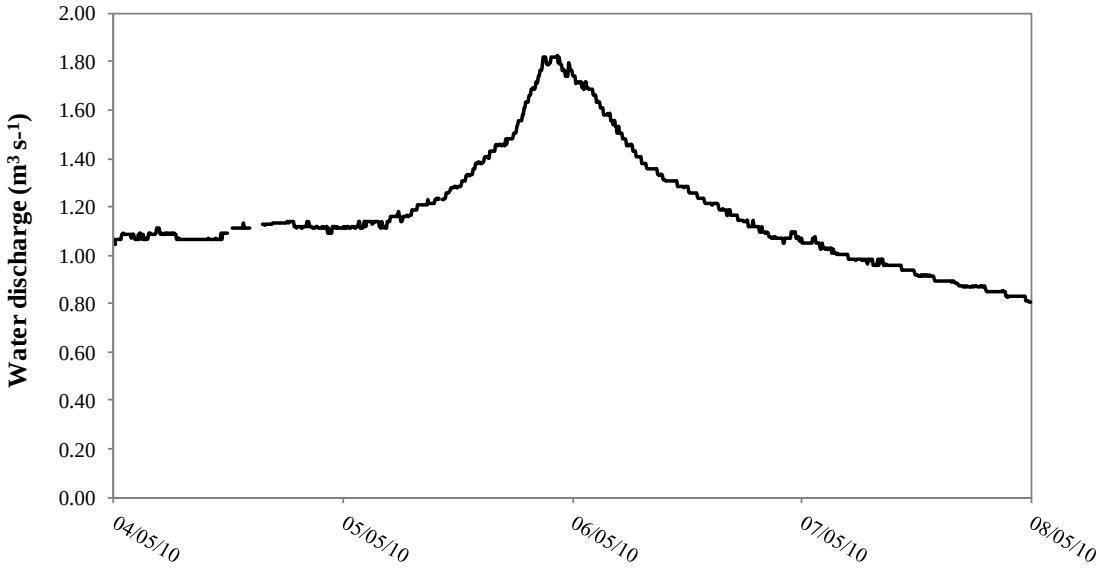

Figure 36: The hydrograph of the flood event occurred on 5th May 2010.

Table 7: Main **c**haracteristics of the floods occurred on 5th May 2010. Q_{peak} is the peak of water discharge (m^3 s^{-1}); RI the recurrence interval (years); BL the bedload volume (m^3); Q_{START} is the discharge in correspondence of which was started the bedload; Q_{END} is the discharge in correspondence of which the bedload ended; T_{BL} is the bedload duration; Blr is the mean bedload intensity (m^3 h^{-1}); Re is the Effective Runoff volume (10^3 m^3).

Q_{peak} (m^3 s^{-1})	RI (years)	BL (t)	Q_{START} (m^3 s^{-1})	Q_{END} (m^3 s^{-1})	T_{BL} (h:m)	BLr (m^3 h^{-1})	Re (10^3 m^3)
1.82	1.5	1.4	1.6	1.5	11:20	0.1	3.7

3.1.1.3. Bedload event on 8th June 2011

In 2011, bedload transport was registered on June, 8. The event was characterized by a peak of water discharge equal to 1.15 m^3 s^{-1} therefore an ordinary flood (Fig. 37). The discharge peaked at 9.30am, after 6 hours of persistent rainfall (23.2 mm cumulated). The hour of occurrence suggests a minor contribution derived by snowmelt respect to the direct runoff due to precipitation. The lack of a contribution provided by the snowmelt could also explain the ordinary discharge recorded during the flood.

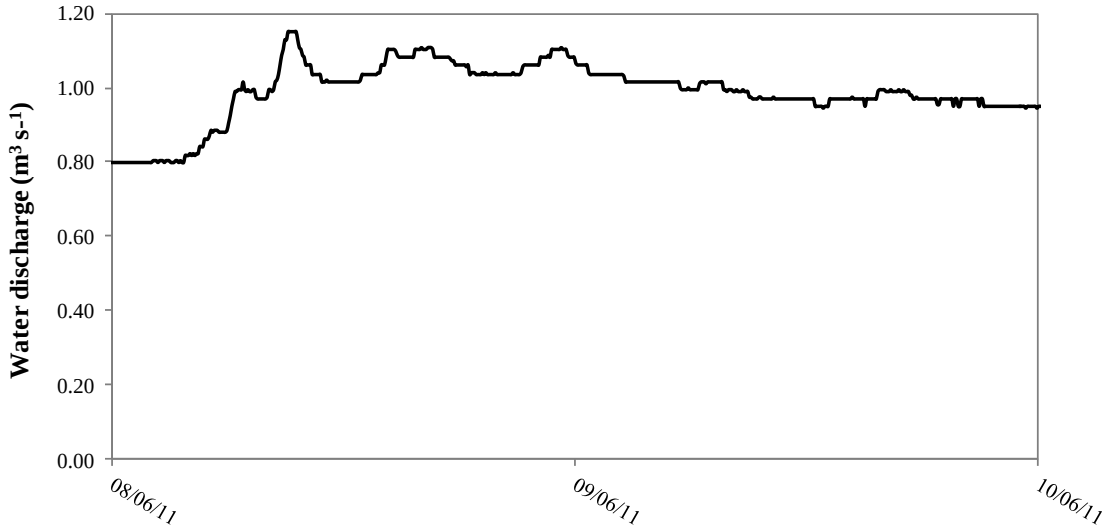

Figure 37: The hydrograph of the flood event occurred on 8th June 2011.

Notwithstanding the low hydraulic forcing, nearly one tons (0.9 t) of coarse material was transported to the monitoring station. The bedload lasted for more than 3 hours, with a bedload rate equal to 0.2 m^3 h^{-1}. Among the recent bedload events (2009-2015), the flood occurred on June 2011 exhibits the lower magnitude both in terms of hydrological and sedimentological features (Tab. 8).

Table 8: Main **c**haracteristics of the floods occurred on 8th June 2011. Q_{peak} is the peak of water discharge (m^3 s^{-1}); RI the recurrence interval (years); BL the bedload (t); Q_{START} is the discharge in correspondence of which was started the bedload; Q_{END} is the discharge in correspondence of which the bedload ended; T_{BL} is the bedload duration; Blr is the mean bedload intensity (m^3 h^{-1}); Re is the Effective Runoff volume (10^3 m^3).

Q_{peak} (m^3 s^{-1})	RI (years)	BL (t)	Q_{START} (m^3 s^{-1})	Q_{END} (m^3 s^{-1})	T_{BL} (h)	BLr (m^3 h^{-1})	Re (10^3 m^3)
1.15	1.1	0.9	1.0	1.1	3:20	0.2	0.8

3.1.1.4. Bedload event on 11th November 2012

In the 2012, significant flood took place in November due to intensive and persistent rainfall. Specifically occurred two subsequent floods on the 5th and 11th November. The event of November, 5 was characterized by a peak water discharge equal to 1.80 $m^3 s^{-1}$, while during the 11th November flood the peak reached 2.10 $m^3 s^{-1}$, then a value similar to the estimated bankfull discharge equal to 2.3 $m^3 s^{-1}$ (Lenzi et al., 2006a). From the hydrograph of the two subsequent floods (Fig. 38), it is possible to observe as the duration and shape of events are quite similar. Despite this similarity, the sediment transport dynamic is fundamentally different among the two floods. Bedload transport was not recorded by the station during the first flood. On the other hand, during the second peak a bedload transport was registered by the ultrasonic sensors. During the 11th November event, the ultrasonic sensors estimated a bedload volume of about 18.40 m^3, but there are some fluctuations in the data, probably caused by the wind that shifts these sensors placed above the bedload storage area. For this reason, for the subsequent analyses only the volume assessed by TLS survey was used. In this case the volume estimated is equal to 14.20 $m^{3,}$ equal to 24.4 t (Tab. 9, Fig. 40). Unfortunately, the 5 minutes ultrasonic sensors data are very scattered and not allow to calculate an exactly bedload transport rate. Taking into account the water discharge data and suspended sediment transport data, is reasonably assumed that bedload is started at a discharge equal to 1.5 $m^3 s^{-1}$ with a transport that lasted 6 hours (Rainato et al., 2013). Due to these conditions, the bedload intensity was estimated equal to 2.3 $m^3 h^{-1}$ then a moderate rate if compared with the other intensities recorded by the station in the last 30 years. On the other hand the Effective Runoff was calculated equal to 4.6 10^3 m^3, in line with the values estimated in the 2009 (5.2 10^3 m^3) and 2010 (3.7 10^3 m^3) events.

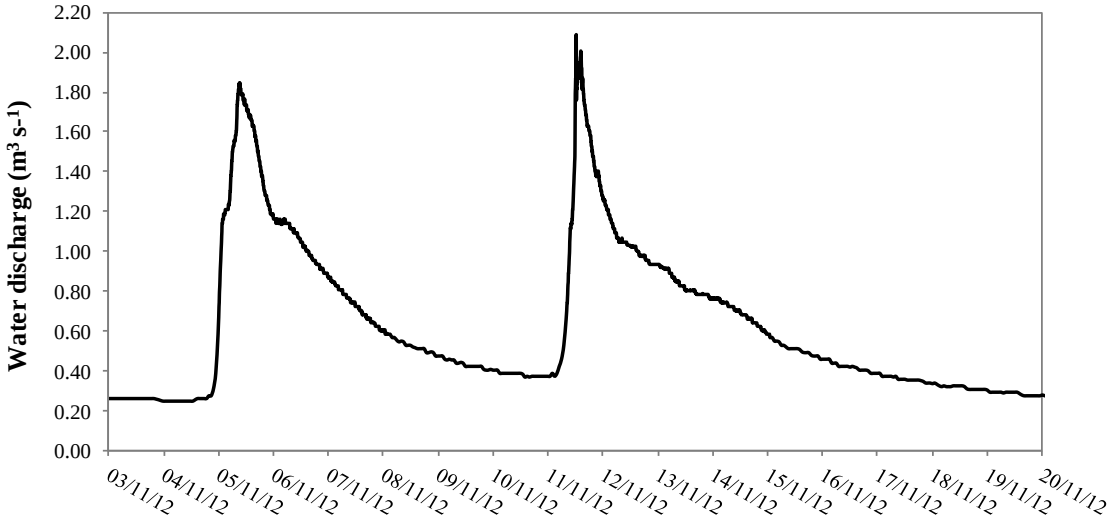

Figure 38: The hydrograph of the flood event occurred on 11th November 2012.

As regards the source area, the field evidences identified a debris flow channel located just upstream of the monitoring station as the main source (Fig. 39, Fig. 40). In the Rio Cordon catchment, this type of channel is a typical source area that provides sediment easily transportable downstream. In this sense, traces of mud along the banks of the debris flow channel were detected during a post-flood survey, confirming the occurrence of a small debris flow. At the same time no geomorphic changes on the main channel of the Rio Cordon were identified. The absence of sediment transport during the flood on 5th November combined with the bedload occurred on November, 11 suggests that the debris flow took place in the days between these two dates.

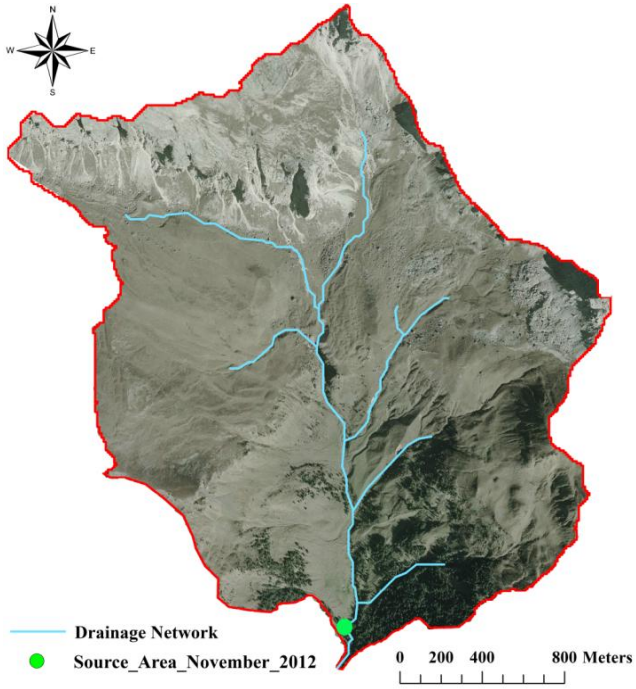

Figure 39: Source area for the bedload event of November 2012

Table 9: Main characteristics of the floods occurred on 11th November 2012. Q_{peak} is the peak of water discharge (m^3 s^{-1}); RI the recurrence interval (years); BL the bedload volume (m^3); Q_{START} is the discharge in correspondence of which was started the bedload; Q_{END} is the discharge in correspondence of which the bedload ended; T_{BL} is the bedload duration; Blr is the mean bedload intensity (m^3 h^{-1}); Re is the Effective Runoff volume (10^3 m^3); D_{16}, D_{50}, D_{84} and D_{90} are the percentiles of the grain size distribution concerning the bedload.

Q_{peak} (m^3 s^{-1})	RI years	BL (t)	Q_{START} (m^3 s^{-1})	Q_{END} (m^3 s^{-1})	T_{BL} (h:m)	BLr (m^3 h^{-1})	Re (10^3 m^3)	D_{16} (mm)	D_{50} (mm)	D_{84} (mm)	D_{90} (mm)
2.10	1.7	24.4	1.5	1.6	6:20	2.3	4.6	23	38	70	79

The grain size distribution (Fig. 41) of the bedload material deposited in the storage area was analyzed through a manual grid by number method, using an inter-distance of 0.60 m, or rather equal to two times the largest clast transported by the event (D_{max}= 0.30 m). Overall,

162 particles were collected and measured. The grain size distribution (GSD) shows as about 100% of the transported material is predominantly gravel, especially small cobble and coarse pebble. The 98.6% of the sediment are finer than 128 mm, while the entire range of particle size is between 11.2 mm and 181 mm. The percentiles were estimated: D_{16} equal to 23 mm, D_{50} is 38 mm, D_{84} is equal to 70 mm while D_{90} is 79 mm. It is worth to noticing that, considering the events investigated in the Rio Cordon (Tab. 1), this GSD shows values among the lowest ever recorded,

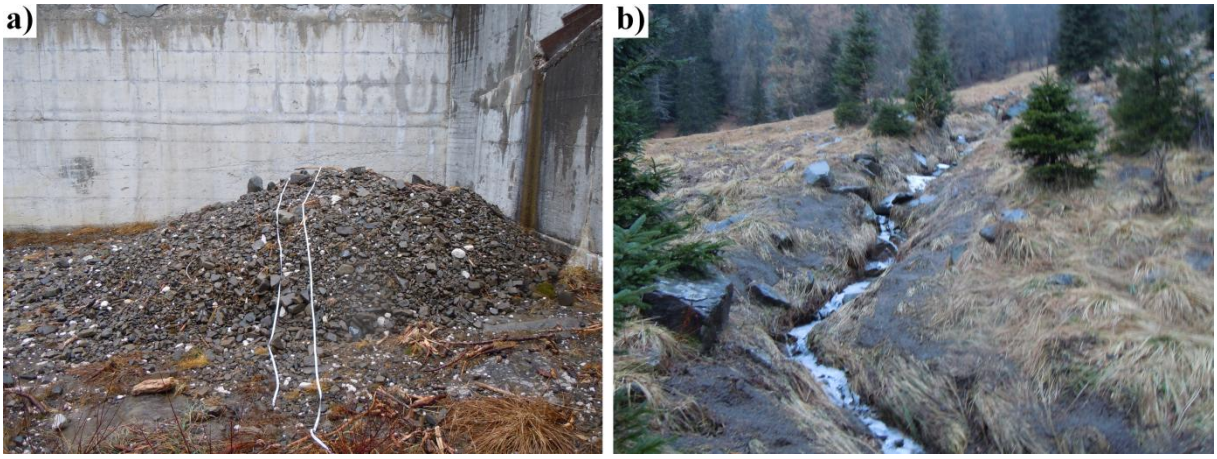

Figure 40: The bedload volume transported by the November 2012 event (a), field evidences along the debris flow channel (b).

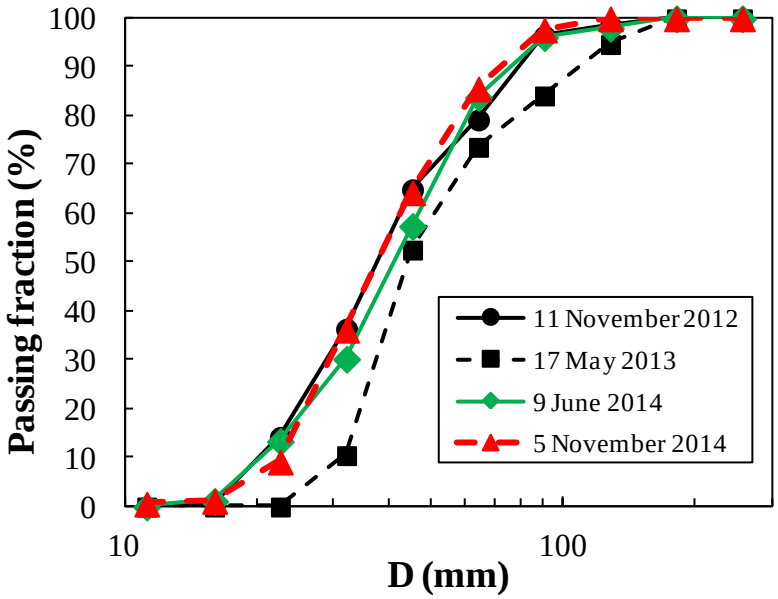

Figure 41: Comparison between the GSD of the material transported by the 4 most recent bedload events.

3.1.1.5. Bedload event on 17th May 2013

In the 2013 the monitoring station recorded bedload transport during May, 17. Also in this case the snowmelt period proved to be a dynamic period to trigger bedload events. The transport took place during a flood characterized by a peak of water discharge equal to 1.96 m3 s-1, reached at the 3.00pm on 17th May 2003 (Fig. 42). As observed during the 2010 event, at the snowmelt was added the contribute of intense rainfalls. In the storage area was deposited 3.8 t of coarse material, then a small amount. Such material was transported in 16 hours, approximately between the 8.00am on May,17 and the 0.30am on May, 18, then during a long time interval. Consequently, the transport rate recorded is very low, equal to 0.1 m^3 h^{-1}. On the other hand the Effective Runoff was estimate as one of the higher of the last years, with a value of 10.2 10^3 m^3 (Tab. 10).

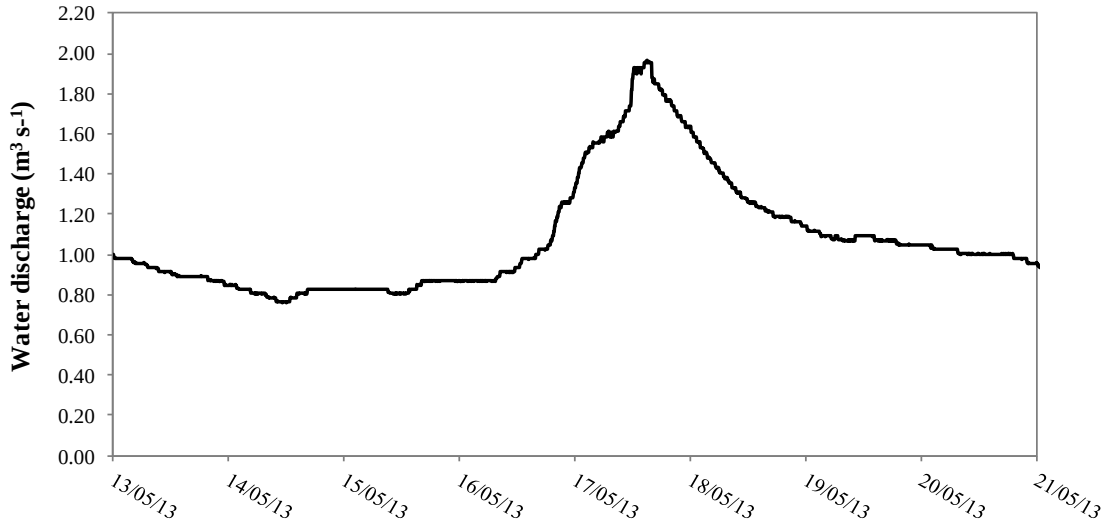

Figure 42: The hydrograph of the flood event occurred on 17th May 2013.

Thanks to the deposition of the bedload material in the storage area, the GSD characterization was performed. The results highlighted as the percentile D_{16} is equal to 33 mm, D_{50} is 44 mm, D_{84} is equal to 90 mm while D_{90} is 110 mm (Tab. 10).

Table 10: Main **c**haracteristics of the floods occurred on 17th May 2013. Q_{peak} is the peak of water discharge (m^3 s^{-1}); RI the recurrence interval (years); BL the bedload volume (m^3); Q_{START} is the discharge in correspondence of which was started the bedload; Q_{END} is the discharge in correspondence of which the bedload ended; T_{BL} is the bedload duration; Blr is the mean bedload intensity (m^3 h^{-1}); Re is the Effective Runoff volume (10^3 m^3); D_{16}, D_{50}, D_{84} and D_{90} are the percentiles of the grain size distribution concerning the bedload.

Q_{peak} (m^3 s^{-1})	RI years	BL (t)	Q_{START} (m^3 s^{-1})	Q_{END} (m^3 s^{-1})	T_{BL} (h:m)	BLr (m^3 h^{-1})	Re (10^3 m^3)	D_{16} (mm)	D_{50} (mm)	D_{84} (mm)	D_{90} (mm)
1.96	1.5	3.8	1.6	1.6	16:30	0.1	10.2	33	44	90	110

These values confirmed that a mix of coarse gravel and small cobbles was transported. Observing the comparison between the GSD of the 2012, 2013 and 2014 events (Fig. 41) it is possible to note that the material transported by the 2013 bedload is the coarsest. In this sense, all percentiles are greater respect to those measured for the other events. Significant is the percentile D90 equal to 110 mm as well as the largest clast transported characterized by a b-axis= 340 mm. Unfortunately, the source area was not determined, but the GDS seems to suggest that the material was provided by a small bank failure.

3.1.1.6. Bedload event on 9th June 2014

In the 2014 a significant bedload event occurred on June, 9. Also in this case the transport took place during a mixed snowmelt-rainfall event, that caused a flood peak equal to 2.06 $m^3 s^{-1}$. Interest to note as the precipitation were not so intensive, in fact the meteorological station recorded 16 mm of precipitation during the 9th June, but this rainfall was concentrated in the afternoon hours when the melt of the snow coverage is more intense. Observing the hydrograph (Fig. 43) it is possible to note the typical daily fluctuations in the discharge during the snowmelt period as well as values continuously above 1 $m^3 s^{-1}$. Due to the abundant snowfall that occurred in winter, the snowmelt period in 2014 has been extended until June. As regards the bedload event the transport lasted for 14 hours between the 2.10pm on June, 9 to 4.10am on June, 10, beginning with a discharge equal to 1.5 $m^3 s^{-1}$ and ending to 1.4 $m^3 s^{-1}$ (Tab. 11). In this sense, the Effective Runoff is 16.6 10^3 m^3. Very significant is the volume transported downstream, equal to 113.0 t (Fig. 46). From the bedload volume point of view, the flood of June 2014 is the sixth most important recorded event. Due to the volume transported also the bedload transport rate assumed a significant value, specifically equal to 4.7 $m^3 h^{-1}$. Regarding the intensity, only the events on October 1987, September 1994 and October 1998 exhibited higher values.

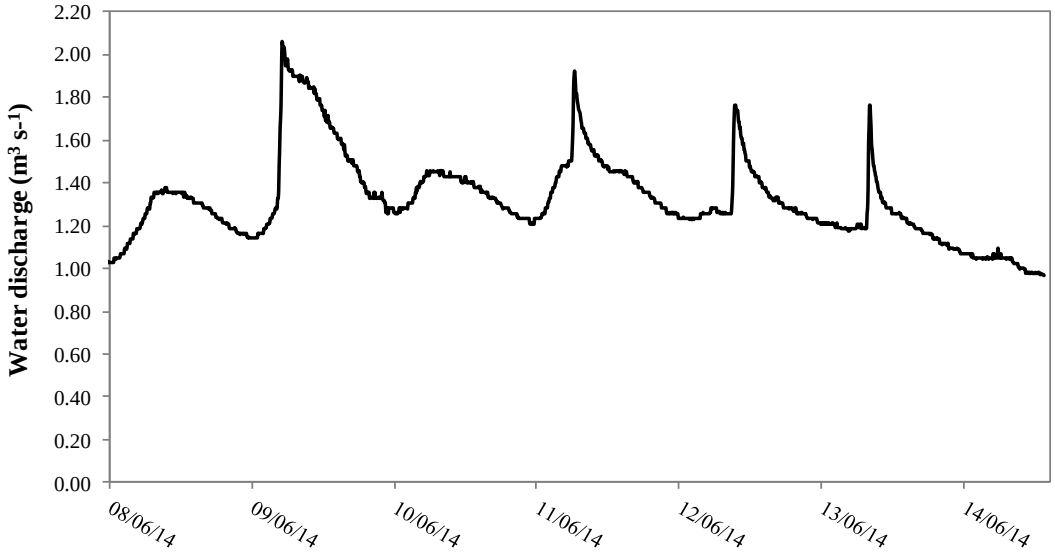

Figure 43: The hydrograph of the flood event occurred on 9th June 2014.

Thanks to the field surveys performed in the week subsequent to the bedload event, the identification of the source area was made possible. A debris flow channel located in the median part of the basin, on the right side, was identified as source area (Fig. 44). The field evidences, as traces of moved loam, showed the occurrence of a debris flow in this zone (Fig.

46). The material produced by this gravitational process reached the channel bed approximately 1300 m upstream the monitoring station. Also in this case, as in 2001 and 2012, a hillslope event provided the main channel of a large quantity of loose sediment then easily transportable downstream.

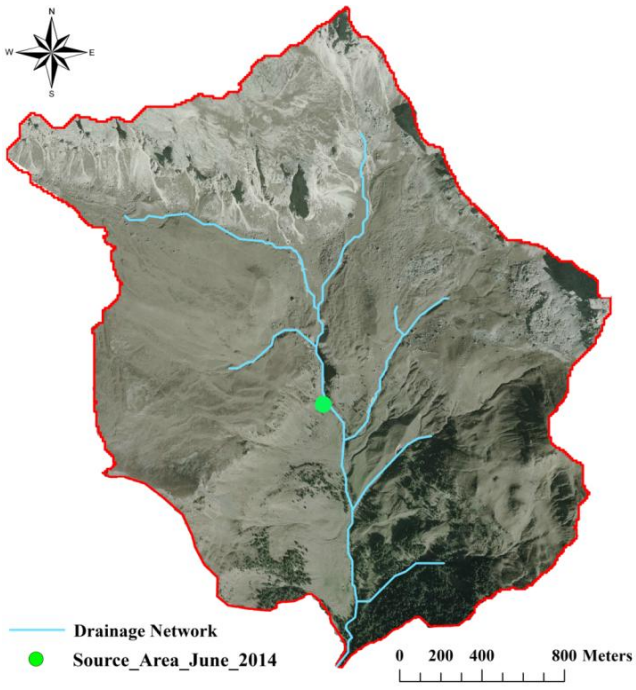

Figure 44: Source area for the bedload event of June 2014

The grain size distribution of the transported material was evaluated by the grid by number method. The largest particle detected in the storage was characterized by a *b-axis* equal to 230 mm. As suggests by the analysis, the material consisted mainly in a coarse gravel (pebble) with some small cobble. Thanks to the collection of 262 clasts, the GSD percentiles were estimated as: D_{16} equal to 16 mm, D_{50} is 41 mm, D_{84} is equal to 64 mm while D_{90} is 76 mm (Fig. 45). As observable in Figure 41, the material transported by the June 2014 event are comparable to those moved by the November 2012 flood. On the other hand, the percentiles are smaller respect to the GSD estimated for the May 2013 bedload. In this sense, it is interesting to note as both bedload events triggered by hillslope processes (November 2012, June 2014) exhibit similar percentiles,. Additionally, such GSD appear finer compared to the May 2013 bedload (bank failure?).

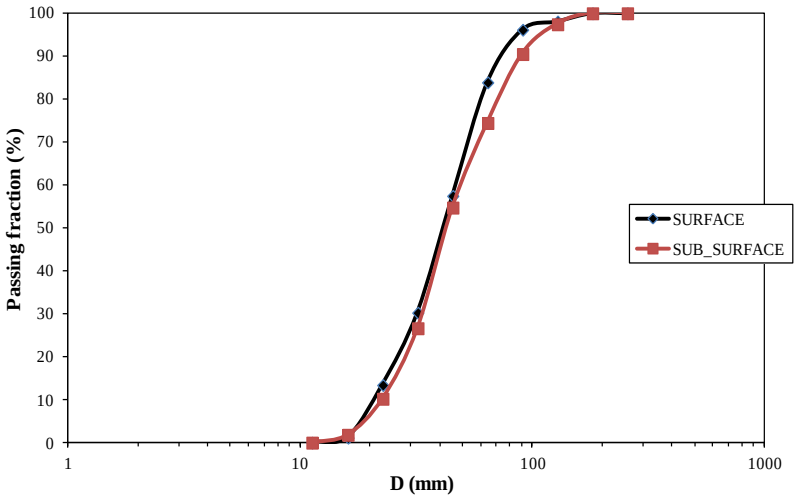

Figure 45: Bedload volume transported during the June 2014 event, comparison between the surface GSD and sub-surface GSD.

The volume transported by the June 2014 event was characterized also as regards the sub-surface GSD. In this case, the sampling was carried out moving the superficial clasts, for a depth equal to 2 D_{max}. The remaining surface represents the sub-surface on which the grid by number method was applied. On the whole, 275 particles were measured and the results of the GSD shows that D_{16s} is equal to 25 mm, D_{50s} is 43 mm, D_{84s} is equal to 79 mm while D_{90s} is 85 mm (Fig. 45). The sub-surface percentiles are larger than those estimated by the surface GSD, highlighting as the superficial clasts were transported by the recession limb of the event, while the larger diameters were moved during the antecedent phase of the hydrograph. Therefore, such analysis allowing to assess the transport dynamic as well as the competence that characterized the different phases of the bedload event.

Figure 46: The bedload volume transported by the June 2014 event (a), the source area of the bedload event (b).

Table 11: Main **c**haracteristics of the floods occurred on 9th June 2014. Q_{peak} is the peak of water discharge ($m^3 s^{-1}$); RI the recurrence interval (years); BL the bedload (t); Q_{START} is the discharge in correspondence of which was started the bedload; Q_{END} is the discharge in correspondence of which the bedload ended; T_{BL} is the bedload duration; Blr is the mean bedload intensity ($m^3 h^{-1}$); Re is the Effective Runoff volume ($10^3 m^3$); D_{16}, D_{50}, D_{84} and D_{90} are the percentiles of the grain size distribution concerning the bedload.

Q_{peak} ($m^3 s^{-1}$)	RI years	BL (t)	Q_{START} ($m^3 s^{-1}$)	Q_{END} ($m^3 s^{-1}$)	T_{BL} (h:m)	BLr ($m^3 h^{-1}$)	Re ($10^3 m^3$)	D_{16} (mm)	D_{50} (mm)	D_{84} (mm)	D_{90} (mm)
2.06	1.7	113.0	1.5	1.4	14:10	4.7	16.6	24	41	64	76

3.1.1.7. Bedload event on 5th November 2014

During 2014 a second bedload event took place, specifically on 5th November 2014. The flood was triggered by heavy and persistent rainfall, i.e. 126.2 mm on November,5 and 237.4 mm between November, 4 a November, 6. The event peaked on November, 5 at 11.55pm (Q_{peak}= 2.06 $m^3 s^{-1}$, Fig. 47) but overall the flood lasted for approximately 30 hours. In this sense, it is worth to noting that the same Q_{peak} characterizes both 2014 events but in November a Re two fold higher was reached (33.3 m^3 10^3).

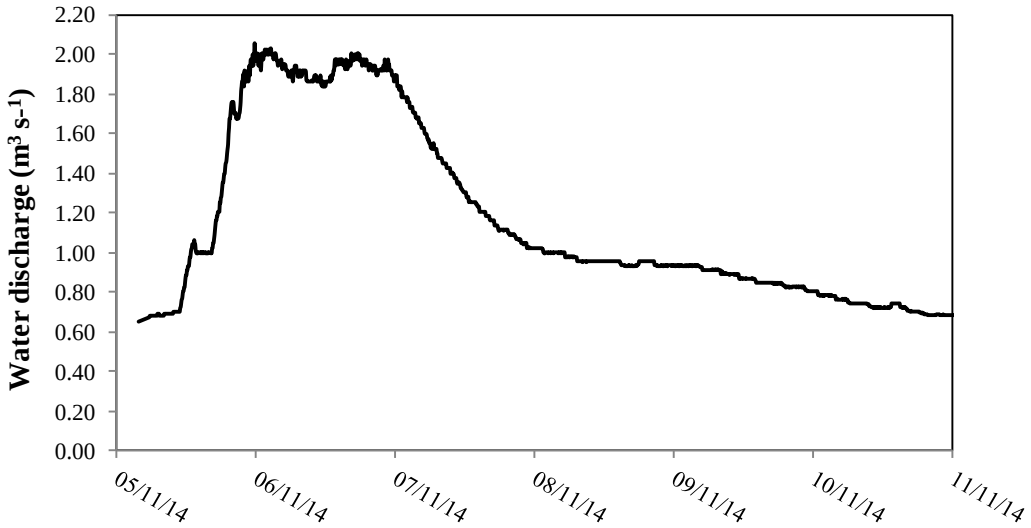

Figure 47: The hydrograph of the flood event occurred on 5th November 2014.

Notwithstanding the high hydraulic forcing occurred during the event (Fig. 48), the bedload has been scarce. Barely 4.6 t of coarse material was transported with a bedload rate of 0.1 $m^3 h^{-1}$ (Tab. 12). A survey was performed during the flood but none active source area was detected. This result would suggest that the most of the coarse sediment was provided by small bank erosions or by loose material located along banks and mobilized by the increased water stage. The bedload accumulated in the storage area was investigated in order to analyze

the GSD. Overall, 174 clasts were collected and measured. The percentiles obtained were: D_{16} equal to 25 mm, D_{50} is 38 mm, D_{84} of 62 mm while D_{90} is 73 mm (Tab. 12). This result is in line with the GSDs assessed for the floods occurred in November 2012 and June 2014, while is slightly dissimilar respect to the material mobilized by the May 2013 flood (Fig. 41).

Table 12: Main **c**haracteristics of the floods occurred on 5th November 2014. Q_{peak} is the peak of water discharge (m^3 s^{-1}); RI the recurrence interval (years); BL the bedload (t); Q_{START} is the discharge in correspondence of which was started the bedload; Q_{END} is the discharge in correspondence of which the bedload ended; T_{BL} is the bedload duration; Blr is the mean bedload intensity (m^3 h^{-1}); Re is the Effective Runoff volume (10^3 m^3); D_{16}, D_{50}, D_{84} and D_{90} are the percentiles of the grain size distribution concerning the bedload.

Q_{peak} (m^3 s^{-1})	RI years	BL (t)	Q_{START} (m^3 s^{-1})	Q_{END} (m^3 s^{-1})	T_{BL} (h:m)	BLr (m^3 h^{-1})	Re (10^3 m^3)	D_{16} (mm)	D_{50} (mm)	D_{84} (mm)	D_{90} (mm)
2.06	1.7	4.6	1.6	1.8	29:45	0.1	33.3	25	38	62	73

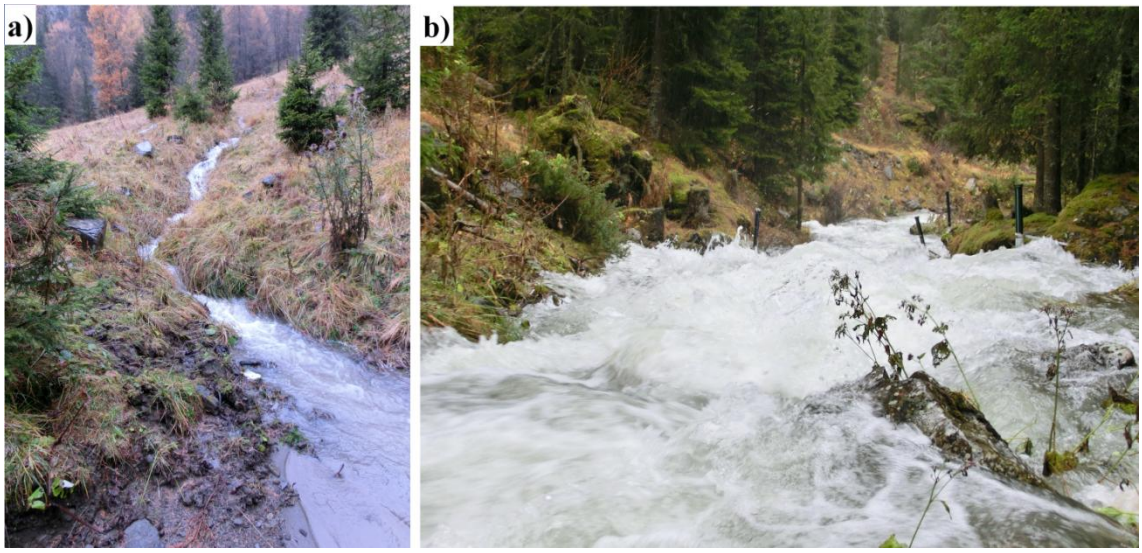

Figure 48: The 5th November 2014 flood event, an ephemeral tributary (a) and the Rio Cordon creek (b).

3.1.2. The long-term dynamic of flood events

The 31 floods recorded at the monitoring station (Tab. 1) since 1986 feature a wide range of hydraulic forcing (peak discharge, duration and effective runoff) and amount transported. While the Q_{peak} ranges within one order of magnitude, from 1.02 to 10.42 $m^3 s^{-1}$, the amount of bedload and suspended load varies by more than 3 orders (i.e. 0.9 t < BL < 1541.7 t). The variability observed in the amounts transported can be appreciated also in the grain size distribution mobilized (Tab. 1). The D_{16} ranges from 18 mm, observed during the October 2005 event, to 65 mm entrained by the September 1994 exceptional flood. Such event transported also the highest D_{50} (116 mm) that appears more than three-fold higher respect to the median percentile mobilized in October 2005 (30 mm). The high magnitude of September 1994 flood is confirmed also by the highest D_{84} and D_{90} recorded, equal to 226 mm and 281 mm, respectively. On the other hand, the lowest 84- and 90- percentiles were entrained by the May 1994 event (52 and 62 mm). Overall, the percentiles transported are positively correlated with the peak of water discharge (Fig. 49). In terms of R^2, the correlation progressively improves with increasing of percentile analyzed. In this sense, the R^2 ranges from 0.624 concerning the relationship Q_{peak}/D_{16} to 0.734 when Q_{peak} is paired to D_{90}.

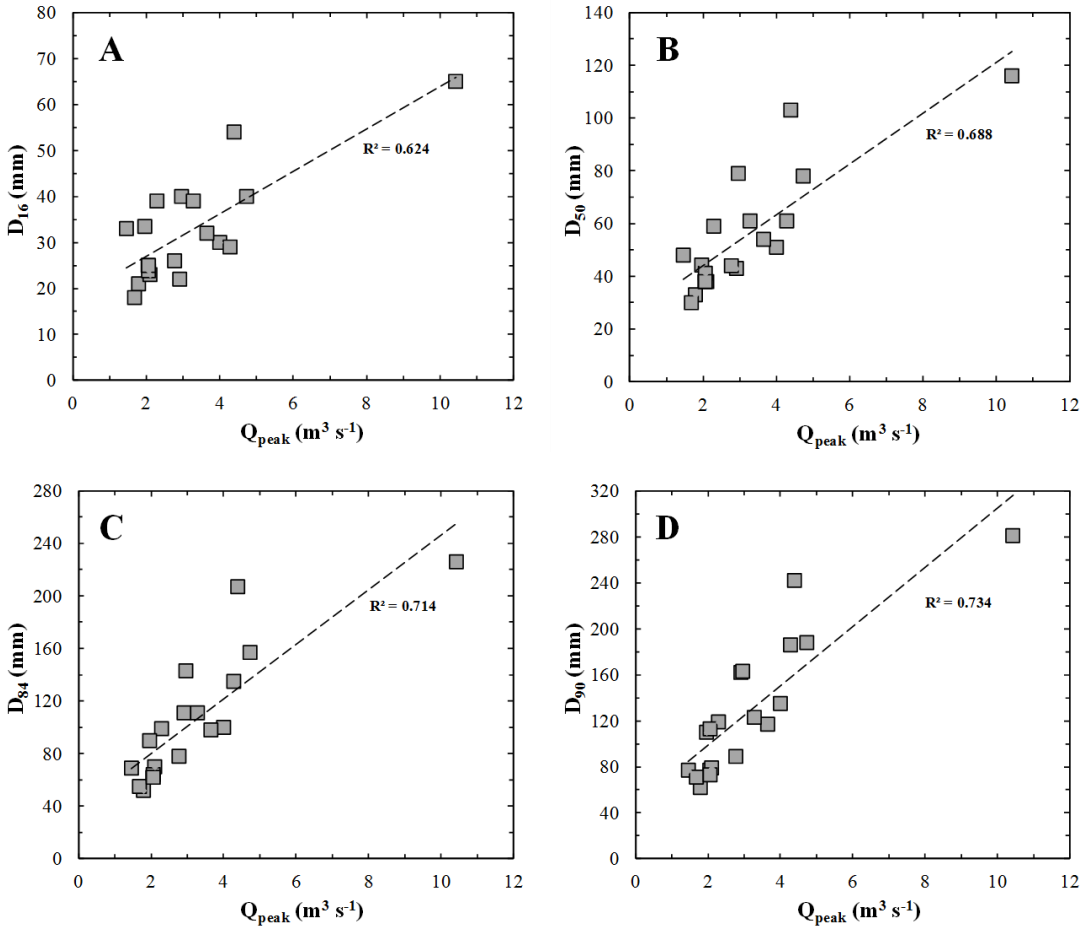

Figure 49: Relationships between Q_{peak} and D_{16} (A), D_{50} (B), D_{84} (C) and D_{90} (D).

The flood on September, 14 1994 was the most severe event recorded in terms of both Q_{peak} (10.42 m^3 s^{-1}) and amount of transported material (BL= 1541.7 t, SSL= 2435.1 t). This event was the only flood able to mobilize more than 1000 t of bedload. With regard to suspended load, the only flood that transported a similar amount of fine material was the May 2001 event (1017.6 t). The event in October 1987 had the second largest recorded Q_{peak} (5.15 m^3 s^{-1}) but although the discharge was half that measured in September 1994, the bedload (BL= 85.6 t) and suspended load (SSL= 131.7 t) were two and one order of magnitude lower, respectively. Instead, the October 1998 flood, which peaked at 4.73 m^3 s^{-1}, transported much higher volumes of coarse and fine material (BL= 516.8 t and SSL= 393.5 t, respectively). The amounts transported by the 31 floods are investigated as a function of the peak of water discharge, using a power-law regression. Bedload (R^2= 0.739) and suspended load (R^2= 0.565) appear positively correlated with Q_{peak} (Fig. 50), also showing that floods of a certain magnitude transported more sediments after the exceptional 1994 flood. Specifically, the coefficient (*a*) of the power-law regressions clearly varies between the events that occurred before and after the September 1994 flood (Tab. 13).

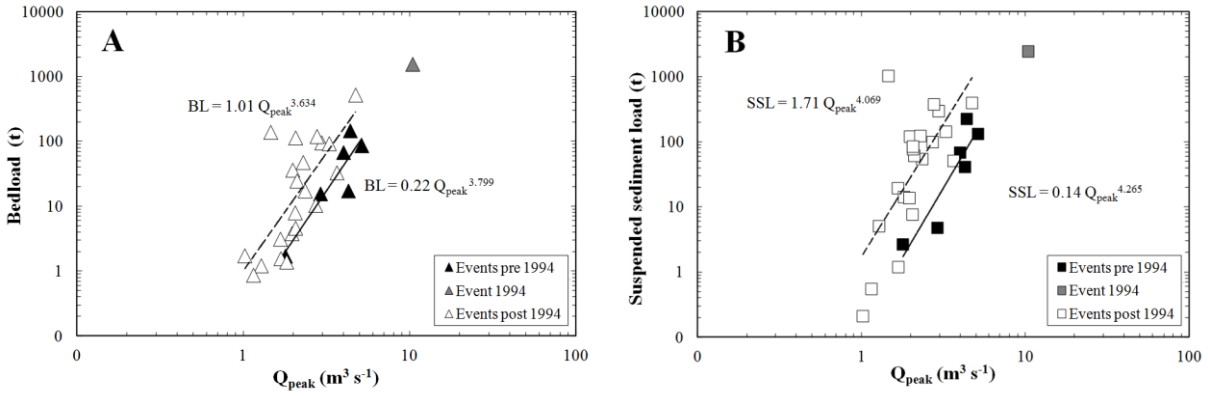

Figure 50: Bedload (A) and suspended sediment load (B) transported by the flood events as a function of their peak discharge. The power-law regressions were applied distinguishing between pre-1994 events (solid lines) and post-1994 events (dashed lines).

Regarding the BL, pre-1994 events exhibit a coefficient *a* equal to 0.22, which exceeds unity (1.01) in the post-1994 period (Fig. 50A). The increase of coefficient *a* is even clearer for the suspended load (Fig. 50B). In this case, *a* increases by more than one order of magnitude, from 0.14 to 1.71 (Tab. 13). A similar behavior appears when the Q_{peak} is plotted versus median diameter (D_{50}) of coarse material transported and deposited in the storage area (Fig. 51A).

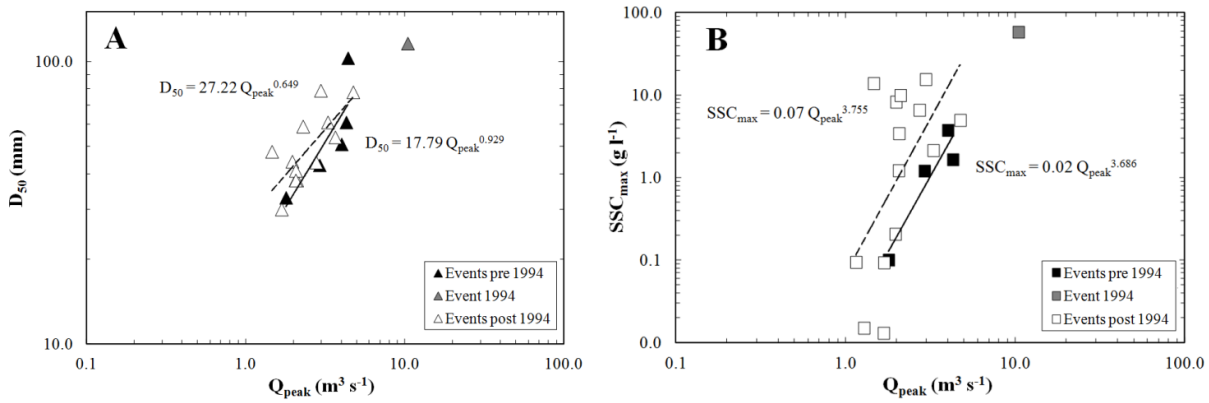

Figure 51: Median diameter (D_{50}) of transported bedload (A) and maximum SSC (B) related to the peak of water discharge. The power-law regressions were applied distinguishing between pre-1994 events (solid lines) and post-1994 events (dashed lines).

As expected, the D_{50} increases with increasing Q_{peak} (R^2= 0.688) and the September 1994 event transported the coarsest mixture (D_{50}= 116 mm). Also, floods that occurred after 1994 transported larger D_{50} if compared with similar pre-1994 events. According to the previous analysis, the median diameters transported by pre- and post-1994 events were investigated. Also in this case a clear change in the coefficient *a* can be appreciated, with an increase from 17.79 (pre-1994) to 27.22 (post-1994). A good power-law regression (R^2=0.694) can also be observed for the maximum suspended sediment load concentration (SSC_{max}, g l^{-1}), which reached the highest value (57.9 g l^{-1},) during the 1994 flood, and after this event was significantly higher than before (Fig. 51B). Coherently with the previous results the post-1994 events show a higher coefficient *a* (0.07) than that evaluated for the pre-1994 events (0.02). Contrary to what is observed regarding the coefficient *a*, it is worth noting that in all equations plotted the exponent *b* does not exhibit significant variations among pre- and post-1994 events (Tab. 13).

Table 13: Fit values for the power-law regressions tested.

	a	***b***	***r²***	***n***
BL pre-1994	0.22	3.799	0.813	6
BL post-1994	1.01	3.634	0.522	21
SSL pre-1994	0.14	4.265	0.830	6
SSL post-1994	1.71	4.069	0.477	21
D_{50} pre-1994	17.79	0.929	0.681	5
D_{50} post-1994	27.22	0.649	0.539	13
SSC pre-1994	0.02	3.686	0.882	4
SSC post-1994	0.07	3.755	0.323	14

3.1.3. Annual sediment yield and partitioning of total sediment load

The annual sediment yields for the period 1986-2014 are reported in Fig. 52. Overall, 14936.9 t were mobilized (Tab. 14). The highest contribution to total sediment load occurred in 1994 (4067.2 t), when 98% of the annual amount was mobilized during the September, 14 event. In addition to 1994, there were relevant contributions to the sediment yield in 1998 (1261.5 t) and 2001 (1742.6 t). Since 2003, the annual sediment yield has been less than 500 t y^{-1}, except in 2009 when it was about 517.9 t (Tab. 14). Taking into account the 29 years of data the mean annual specific yield was evaluated as 103.0 t km^{-2} y^{-1}. The value ranges from 813.4 t km^{-2} y^{-1} assessed in 1994 to years like 2003 when only 2.4 t km^{-2} y^{-1} were recorded.

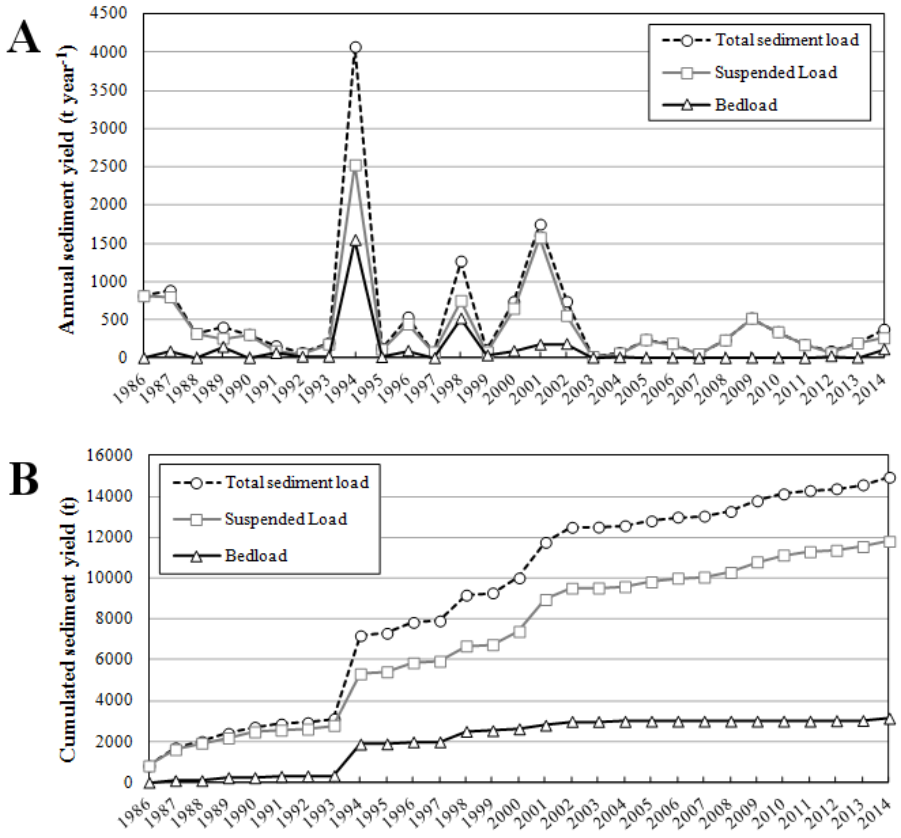

Figure 52: Annual (A) and cumulated (B) sediment yield measured in the Rio Cordon basin from 1986 to 2014.

The highest annual yields of suspended load fraction were recorded in 1994 (2523.8 t), 2001 (1568.6 t), 1986 (806.9 t), 1987 (792.1 t) and 1998 (744.7 t). The relatively high suspended sediment transport in 2001 was due to the mud flow during the snowmelt period, which originated 1017.6 t of fine sediment. From 2001 to the present, the suspended sediment load shows annual yields permanently one order of magnitude lower. Less than 100 t of fine material were transported during 1991, 1992, 1997, 1999, 2003, 2004, 2007 and 2012 (Tab.

14). Interestingly, 50% of the total suspended load transported in 29 years (11794.6 t) was mobilized during flood events (5858.7 t).

The bedload fraction exhibits annual sediment yields constantly lower than the suspended load, with the main contributions observed in 1994 (1543.4 t), 1998 (516.8 t), 2002 (183.4 t), 2001 (174.0 t), 1989 (145.6 t) and 2014 (117.6 t). In addition to the already mentioned September 1994 event 1998 also gives an important annual contribution to the bedload yield, mainly due to a flood caused by autumn rainfall. More recently, bedload yield has reduced considerably, and especially between 2003 and 2011 the annual bedload yield has been constantly lower than 10 t y^{-1} (Tab. 14).

Table 14: Suspended sediment load (SSL, t), bedload (BL, t), total load (TL, t) and bedload fraction (BL_f) recorded year to year in the Rio Cordon instrumented basin .

	SSL (t)	**BL (t)**	**TL (t)**	**BL_f**
1986	806.9	0.0	806.9	0.00
1987	792.1	85.6	877.7	0.10
1988	312.7	0.0	312.7	0.00
1989	251.7	145.6	397.3	0.37
1990	302.1	0.0	302.1	0.00
1991	86.9	67.2	154.1	0.44
1992	50.6	15.5	66.1	0.23
1993	175.5	17.2	192.7	0.09
1994	2523.8	1543.4	4067.2	0.38
1995	110.8	10.3	121.1	0.09
1996	436.2	94.7	530.9	0.18
1997	73.9	0.0	73.9	0.00
1998	744.7	516.8	1261.5	0.41
1999	73.5	32.7	106.2	0.31
2000	641.6	92.2	733.8	0.13
2001	1568.6	174.0	1742.6	0.10
2002	551.0	183.4	734.4	0.25
2003	10.3	1.7	12.1	0.14
2004	58.6	7.9	66.6	0.12
2005	232.8	1.6	234.4	0.01
2006	184.2	1.2	185.4	0.01
2007	49.7	0.0	49.7	0.00
2008	229.0	0.0	229.0	0.00
2009	514.8	3.1	517.9	0.01
2010	336.1	1.4	337.4	0.00
2011	167.0	0.9	167.8	0.01
2012	62.3	24.5	86.7	0.28
2013	189.3	3.8	193.1	0.02
2014	257.8	117.6	375.4	0.31
TOTAL	**11794.6**	**3142.2**	**14936.9**	**0.21**

The partitioning of bedload and suspended sediment yield demonstrates that 79% of the sediment transported over the 29 years was transported as suspended load. Using published data concerning Eastern Alpine rivers, Schlunegger and Hinderer (2003) proposed a formula to predict the long-term fractions as a function of the basin area (A, km^2):

$$SSL_f = 0.475 + 0.0506\ ln\ (A) \quad \text{Eq.5}$$

more recently, Turowski et al. (2010), collecting the existing data and using the above-mentioned approach, suggested the equation:

$$SSL_f = 0.550 + 0.040\ ln\ (A) \quad \text{Eq.6}$$

If applied to the Rio Cordon, the formulas predict a SSL fraction (SSL_f) of 0.56 and 0.61, respectively. Such values are clearly lower than the 0.79 obtained using the field data. Significant annual variations are evident in the long-term partitioning. The annual bedload fraction ranges from 0.44 in 1991 to 0.00 for the years with no bedload transporting events (1986, 1988, 1990, 1997, 2007 and 2008). The variability is also appreciable analyzing the partitioning at a shorter term (event-scale). In this case, while the October 1992 event shows a bedload fraction of 0.77, a completely different partitioning was recorded during the November 2014 flood when bedload fraction reached 0.05. It is worth noting that the average partitioning varies notably between the periods 1986-1993 and 1994-2014, with the bedload fraction increasing from 0.11 to 0.24. Such temporal variation can also be observed in the mean annual sediment production. Particularly, the mean annual specific yield before 1994 is 77.7 t km^{-2} y^{-1} which then increases to 112.6 t km^{-2} y^{-1}.

3.1.4. Seasonal suspended load yield

If the seasonal yield of the suspended load fraction is taken into consideration, the snowmelt contribution clearly prevails (fraction > 90%) in 1988, 1990, 2001, 2008, 2009 and 2013, while the autumnal transport is particularly important in 1994, 1996, 1998, 2000 and 2002 (Fig. 53). The summer contribution appears infrequently and is concentrated mainly in the first years of the monitoring period. In 1994 and 2001, the seasonal yield clearly depends on the period in which the high magnitude floods took place. Over the long term, a mixed prevalence of snowmelt and summer contributions can be appreciated in the pre-1994 period, when only 6.4% of suspended load was originated in autumn. From 1994 and for the next

decade, autumn floods were the main factor of sediment yield. An exception to this trend is 2001, when due to the above-mentioned mud flow in May, the snowmelt contribution prevails. In recent years a new prevalence of snowmelt yield has been observed. More specifically, since 2005 the snowmelt contribution again predominates with an average annual percentage of 71.6% (2005-2014). Overall, in the 29 years the autumn contribution accounts for 43.5% while the snowmelt and summer contributions are 37.3% and 19.3%, respectively.

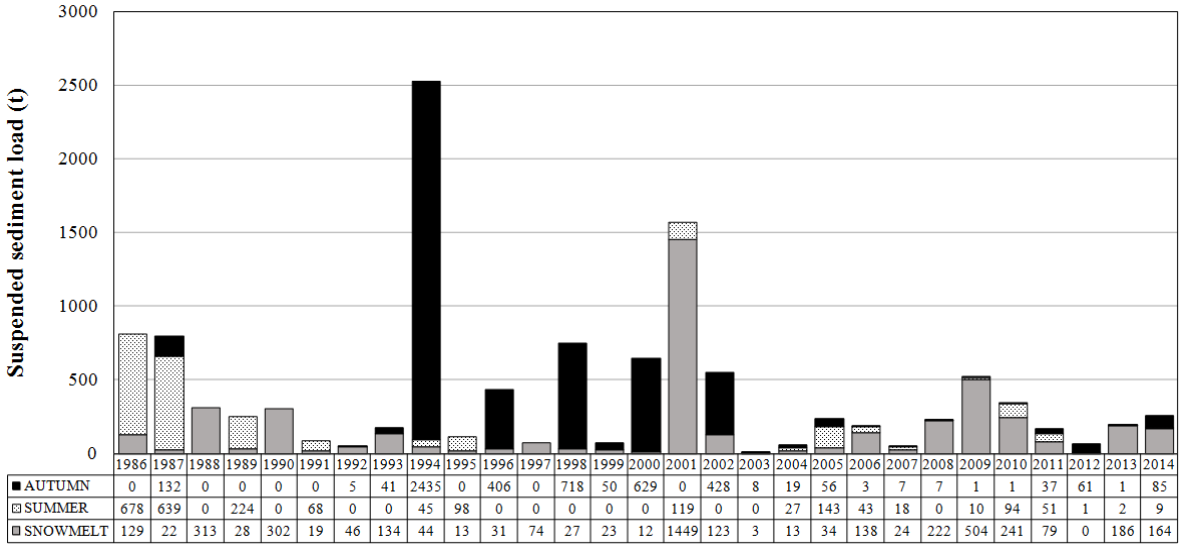

	1986	1987	1988	1989	1990	1991	1992	1993	1994	1995	1996	1997	1998	1999	2000	2001	2002	2003	2004	2005	2006	2007	2008	2009	2010	2011	2012	2013	2014
AUTUMN	0	132	0	0	0	0	5	41	2435	0	406	0	718	50	629	0	428	8	19	56	3	7	7	1	1	37	61	1	85
SUMMER	678	639	0	224	0	68	0	0	45	98	0	0	0	0	0	119	0	0	27	143	43	18	0	10	94	51	1	2	9
SNOWMELT	129	22	313	28	302	19	46	134	44	13	31	74	27	23	12	1449	123	3	13	34	138	24	222	504	241	79	0	186	164

Figure 53: Seasonal suspended sediment yield measured in the period 1986-2014 in the Rio Cordon basin

3.1.5. Temporal trend

The temporal trends of bedload and suspended load yields can be generated using the available data (Fig. 54). In order to compare events of different magnitude and duration, the floods are analyzed in terms of ratio between transport load (both BL and SSL) and the effective runoff of each flood. Although the suspended load exhibits a more scattered trend with respect to bedload, Figure 54 depicts different phases of sediment availability and transport efficiency. Before the exceptional 1994 flood, the BL/Re and SSL/Re ratios exhibit low values (< 2.5) and tend to decrease over time. During this period, the lowest degree of transport efficiency was achieved by the May 1994 event when a BL/Re of 0.3 and SSL/Re of 0.5 were measured. This initial trend was interrupted by the occurrence of the September 1994 flood. Due to its high magnitude, during this event the BL/Re ratio reached the highest value so far recorded (58.0). The SSL/Re ratio is also very significant, achieving an extremely high value (91.5). During the event the ratios increased by two orders of magnitude if compared with the values registered before. In the following years, a new decreasing tendency

is observed, but this trend originates from flood events characterized by ratios clearly higher with respect to the pre-1994 period. Such higher transport efficiency lasted for approximately 10 years. In fact, the ratios have only returned to values comparable to those observed before 1994 since 2005 (May 2005; BL/Re = 0.5, SSL/Re = 0.4). After the exceptional 1994 flood, the May 2001 event represents an outlier, especially regarding the suspended load events. During this flood the SSL/Re ratio (119.7) exceeded the one measured in the September 1994 event, demonstrating the high transport efficiency of fine material that occurred as a consequence of mud flow. Contrary to what was observed subsequently to the September 1994 event, the May 2001 event has not led to a change in the general trend. In the most recent years the high transport efficiency exhibited by the November 2012 (BL/Re = 5.4) and June 2014 (BL/Re = 6.8) bedload events are worth highlighting, which also represent a significant interruption to the recent decreasing trend.

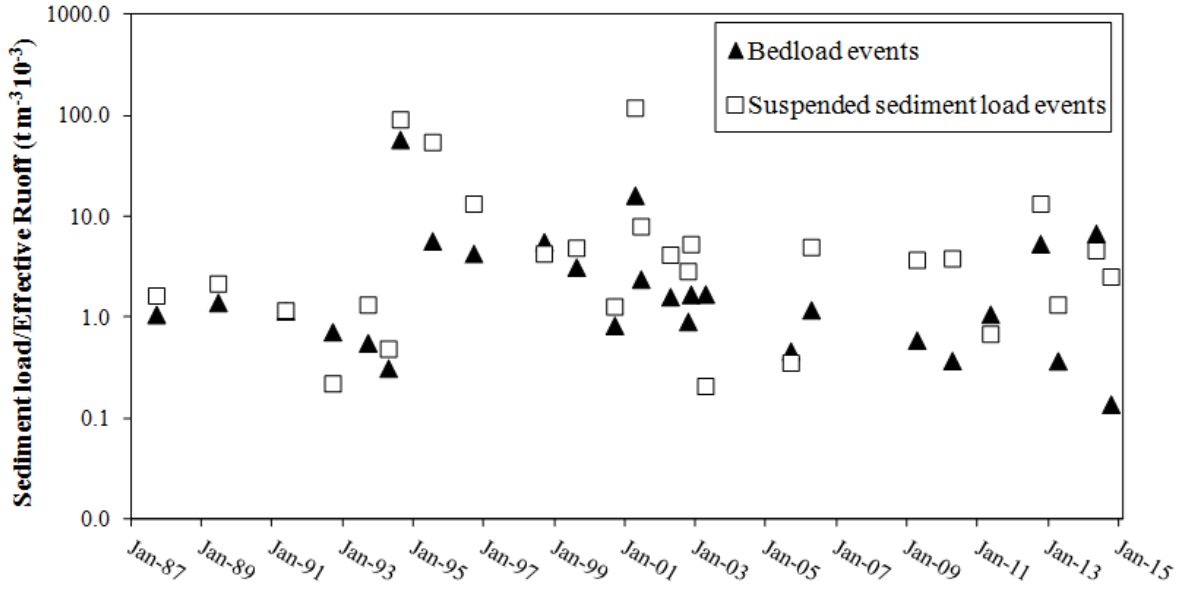

Figure 54: Temporal trend about the bedload/effective runoff and suspended sediment load/effective runoff ratios

3.2. Rio Cordon: Tracing bedload transport using PIT tracers

3.2.1. Measurement campaign and recovery rates

Since the PITs installation, 11 surveys were performed in order to monitoring the tracer dynamics (Fig. 55). In Table 15 are reported the main characteristics of the surveys and periods monitored. From 2010 to 2012, the displacements were investigated annually while during my PhD period the surveys were performed more frequently (i.e. on average 112 days between survey to survey). Previously the PhD period, the tracer inventories were executed exclusively to analyze the travel distance caused by significant flood events (i.e $Q_{peak} > 2.0$ m^3 s^{-1}). Since 2013 (beginning of PhD), the surveys were performed also to investigate the displacement due to low and moderate events (i.e $Q_{peak} < 2.0$).

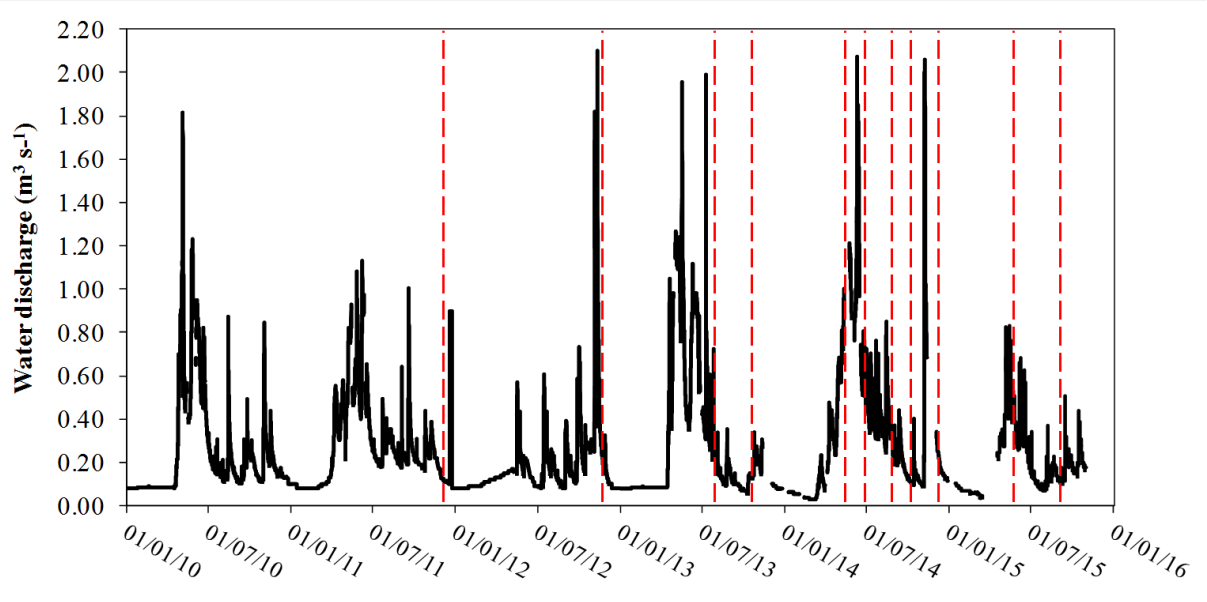

Figure 55: Discharge time series during the study period, the red dashed lines correspond to the PIT surveys performed

As observable in Table 15, for each period monitored, both the peak of water discharge (Q_{peak}) and peak of unit stream power ω_{peak} were estimated. The use of a dimensionless value (ω_{peak}) to describe the hydraulic forcing conditions allows to compare between them the results obtained in different study areas. In this case the data obtained in the Rio Cordon creek were compared with those acquired in the Estero Morales stream. Due to the tricky conditions in which the PIT monitoring have been executed (high-gradient channels), the positioning of the tracers is assumed as affects by a certain degree of uncertainty. To obviate to this potential error, in this work only the differences of position (i.e. displacement) > 1 m were accounted.

Table 15: Date of the PIT survey, Q_{peak} and ω_{peak} occurred during the period monitored, mean travel distance of the tracers (Li), number of PIT detected (n), recovery rate (Rr) and extent in days of the period monitored.

Survey	Q_{peak} ($m^3 s^{-1}$)	ω_{peak} ($W m^{-2}$)	Li (m)	n (*n*)	Rr (%)	T (days)
03/12/2011	1.82	390.90	7.03	91	36	581
22/11/2012	2.10	451.78	82.60	194	78	355
25/07/2013	1.96	421.66	13.10	194	78	245
14/10/2013	0.72	155.76	2.74	162	65	81
15/05/2014	1.00	215.35	3.18	215	86	213
01/07/2014	2.06	443.17	114.02	192	77	47
25/08/2014	0.85	182.22	2.78	176	75	55
29/10/2014	0.44	94.44	1.23	172	73	65
24/11/2014	2.06	443.17	90.94	166	70	26
18/05/2015	0.83	178.13	1.13	154	65	175
26/08/2015	0.68	146.93	1.08	160	68	100

During the study period, the peaks of unit stream power vary from 94.44 W m^{-2} to 451.82 W m^{-2}, while the related mean transport distances (Li) range from 1.08 m to 115.24 m, varying by two order of magnitude (Tab. 15). Different recovery rates (i.e. PITs detected on the total population of tracers) were achieved during the 11 surveys, in fact the percentages range from 36% in the first inventory in December 2011 to 86% reached during the May 2014 survey. Generally, the recovery rate is increased in the time with temporary reductions observable in the surveys of November 2012, July 2014, November 2014, due to the occurrence of significant floods. Slightly less than 70% of tracers population was detected during the recent inventories performed in 2015 that reached recovery rates equal to 65% and 68%, respectively.

3.2.2. Influence of grain size on the displacement

In order to investigate the influence of grain size characteristics on the sediment entrainment, the tracers mobilized were grouped on the basis of the relative peak of water discharge. Once grouped, the tracers were reclassified according to their *b-axis*, using the ϕ size classes equal to 45.3 mm, 64 mm, 90.5 mm, 128 mm and 181 mm, and finally the mean travel distance was estimated for each ϕ size class. The Fig. 56 shows the results of the Di/Li relationship, for the three magnitude of events occurred, i.e. low when $Q_{peak} < 1.0$ $m^3 s^{-1}$, moderate if $1.0 < Q_{peak} < 2.0$ $m^3 s^{-1}$ and high magnitude in case of $Q_{peak} > 2.0$ $m^3 s^{-1}$. Overall, the number of tracers entrained increases with increasing the magnitude of flood events. In

this sense, 52 PITs were mobilized by the low magnitude floods, while 142 and 248 were entrained by the moderate and high magnitude events, respectively. An increasing trend can be observed also in the relationship between the classes of Q_{peak} and Li. Specifically, the mean transport distance gradually increases by one order of magnitude among low-moderate-high flood events. Notably, the low and moderate magnitude events exhibit mean transport distance equal to 2.60 m to 10.10 m, respectively, while in the high magnitude flood Li abruptly increase to 105.5 m.

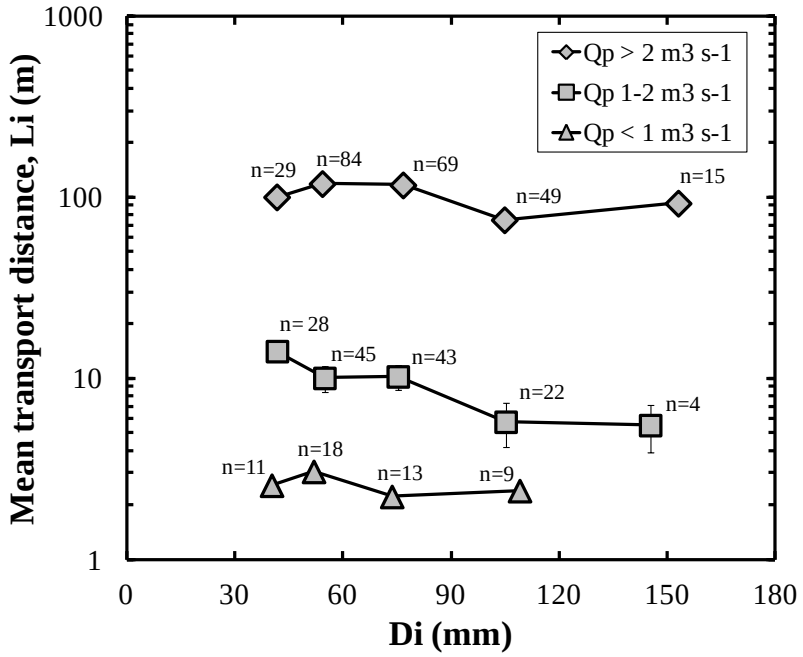

Figure 56: Relationship between mean transport distances, with standard errors and five particle size classes. Analysis performed on the three peak discharge classes observed in the Rio Cordon.

In terms of grain size influence, the results seem to suggest that the displacement was affected by the particle size, especially during the low and moderate floods. In these events Li decreases with increasing of *b-axis*, highlighting a size-selective transport. On the other hand, the displacements showed by the high magnitude floods appear barely affected by the particle size with Li that remains relatively steady with increasing of *b-axis*. These results suggest the occurrence of equal-mobility conditions during the highest floods, that are also the only events able to mobilize a significant number (i.e. 15) of larger tracers (ϕ size class=181 mm).
The influence of the grain size on the sediment entrainment was investigated also analyzing the relationship between Q_{peak} and GSD of the tracers mobilized (D_p). For this purpose, were taken into account only the surveys in which more than 20 displacements were detected, considering 20 *b-axis* as threshold to obtain a proper grain size distribution. In such analysis,

the inventories carried out in 2011 and 2012 were not accounted because characterized by a different tracers population, i.e. performed previously to the installation of 50 PITs in November 2012. The results highlighted that Q_{peak} and the *b-axis* of percentiles mobilized show a positive correlation (Fig. 57). The peak of discharge appears better related with D_{16p} (Fig. 57A), D_{50p} (Fig. 57B) and D_{90p} (Fig. 57D), while the correlation is weak with D_{84p} (Fig. 57C).

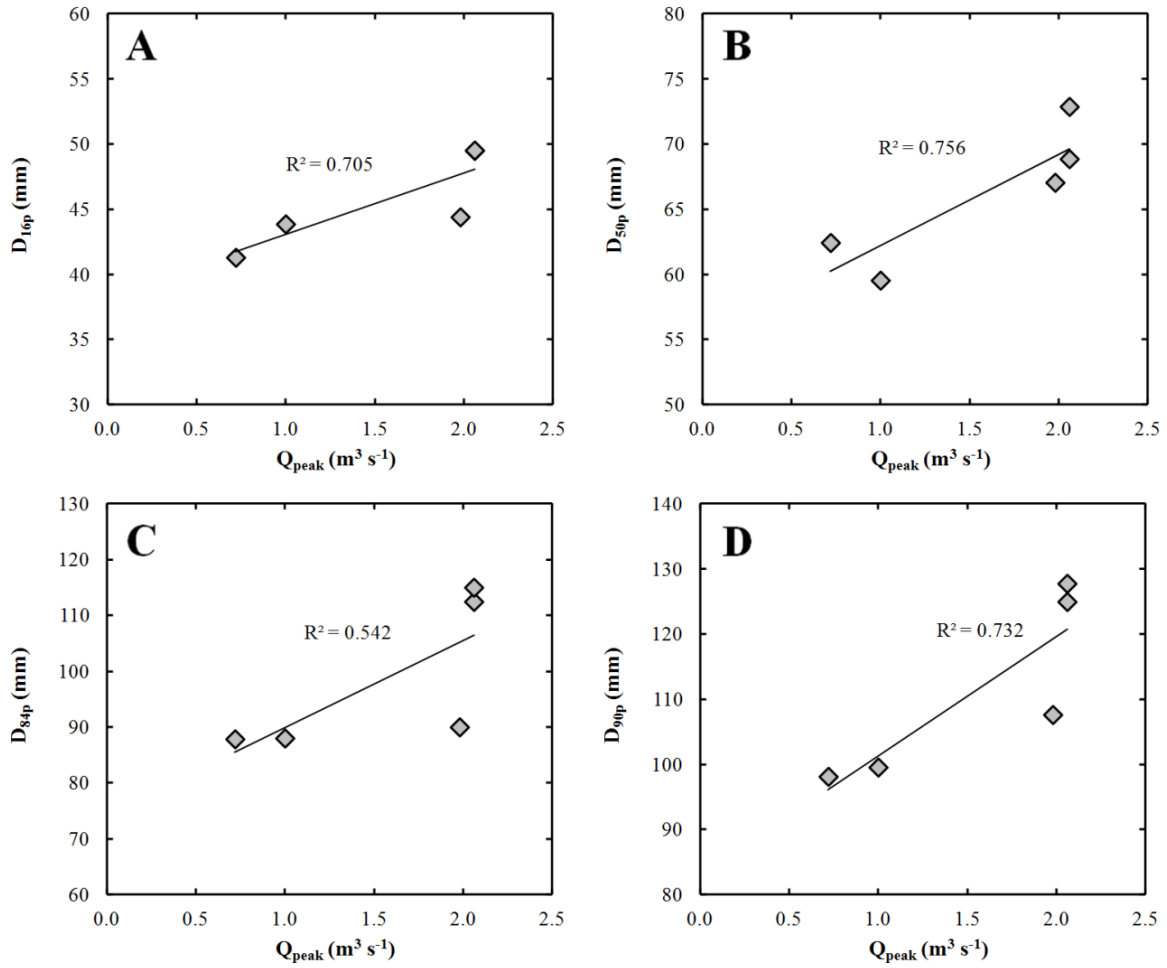

Figure 57: Relationship between Q_{peak} and D_{16} (A), D_{50} (B), D_{84} (C) and D_{90} (D) of tracers entrained in the Rio Cordon.

Comparing between them the Q_{peak}/D_p relationships we can observe that the *b-axis* increase with increasing the Q_{peak} (Fig. 58). Also, the highest water discharges were characterized by more scattered GSD, respect to those observable when $Q_{peak} < 1$ m^3 s^{-1}. Using a linear regression to investigate the Q_{peak}/D_p relationships, it is possible to observe that, as expected, the intercept increases with the raising of percentile considered. Additionally, it is worth to noticing that the regressions become progressively more steeper, with the slope (or *a* coefficient) that increases from 4.72 in D_{16p} to 18.38 for D_{90p}. These results suggest that under

equal hydraulic forcing conditions, the coarse material (i.e. D_{84p}, D_{90p}) exhibits a larger variability in terms of relative *b-axis* entrained, increasing more respect to the lower percentiles. This result appears consistent with a condition of size-selective transport.

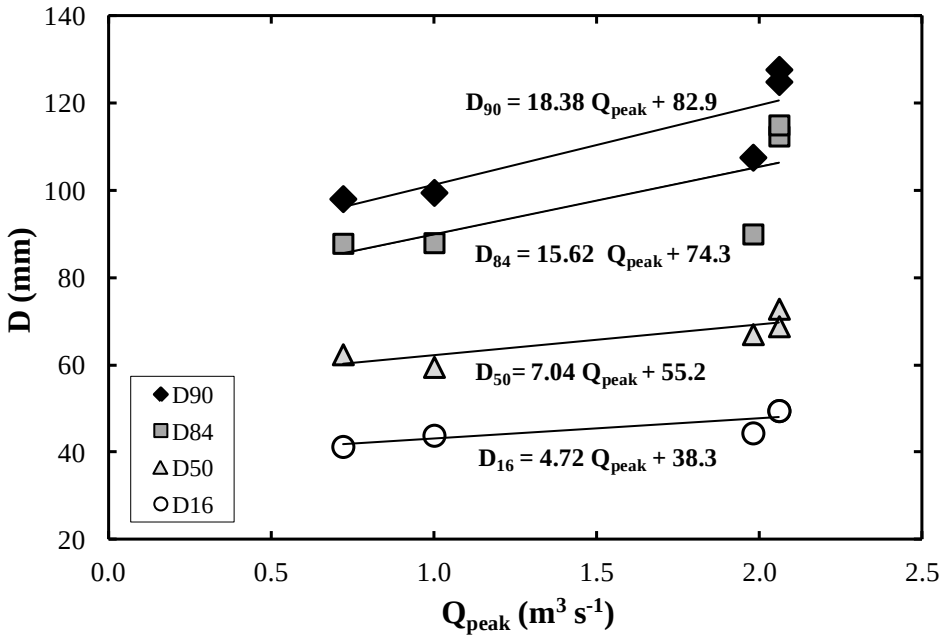

Figure 58: Comparison between the relationships Q_{peak}/D_P of tracers entrained in the Rio Cordon.

3.2.3. Scaling relationships

Once analyzed the influence of particle size on sediment entrainment, the relationship among hydraulic forcing and tracers displacement was investigated. The analysis was focused on the assessment of the scaling relationships between Li and the variable hydraulic forcing conditions that affect a tracer mobilized. To achieve this aim, for each displacement, the flow duration curve was realized and consequently the 25th (ω_{25}), 50th (ω_{50}) and 75th (ω_{75}) percentiles of unit stream power were calculated. These significant percentiles, with the ω_{peak}, are used in order to test their capacity to explain the relationship among hydraulic forcing and tracers displacement. First, Li were plotted as a function of this significant percentiles (Fig. 59). Notwithstanding the weak relationships, the transport distance appears positively correlated with ω_{50}, ω_{75} and ω_{peak} (Fig. 59B-D) while the data in ω_{25}/Li are quite scatter (Fig. 59A). The positive correlation observed enhances with increasing the percentile of unit stream power, reaching the best performance among ω_{peak} and Li (R^2= 0.778).

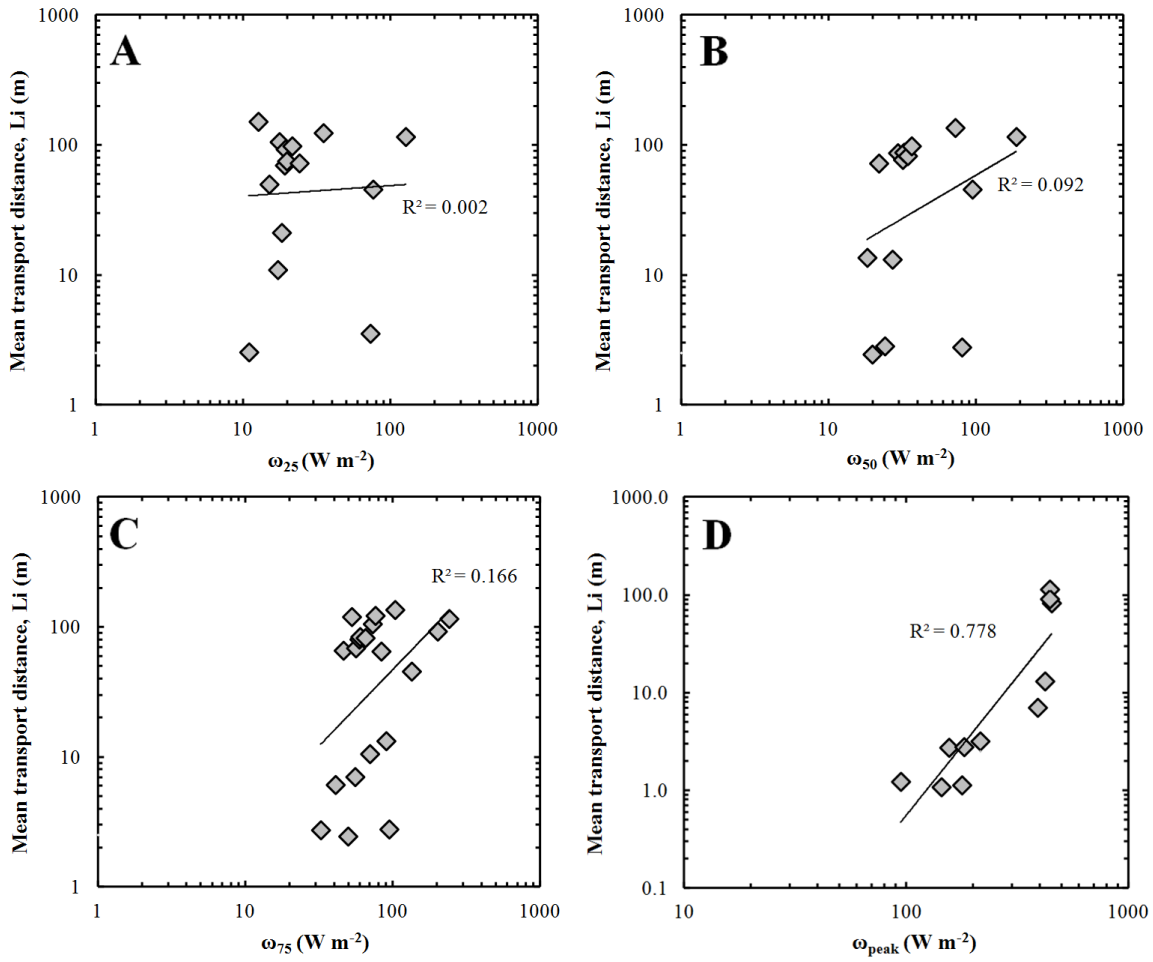

Figure 59: Relationships between the stream power percentiles and mean transport distance in the Rio Cordon. Li is related to ω_{25} (A), ω_{50} (B), ω_{75}(C) and ω_{peak} (D).

A further analysis was performed, testing Li as a function of the ratios among the significant percentiles. The six possible ratios were tested and the results are reported in Fig. 60. As it is possible to note all relationships show a positive trend, but exhibiting scarce correlations. The weakest correlations are observable with the ratios ω_{75}/ω_{50} (Fig. 60C), $\omega_{peak}/\omega_{25}$ (Fig. 60D), $\omega_{peak}/\omega_{50}$ (Fig. 60E) and $\omega_{peak}/\omega_{75}$ (Fig. 60F) in which the data are notably scattered. The correlation partly improves when Li is related to ω_{75}/ω_{25} (Fig. 60B) and particularly with ω_{50}/ω_{25} (R^2= 0.308), when the regression appears to be slightly steeper (Fig. 60A).

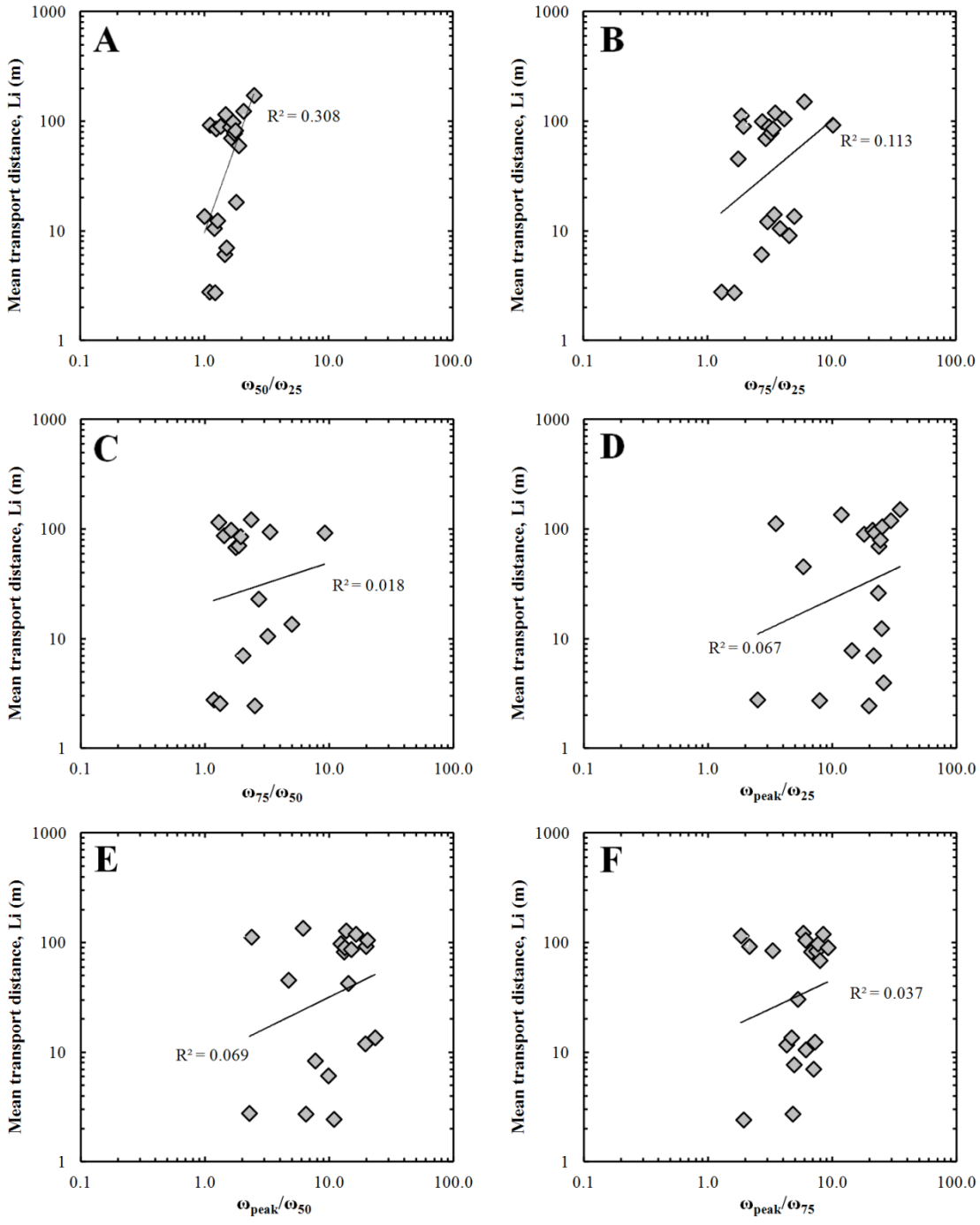

Figure 60: Relationships between the percentile ratios and mean transport distance in the Rio Cordon. Li is related to ω_{50}/ω_{25} (A), ω_{75}/ω_{25} (B), ω_{75}/ω_{50} (C), $\omega_{peak}/\omega_{25}$ (D), $\omega_{peak}/\omega_{50}$ (E) and $\omega_{peak}/\omega_{75}$ (F).

3.3. Estero Morales: Tracing bedload transport using PIT tracers

3.3.1. Measurement campaign and recovery rates

In the Estero Morales, the surveys aimed to the bedload tracing were performed during the austral summer 2014, specifically from January 2014 to March 2014. Overall, 14 PIT inventories were performed, starting on January, 29 to terminate on March, 7 with on average a survey every 2.7 days (Fig. 61). Contrary to the Rio Cordon, where the PIT were installed in 2010, in the Estero Morales the tracers were seeded in January 2014 for the first time. Despite this short-term study period, the particular hydrological conditions that characterizes the Andean basin allowed to investigate the tracers with a wide range of water discharges.

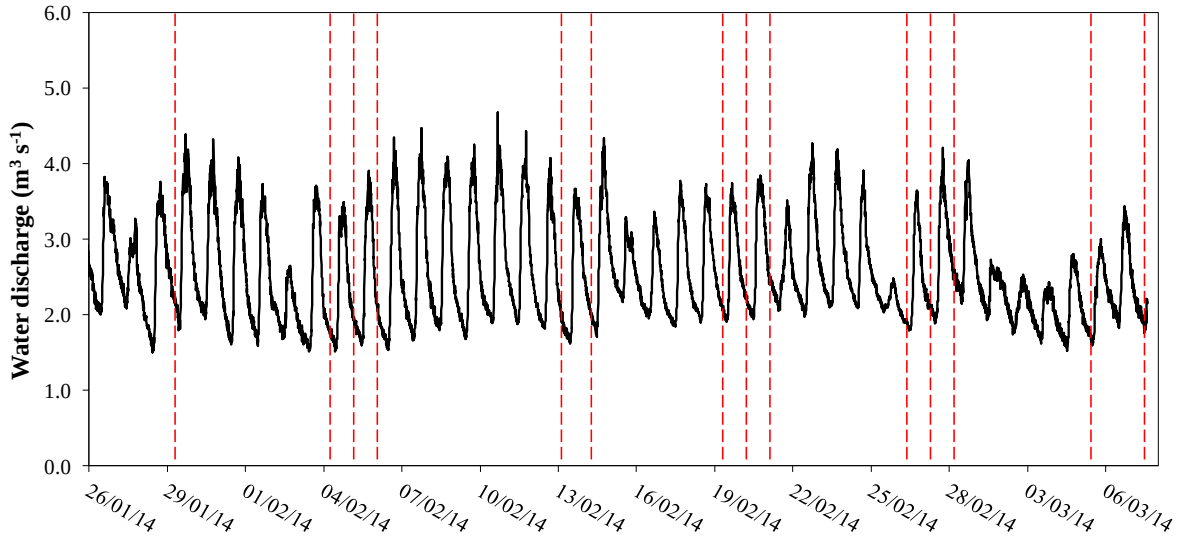

Figure 61: Discharge time series during the study period, the red dashed lines correspond to the PIT surveys performed.

Coherently to the approach used in the Rio Cordon, also in the Estero Morales the hydraulic forcing were expressed by the peak of water discharge (Q_{peak}) as well as the peak of unit stream power ω_{peak}. Also, the displacements < 1m were not taken into account for the subsequently analysis. In terms of hydrological conditions the glacial melt occurred during the summer 2014 allowed to investigate the bedload transport with daily fluctuations in the water discharge and high hydraulic forcing. Notably, the unit stream power peaks are higher respect those observed in the Rio Cordon, ranging from 627.11 W m^{-2} to 872.86 W m^{-2}. Notwithstanding the limited range exhibited by the stream power per unit area, the mean transport distances (Li) vary of more than one order of magnitude, ranging from 6.51 m to 185.36 m (Tab. 16).

Table 16: Date of the PIT survey, Q_{peak} and ω_{peak} occurred during the period monitored, mean travel distance of the tracers (Li), number of PIT detected (n), recovery rate (Rr) and extent in days of the period monitored.

Survey	Q_{peak} ($m^3 s^{-1}$)	ω_{peak} ($W m^{-2}$)	Li (m)	n (*n*)	Rr (%)	T (days)
29/01/2014	3.77	701.93	27.44	35	44	1
04/02/2014	4.39	818.38	93.08	54	44	6
05/02/2014	3.49	651.15	8.40	79	44	1
06/02/2014	3.91	728.69	12.37	111	64	1
13/02/2014	4.68	872.86	122.51	85	41	7
14/02/2014	3.67	684.09	43.51	111	50	1
19/02/2014	4.34	808.75	54.28	134	53	5
20/02/2014	3.49	651.15	16.24	145	51	1
21/02/2014	3.85	717.44	22.39	150	49	1
26/02/2014	4.27	796.27	52.52	157	47	5
27/02/2014	3.36	627.11	6.51	198	54	1
28/02/2014	4.21	784.20	8.41	222	61	1
05/03/2014	4.04	753.51	185.36	58	16	5
07/03/2014	3.44	640.87	21.28	226	86	2

During the measurement campaign the recovery rates varied from 16% in the inventory carried out on March, 5 to 86% reached in the last survey on March, 7. This large variability in the recovery rates is due to the large extent of the reach investigated in Estero Morales creek (i.e. 720 m) and by the rapid fluctuations in water stage. In case of an abruptly increase of discharge during the field surveys, the study reach was only partially investigated (i.e. January, 29; March, 5) and thus the tracers were only in part detected.

3.3.2. Influence of grain size on the displacement

Consistently to the method employed in the Rio Cordon, also in the Estero Morales dataset the tracers mobilized were grouped on the basis of their *b-axis*, evaluating the related mean travel distance. Also in this case, the displacements were reclassified in three classes according to the peak of water discharge. In terms of particle sizes, the tracers installed in the Estero Morales creek are characterized by a wider range of *b-axis* compared to the Rio Cordon. Specifically, also the 32mm-size class is represented in the PIT population. The Di/Li relationship, for the three magnitude of events occurred, is shown in Fig. 62. In the Estero Morales the magnitude of events was classified as: low when $Q_{peak} < 4.0$ m^3 s^{-1}, moderate with $4.0 < Q_{peak} < 4.5$ m^3 s^{-1} while high magnitude with $Q_{peak} > 4.5$ m^3 s^{-1}. The number of

tracers mobilized by each class of flood magnitude increases between the low magnitude (n=180) to the moderate magnitude floods (n=226), while decrease in the high events (n=88). In this sense, it is to stress out that low and moderate magnitude classes accounted 8 and 5 surveys, respectively, while 1 inventory is represented by the high magnitude events. In terms of mean transport distance an augment is observable with increasing the floods magnitude. The low and moderate magnitude events show a mean displacement quite similar, equal to 32.82 m and 42.27 m, respectively. Li abruptly increases with the high magnitude event, reaching 282.59 m.

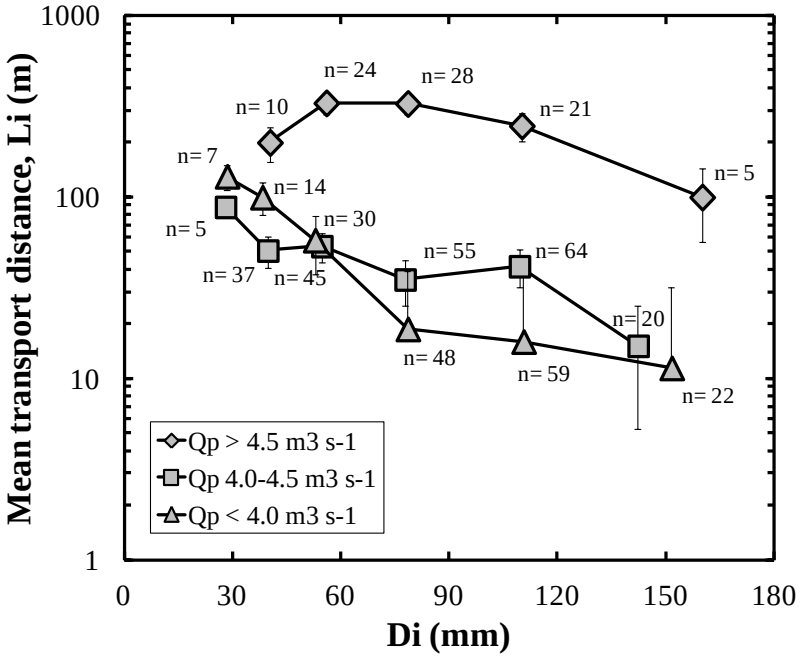

Figure 62: Relationship between mean transport distances, with standard errors and six particle size classes. Analysis performed on the three peak discharge classes observed in the Estero Morales.

Focusing on the grain size influence, the low and moderate magnitude floods were characterized by a similar behavior. In fact, the tracers displacement decreases with increasing the particle size. This results suggests that in the low and moderate floods a size-selective transport occurred. Contrary to what is expected, in the finer *b-axis* classes (i.e. size classes 32-64mm) the low magnitude floods showed higher displacements respect to the moderate magnitude events. In the coarser sediment such behavior is inverted. It is worth to noticing that a lower number of coarse tracers (size class=181 mm) was entrained by the high magnitude flood (n=5) compared to those mobilized by low (n=20) and moderate (n=22), but the PITs transported by the high hydraulic forcing appear larger. The flat trend exhibited by the curve of the high magnitude event, suggests that during such flood the displacement was

unaffected by the particle size. In turn, this evidence seems to suggest the occurrence of equal-mobility conditions due to the high hydraulic forcing.

In line with the Rio Cordon analysis, also in the Estero Morales the relationship between Q_{peak} and GSD of the tracers mobilized was investigated (Fig. 63). Also in this case, merely the surveys with more than 20 displacements were taken into account. Thus, 6 inventories were used in this analysis. The results show quite scattered relationships. Specifically, the regression worsens with increasing the percentile investigated. A positive correlation can be observed in the D_{16p}/Q_{peak} relationship (Fig. 63A). In the D_{50p}/Q_{peak} (Fig. 63B) and D_{90p}/Q_{peak} (Fig. 63D) regressions, the *b-axis* of percentiles not exhibit a clear variation with increasing the peak of water discharge, showing a flat trend. Moreover, the D_{84p} appears negatively correlated with Q_{peak} (Fig. 63C). Overall, none clear relationship was detected among Q_{peak} and GSD of the tracers mobilized.

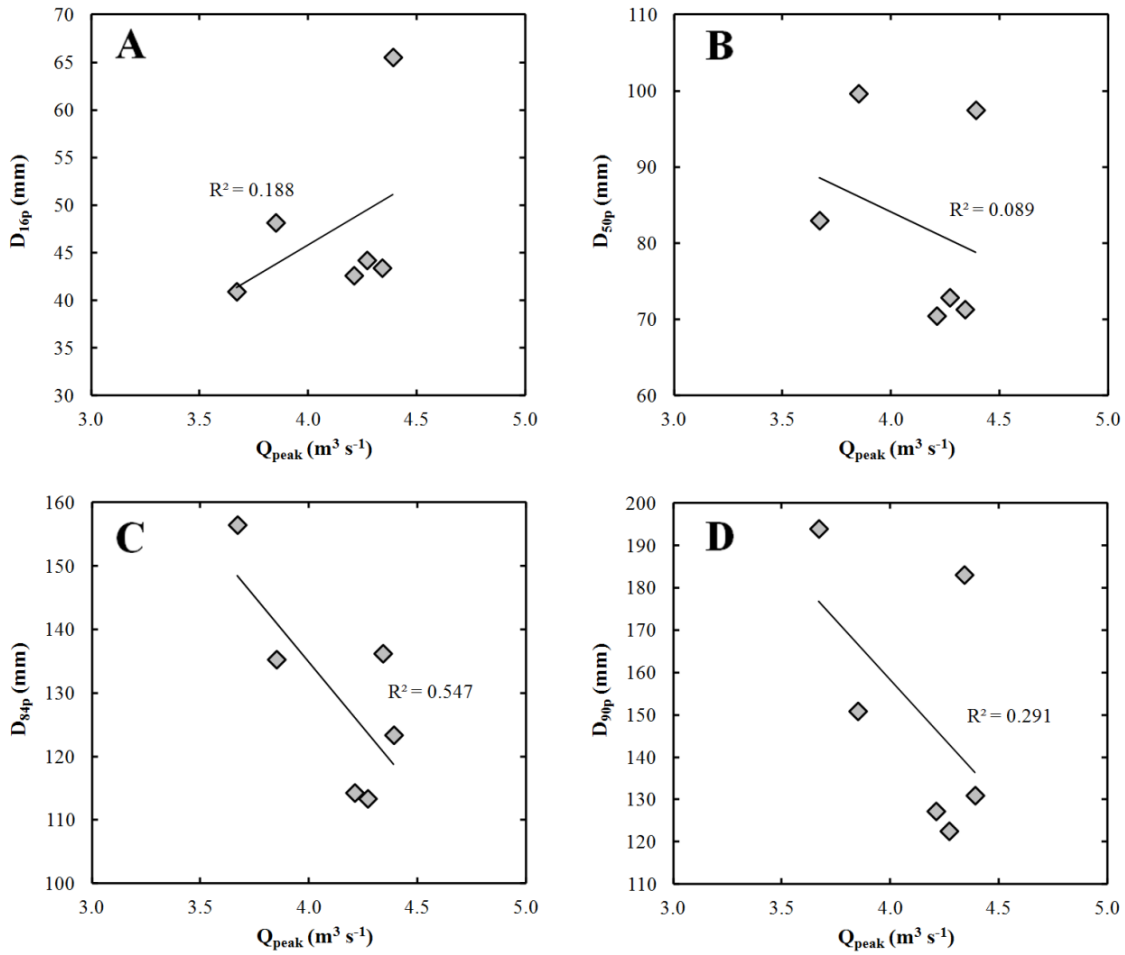

Figure 63: Relationship between Q_{peak} and D_{16} (A), D_{50} (B), D_{84} (C) and D_{90} (D) of tracers entrained in the Estero Morales.

The lack of a clear relationship between Q_{peak} and GSD of the tracers mobilized can be observed also comparing the linear regressions obtained (Fig. 64). In this sense, only D_{16p} shows a positive correlation with an *a* coefficient (i.e. slope) equal to 11.89. The other percentiles are characterized by flatter regression lines, with slope that ranges from to 2.39 (D_{50p}) to negative values, i.e. -6.86 (D_{84p}) and -2.17 (D_{90p}). Additionally, the range of percentiles mobilized not increases with increasing peak of water discharge, with the prevailing of trends highly scattered.

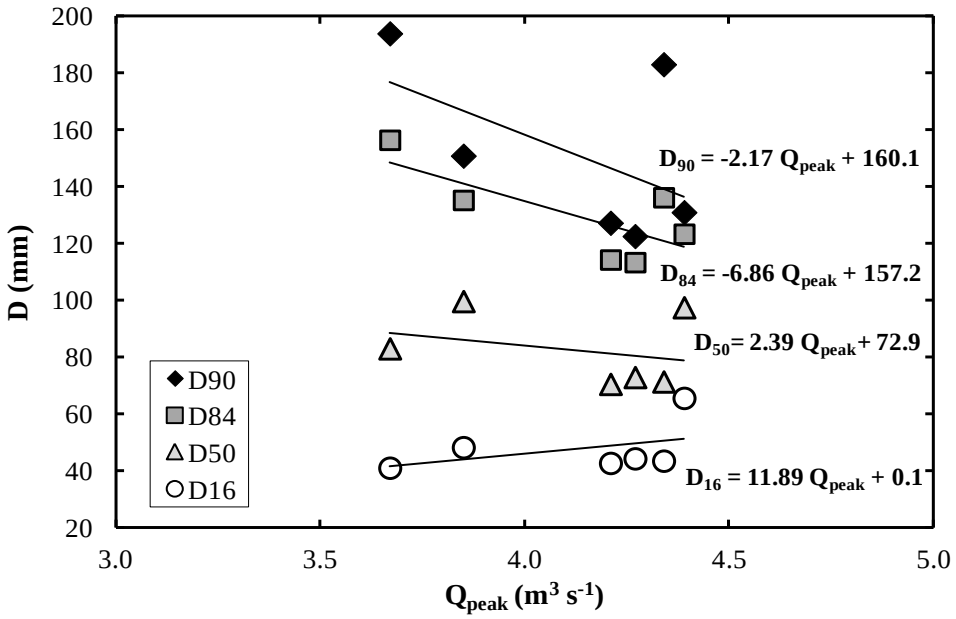

Figure 64: Comparison between the relationships Q_{peak}/D_p of tracers entrained in the Estero Morales creek.

3.3.3. Scaling relationships

Also in the Estero Morales the influence of hydraulic forcing on tracer displacements was investigated. Particularly the scaling relationships between Li and the significant percentiles of ω (25th, 50th, 75th and peak) were tested (Fig. 65). Overall, the mean transport distance appears weakly correlated with the ω percentiles. As already observed in the Rio Cordon, the correlation augments with increasing the percentile of unit stream power. In this sense, the best correlation (R^2= 0.460) can be observed between Li and ω_{peak} (Fig. 65D). The ω_{25}/Li and ω_{50}/Li relationships show a negative correlation (Fig. 65A-B), while the mean transport distance increases with increasing ω_{75} and ω_{peak} (Fig. 65C-D).

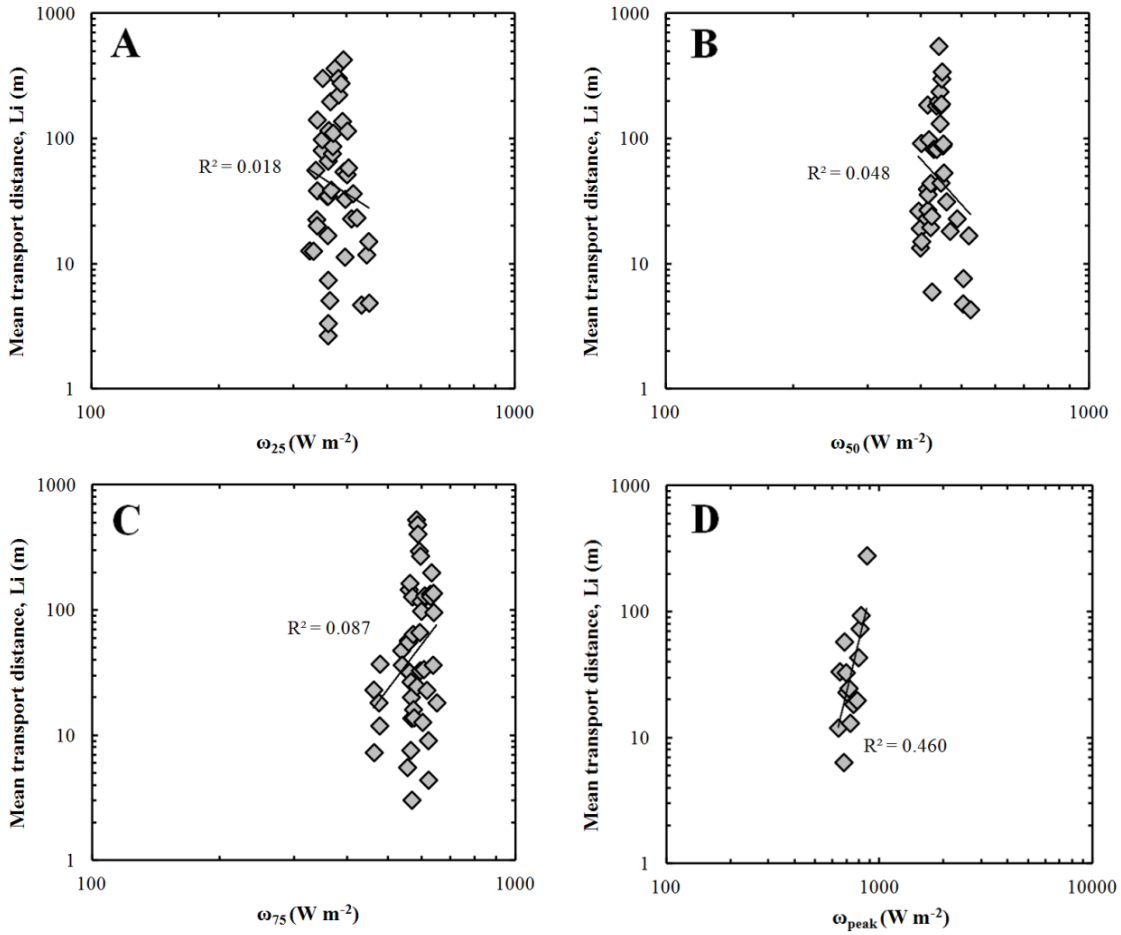

Figure 65: Relationships between the stream power percentiles and mean transport distance in the Estero Morales. Li is related to ω_{25} (A), ω_{50} (B), ω_{75}(C) and ω_{peak} (D).

In the light of the results reported, the mean transport distance was also tested as a function of the ratios between ω-percentiles (Fig. 66). Li is positively correlated with all ratios investigated, in particular appears better related with $\omega_{peak}/\omega_{25}$ (Fig. 66D) and $\omega_{peak}/\omega_{50}$ (Fig. 66E). In the remaining ratios, the correlation is constantly positive but quite weak (R^2= 0.114-

0.199). If compared to the significant percentile of unit stream power (i.e. 25th, 50th, 75th and peak), the ratios between ω percentiles appear better related with the mean transport distance. This better relationship is appreciable both in terms of positive correlation and square error. Interestingly, in the Estero Morales the scaling relationships investigated exhibit a very steep trend.

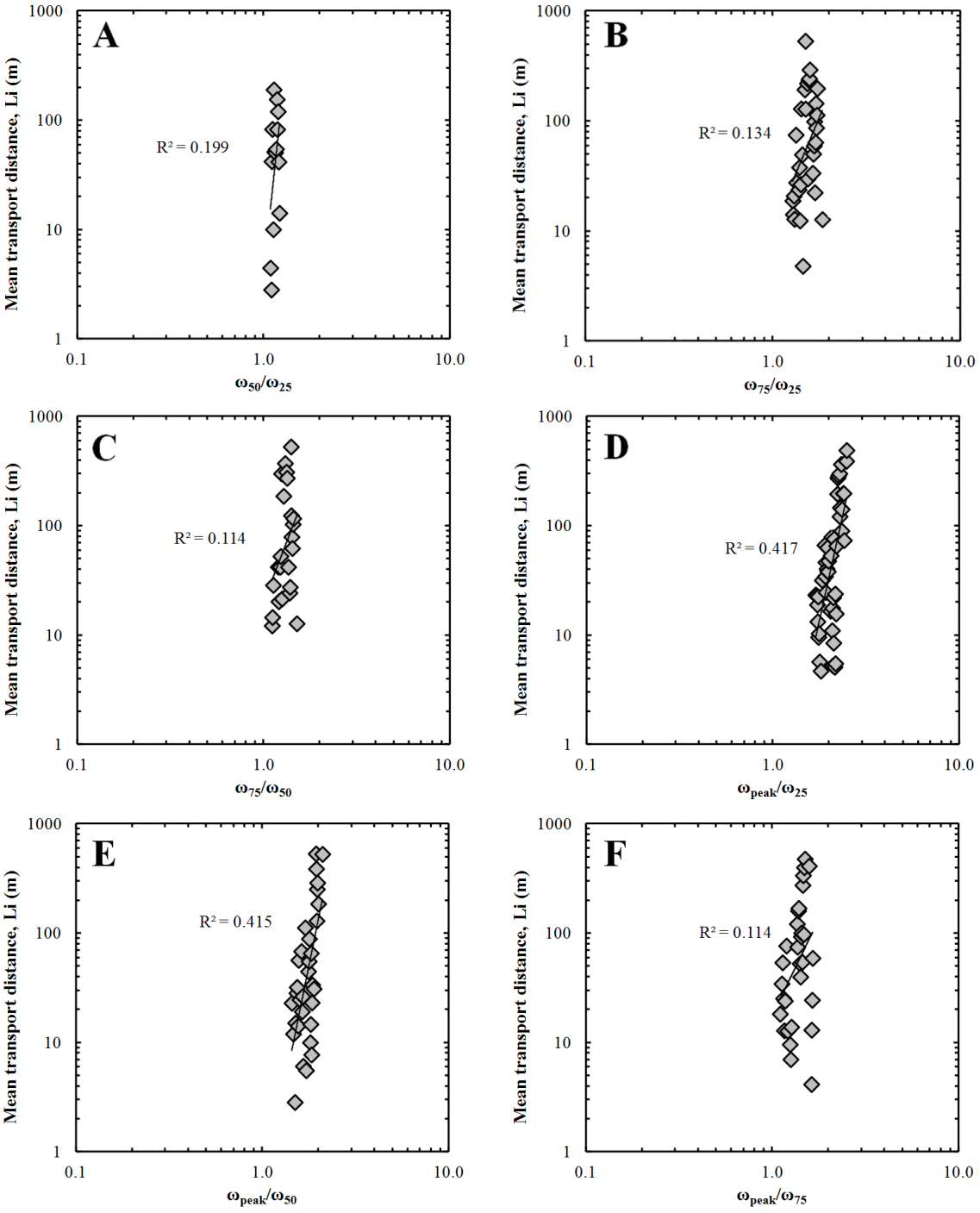

Figure 66: Relationships between the percentile ratios and mean transport distance in the Estero Morales. Li is related to ω_{50}/ω_{25} (A), ω_{75}/ω_{25} (B), ω_{75}/ω_{50} (C), $\omega_{peak}/\omega_{25}$ (D), $\omega_{peak}/\omega_{50}$ (E) and $\omega_{peak}/\omega_{75}$ (F).

4. CHAPTER FOUR - DISCUSSIONS

4.1. Rio Cordon: Temporal trend of sediment yield

4.1.1. Sediment yield

The analyses performed on the data produced by the Rio Cordon monitoring station highlighted that the total sediment load reached nearly 15000 from 1986 to 2014, corresponding to a mean sediment yield of 103 t km^{-2} y^{-1}. This value is consistent with the results obtained by Hinderer et al. (2013) who, reviewing the data published on 202 Alpine basins, reported a range of mean sediment yield between 50 and 5000 t km^{-2} y^{-1}. Among the southern calcareous Alpine basins with comparable features (unglaciated, basin area<500 km^2), the Rio Cordon exhibits a relatively low sediment yield. In fact, in this lithotectonic zone the observed sediment yield varies between 100-500 t km^{-2} y^{-1} (Hinderer et al., 2013). Results from Rio Cordon are relatively comparable with what was reported by Tropeano (1991) in the Sauglio stream, eastern Italian Alps. In this catchment (6.8 km^2; similar to the Rio Cordon), a sediment production of 157.0 t km^{-2} y^{-1} was assessed in the period 1986-1989. In the Rio Cordon, the average sediment yield increases from 77.7 (pre-1994 period) to 112.6 t km^{-2} y^{-1} (from 1994 to 2014). Such behavior seems to suggest that the September 1994 flood induced a change in the sediment availability that led to increased amounts mobilized during the post-1994 period.

Observing the annual contribution of the 1994 flood on the overall sediment yield (Fig. 52, Tab. 14), it appears that 1994 plays a key role in the budget estimated on the 29 years of monitoring. The 4067.2 t transported in that year accounted for 27.2% of the total sediment load mobilized between 1986-2014. In turn, the annual contribution recorded in 1994 is strongly dominated by the September 1994 flood, which transported 3976.8 t, i.e. 97.7% of the annual sediment production and 26.6% of the total sediment load. Contributions higher than 1000 t y^{-1} were recorded in 1998 (1261.5 t) and 2001 (1742.6 t) accounting for 8.4% and 11.6% of the total sediment load, respectively. Also in these cases the annual contributions are dominated by the sediment load mobilized by large flood events. Specifically, the October 1998 event transported 910.3 t that represents 72.2% of the annual production and 6.1% of the total sediment load. The mud flow that occurred in May 2001 mobilized 1155.4 t, which accounted for 7.7% of the budget estimated over 29 years and for 66.3% of the annual sediment contribution. In the remaining years, the annual contributions are markedly below 1000 t y^{-1}, with an evident phase of limited sediment yield since 2003. Overall, the influence of floods is clear taking the 6 large events (RI > 5 years) into account. These floods

transported a sediment load of 5667.6 t, corresponding to 37.9% of the total load. If we add the May 2001 event, characterized by ordinary magnitude (RI = 1.2 years) but unlimited sediment supply conditions (Lenzi et al., 2003), the amount transported increases to 6823 t, i.e. 45.7% of the total sediment budget. These results suggest that in three decades of monitoring, the sediment budget in the Rio Cordon was mainly controlled by the occurrence of large floods, and particularly by the exceptional event in September 1994. The importance of this event on the overall sediment budget confirms that exceptional floods, rarely evaluated in short-term monitoring projects, can strongly influence the budget over the long-term (Sadler, 1981; Kirchner et al, 2001; Turowski et al., 2010). Even analyzing the bedload and suspended load fractions separately, the influence of the large events is confirmed. The seasonal contribution of the suspended load (Fig. 53) is clearly dominated by the period of occurrence of such floods while the amount provided by the large events is 27.9% of the total suspended load, a contribution that increases to 36.6% if the May 2001 event is taken into account. Altogether, the 31 recorded events (Tab. 1) accounted for 49.6% of the total suspended load, with the September 1994 flood that alone contributed 20.6%. As to the bedload, the large floods supplied 75.6% of the coarse sediments mobilized over 29 years. Also, the key role of the September 1994 flood is even clearer. In fact, 49.1% of the coarse material transported in the last 29 years was provided by this event, suggesting that the high magnitude events may provide a large part of the bedload transported over the long term. Once the impact of large flood events has been proved, the relatively low sediment yield can probably be explained by the lack of such events, especially in recent years. The absence of significant floods since 2003 has led to a bedload contribution constantly lower than 10 t y^{-1}, a trend that was partially interrupted by ordinary floods that occurred in 2012 and 2014. Reflecting the same trend, the suspended load just in 2009 exceeded 500 t y^{-1} as a consequence of an extensive and persistent snowmelt.

4.1.2. Long-term partitioning

The long-term partitioning obtained in the Rio Cordon exhibits the clear prevalence of SSL contribution, with a fraction equal to 0.79. If compared to the fractions predicted by the equations used by Schlunegger and Hinderer (2003) and Turowski et al. (2010), the observed SSL contribution appears clearly higher. Specifically, the equations overestimate the BL fraction, under-predicting the SSL contribution by about one quarter. As reported by the authors these formulas allow a prior and rough assessment, using published data that show wide scatter and not taking into account the singularities of the basins. However, the

partitioning estimated is consistent with the values noted in similar Alpine basins (unglaciated, A<500 km^2), where SSL fractions between 0.37-1.00 were observed (Durst, 1990; Lauffer and Sommer, 1982; Lenzi et al., 2003). As also recognized in other mountain basins by Turowski et al. (2010), a large variability in the annual and floods fractions was detected in the Rio Cordon. Interestingly, the partitioning found over the long term may not reflect the conditions during the large floods. Similarly to what was observed by Beecroft (1983) who during a large outburst flood from the Tsidjiore Nouve Glacier (Switzerland Alps) noted a BL fraction of about 0.70 compared to the long-term bedload fraction of 0.44 (Gurnell et al., 1988), the September 1994 flood in the Rio Cordon had a BL fraction of 0.39, i.e. 185% higher than the bedload fraction averaged over 29 years (0.21). Despite the lack of a clear relationship between discharge and degree of partitioning, the 1994 flood shows that exceptional events contribute disproportionately more to bedload over the long term than any other ordinary event. Also, a change in the partitioning can be appreciated between pre- and post-1994, reflecting the sediment yield trend. The increase in the BL fraction from 0.11 pre-1994 to 0.24 during the 1994-2014 period appears to be consistent with a higher availability of coarse and loose material subsequent to the September 1994 event.

4.1.3. Temporal trend on sediment dynamics

As expected, the bedload and suspended load mobilized by the floods scaled roughly linearly with the peak of water discharge, increasing with the increase of hydraulic conditions. Such a scaling relationship was also observed investigating the D_{50} and SSC_{max}. In this case, the power-law regressions were used in the light of the change in sediment dynamics induced by the September 1994 event and detected by the previous analyses. Distinguishing between pre- and post-1994 events, a significant increase in the coefficient *a* of this relationship was observed, providing evidence of an increased sediment availability after the 1994 event. Specifically, the results obtained by the BL/Q_{peak} and SSL/Q_{peak} relationships highlighted that the events occurring after the September 1994 flood transported larger amounts of sediments than similar events in the pre-1994 period. In addition, the increase of coefficient *a* in the D_{50}/Q_{peak} and SSL/Q_{peak} relationships suggests that the higher sediment availability has been coupled to the supply of larger coarse material as well as looser fine sediment. The reactivation of several old sediment source areas, the triggering of new ones and the removal of the armour layer caused by the September 1994 flood can mostly explain these observations. Even if the analysis was focused on the short-term dynamics (flood event), the effect can be constantly detected for the post-1994 events. This evidence seems to broadly

confirm the role of the September 1994 event, which altered the sediment fluxes observed until then, increasing sediment availability and transport efficiency over the long term. Having demonstrated that the exceptional event clearly triggered a change in sediment dynamics, the aim has been to determine the "temporal effect" of such an event. In this sense, the temporal trend (Fig. 54) exhibited by flood events over the 29 years allows phases to be identified characterized by different sediment availability conditions. As already discussed in part by Lenzi et al. (2004), a general decreasing trend can be observed in the Rio Cordon basin over the long term. Such a tendency is due to the gradual depletion of sediment availability and can first be detected in the 1986-1993 period. This initial phase was abruptly interrupted by the September 1994 flood, which features BL/Re and SSL/Re ratios of about two magnitudes higher than the pre-1994 events. The high sediment supply from the source areas, the large amounts of sediment eroded from the hillslopes and stored in the stream network but above all the great quantity of in-channel loose material derived from the armour layer elimination coupled with the increased transport capacity favored by step-pool removal (Lenzi, 2001; Comiti et al., 2005) have led to an increase in the sediment availability and then in the transport efficiency displayed by the post-1994 flood events. The temporal trend seems to suggest that this period of high sediment transport efficiency was exhausted in about 10 years (1994-2004). The post-1994 decreasing trend was interrupted by the event in May 2001 and more recently by the November 2012 and June 2014 floods, i.e. by events with unlimited or quasi-unlimited supply conditions induced by hillslopes gravitational phenomena. Contrary to what is observed for the September 1994 flood, in these cases no significant variations can be appreciated in the post-events trend, suggesting no influence on the long-term transport efficiency. Evidence of short-timescale effects can be partially detected as a consequence of the May 2001 flood. The immediately subsequent event that took place in July 2001 (Q_{peak}=1.98 $m^3 s^{-1}$; Re= 15.0) features hydraulic forcing conditions fully comparable with the recent May 2013 flood (Q_{peak}=1.96 $m^3 s^{-1}$; Re= 10.2) but despite this similarity the total load transported (155.5 t) in 2001 was one magnitude higher with respect to 2013 (17.5 t), suggesting higher sediment availability probably triggered by the material mobilized in May 2001. The different influence on the post-transport efficiency can be explained by the lower magnitude of the events with respect to the September 1994 flood and particularly by the limited effects induced on the source areas. Notably, the equivalence in the GSDs assessed in 2004 and 2014 appears to be consistent with the persistence of the armour layer, even after the recent high-transport efficiency floods. Similarly to what was observed during the pre-1994 phase, a low transport efficiency has been exhibited by the floods since 2005. The progressive

consolidation of the step-pool configuration (Lenzi, 2001) combined with the reestablishment of the channel-bed armouring and the depletion of the material supplied by the 1994-source areas would explain this recent phase characterized by low sediment availability, which is particularly evident in the bedload behavior.

4.1.4. The effects of antecedent floods on sediment production

The long-term analysis of sediment production in the Rio Cordon demonstrated that the September 1994 flood influenced the sediment transport of subsequent floods, having thus determined a certain "memory effect" in the basin (Hinderer et al., 2013), consisting of the creation of new source areas, reactivation of old ones and thus intensifying the sediment delivery over a long-timescale (Rickenmann et al., 1998; Lenzi and Marchi, 2000; Turowski et al., 2009; Morche and Bryk, 2010; Bennett et al., 2013). The investigation of the flood events clearly demonstrated that in the post-1994 period a variation occurred in the sediment dynamics, resulting in an increase of the amounts transported accompanied by larger diameters and concentrations mobilized. The exceptional event also led to a change in both sediment yield and partitioning. On a long-timescale the temporal trend highlighted the succession of three periods characterized by different sediment dynamics. After the September 1994 event there was a high transport efficiency phase that lasted for about a decade. In these terms, the 1994-2004 period clearly differs with respect to the conditions observed pre-1994 (1986-1993) and between 2005-2014. A coincident temporal behavior can be broadly identified in the seasonal contribution of suspended load. In the 1994-2004 period, opposite conditions were detected if compared to what was observed prior to the exceptional event. This involves an initial period with a mixed seasonal contribution, in which snowmelt and summer contributions prevailed over the autumn yield (Tab. 17). After 1994, the autumn contribution clearly prevailed for approximately 10 years with a mean yield of 426.7 t y^{-1} (Tab. 17), probably suggesting the availability of the sources of fine sediment easily mobilized by the frequent autumn rainfall. Once this supply was exhausted, the limited amounts transported by suspension since 2005 have been mobilized mainly during the snowmelt period.

The mean sediment yield in the three periods was evaluated in the light of this consistent temporal behavior. The results obtained show that the first period (1986-1993) with an average sediment yield of 77.7 t km^{-2} y^{-1} was followed by the second (1994-2004) with a clearly amplified sediment production of 171.8 t km^{-2} y^{-1}, while in the third period (2005-2014) this value decreased to 47.4 t km^{-2} y^{-1} (Fig. 67; Tab. 17). The same approach was used

regarding the partitioning. While in the 1986-1993 period the bedload contribution was 0.11, in the 1994-2004 period the BL fraction increased to 0.28 and then strongly decreased to 0.06 in the 2005-2014 period (Fig. 68: Tab. 17).

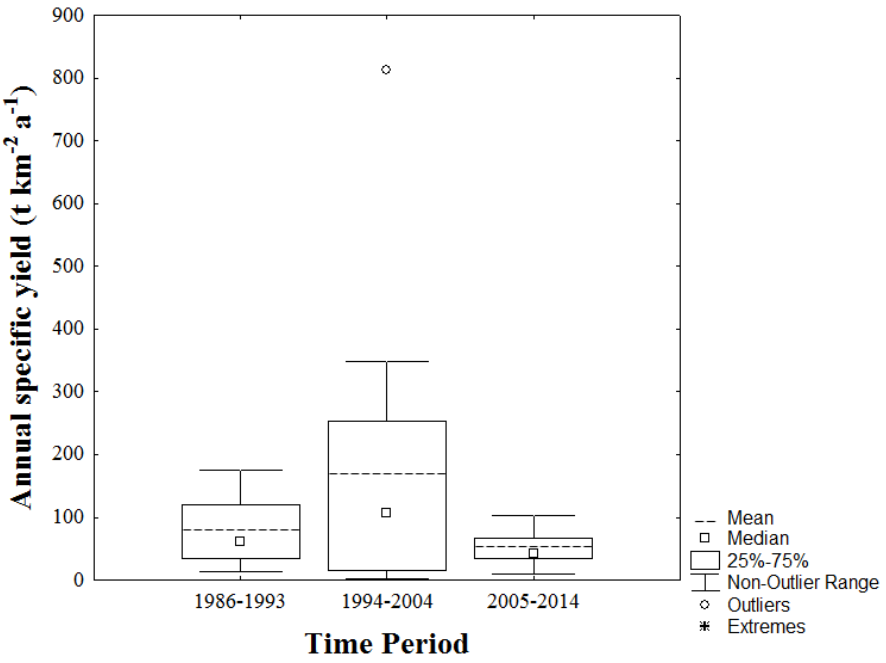

Figure 67: Mean annual specific yield occurred during the 3 periods characterized by different sediment availability conditions.

The partitioning thus appears to be consistent with the results obtained by the D_{50}/Q_{peak} relationship, suggesting the higher availability of coarse loose material following the September 1994 flood that persisted for approximately a decade. Apparently, the evidence supports the hypothesis that the September 1994 event in the Rio Cordon caused a memory effect in the sediment dynamics, whose influences impacted the basin for roughly 10 years.

Table 17: BL fraction, mean sediment yield and seasonal SSL contribution occurred during the 3 periods characterized by different sediment availability conditions.

Period	BL fraction	Sediment yield	SSL		
			Snowmelt contribution	Summer contribution	Autumn contribution
		(t km^{-2} y^{-1})	(t y^{-1})	(t y^{-1})	(t y^{-1})
1986-1993	0.11	77.7	123.9	201.4	22.2
1994-2004	0.28	171.8	164.6	26.3	426.7
2005-2014	0.06	47.4	159.2	37.2	25.9

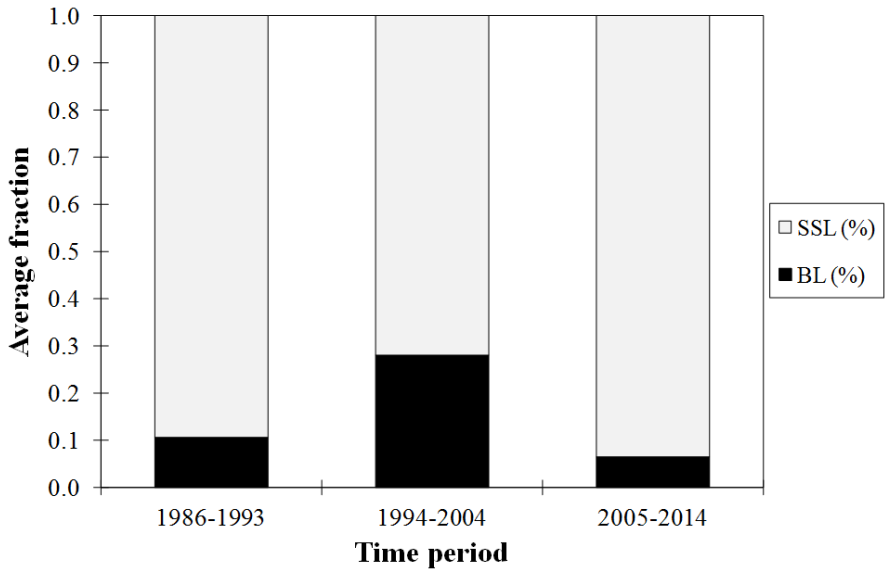

Figure 68: Average partitioning occurred during the 3 periods characterized by different sediment availability conditions.

4.1.5. Influence of sediment supply on the bedload equation performances

The availability of bedload field observations in the Rio Cordon enabled us to test the performance of 3 popular bedload equations (Meyer-Peter and Muller, 1948; Schoklitsch, 1962; Rickenmann, 1991). In particular the ratio between the observed bedload (Bl_{obs}) and predicted bedload (Bl_{pred}) was used in order to investigate the capacity to predict floods characterized by different sediment availability conditions. For this purpose, 5 flood events were taken into account: those that occurred in October 1993, September 1994, October 1996, May 2002 and November 2014 (Tab. 18). These events were selected because they had the same magnitude of effective runoff with values that range between 22.0 to 33.3 10^3 m^3 and occurred in periods with different sediment availability conditions. The results obtained show that the bedload equations give poor performances (Tab. 18). Firstly, the formulae greatly overestimate the Bl_{obs}, over-predicting about 3 fold the bedload transported by the exceptional September 1994 flood. Secondly, the Bl_{pred} estimate a bedload roughly constant among the 5 floods, varying from 1952 to 5748 tons while the Bl_{obs} varies by three orders of magnitude, ranging from 4.6 to 1541.7 tons. These results suggest that the bedload equations cannot depict the different sediment availability conditions in the Rio Cordon assuming sediment supply ~ transport capacity, whereas it appears to be evident that events having similar hydrological conditions may mobilize very different bedload amounts, depending on the period (i.e. sediment availability) in which they occurred. In this sense, an interesting attempt to improve the equation performances considering the sediment availability conditions was

made by Barry et al. (2004). The authors achieved significant results proposing a power-law equation in which the coefficient is a factor of basin area while the exponent is related to bedload sediment supply, understood as the degree of channel armouring.

Table 18: Characteristics of the 5 flood events compared and results obtained by the bedload equations

Date	Re	BL_{obs}	Meyer-Peter & Muller		Schoklitsch		Rickenmann	
			Bl_{pred}	Bl_{obs}/Bl_{pred}	Bl_{pred}	Bl_{obs}/Bl_{pred}	Bl_{pred}	Bl_{obs}/Bl_{pred}
	(10^3 m^3)	(t)	(t)		(t)		(t)	
2 October 1993	30.7	17.2	4070	0.004	4800	0.004	4276	0.004
14 September 1994	26.6	1541.7	4223	0.365	4581	0.337	4280	0.360
16 October 1996	22.0	94.7	2731	0.035	4539	0.021	3682	0.026
04 May 2002	29.4	47.2	1952	0.024	3989	0.012	3154	0.015
5 November 2014	33.3	4.6	2766	0.002	5748	0.001	4572	0.001

It is worth noticing that the Bl_{obs}/Bl_{pred} ratio in the Rio Cordon seems to be a good proxy of the transport efficiency conditions, in particular assuming $Bl_{obs}/Bl_{pred} \sim 1$ equal to absolute supply condition. Considering Meyer-Peter and Muller (1948), Bl_{obs}/Bl_{pred} equal to 0.004 seems to suggest a manifestly low transport efficiency during October 1993. Coherently with the flood magnitude, the highest ratio (0.365) was reached by the September 1994 flood, which still remained clearly below the hypothetical maximum value 1 (i.e. unlimited supply condition). In the October 1996 and May 2002 events, the increased sediment availability triggered by the memory effect led to Bl_{obs}/Bl_{pred} of 0.035 and 0.024, respectively, i.e. one magnitude higher with respect to the pre-1994 condition. The decreasing trend that can be appreciated since September 1994 appears to be consistent with the exhaustion of the memory effect. In this sense, the recent November 2014 flood exhibits a Bl_{obs}/Bl_{pred} of 0.002, fully comparable to the ratio evaluated on October 1993, suggesting a return to the supply-limited conditions observed before the September 1994 flood. If the Bl_{obs}/Bl_{pred} ratios are plotted over time, the trend obtained appears be consistent with the temporal behavior detected by the previous analyses (Fig. 69), supporting the evidence of an alteration in the sediment dynamics induced by the exceptional 1994 flood.

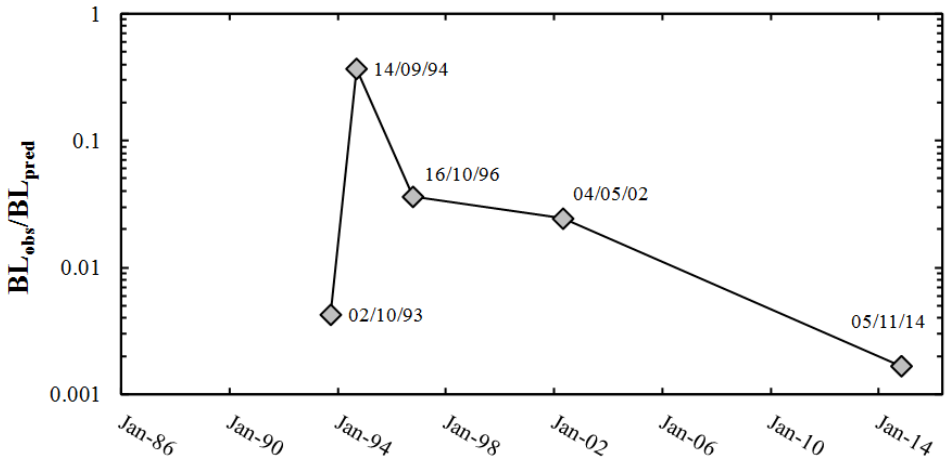

Figure 69: Ratio between Bedload Observed and Bedload Predicted (Meyer-Peter & Muller, 1948) for the five flood events compared.

4.2. Tracing bedload using PIT tracers: comparison among the two study cases

4.2.1. Periods monitored and performance of the surveys

In the Rio Cordon, the PIT inventories carried out since the 2011 have allowed to investigate the tracer dynamics due to a wide range of hydraulic forcing conditions, considering both high magnitude floods ($Q_{peak} > 2$ m^3 s^{-1}) but also the effects triggered by low-moderate events ($Q_{peak} < 2$ m^3 s^{-1}). In the Estero Morales, the measurement campaign was focused during the austral summer 2014 (i.e. January-March), when the glacier-melt contribution guarantees significant peaks in water discharge. In this sense, despite the short-term study period, a large range of hydraulic forcing was monitored, particularly due to the daily fluctuations that characterized this glacierized basin during the melt phase. In terms of peak of unit stream power (ω), in the Rio Cordon the monitored floods range between 94.44 W m^{-2} to 451.78 W m^{-2}. On the other hand, the hydraulic forcing investigated in the Estero Morales are characterized by a smaller range in terms of ω_{peak} (627.11-872.86 W m^{-2}), but with conditions overall higher compared to those analyzed in the Rio Cordon.

The recovery rates (Rr) were progressively increased in the Rio Cordon surveys, thanks to a increasing efficiency in the field-activities as well as in tracers detection. The reduction in Rr, observable especially after the large floods, is due to the transport of several tracers from the channel bed to the storage area of the monitoring station, over the bankfull-width and into the deep pools, thus in positions tricky to detected by the mobile antenna (range detection ~ 0.50 m). An example of this, is the decrease of recovery rates observable in 2015 surveys and due to large quantity of PITs actually located in large pools that characterized the Rio Cordon

channel bed. This tracers clustering was mainly caused by the high-moderate magnitude events that occurred in 2014. In this sense, a new flood could re-make available the tracers now trapped in the deep pools. Comparing the two measurement campaigns, in Rio Cordon and Estero Morales was reached an average recovery rate equal to 50% and 70%, respectively. In the Estero Morales the lower recovery rate can be partly explained by the larger extent of the study reach, two fold higher respect to that investigated in the Rio Cordon. Moreover, in the Estero Morales the PIT monitoring were carried out during persistent high hydraulic forcing conditions (i.e. daily fluctuations), while in the Rio Cordon the tracer inventories were performed in post-flood phases, i.e. during more suitable conditions for the channel investigation. In either cases, the mean recovery rate appears in line with the values obtained by similar works concerning the bedload tracing by PIT tracers (Lamarre et al., 2005; Liebault et al., 2012; Schneider et al., 2014; Houbrechts et al., 2015).

4.2.2. The sediment entrainment was affected by particle size?

In the Rio Cordon, the number of tracers mobilized increases with increasing the flood magnitude. Such trend can be partly observed also in the Estero Morales, where only 1 survey was represented by the high magnitude floods, respect to the 8 and 5 surveys accounted in the lower magnitude events (i.e. low and moderate). In terms of sediment entrainment, the results highlighted that in both study areas the mean transport distance increases with increasing the flood magnitude. Specifically, in the Rio Cordon the mean transport distance increases exponentially among low-moderate-high magnitude events, augmenting of one order of magnitude in each magnitude class. A similar dynamic was observed in the Estero Morales, where the low and moderate magnitude floods show a comparable mean transport distance, while a strongly increment in the mean displacement was triggered by the high magnitude events.

Focusing on the influence of particle size on the sediment entrainment, similar dynamics were observed in the study areas. In either cases, the relative low and moderate magnitude floods exhibit a size selective transport, in which the mean transport distance decreases with increasing the particle size. Thus, in the low and moderate hydraulic forcing the sediment entrainment appears affected by the sediment grain size. On the other hand, the high magnitude floods show equal mobility conditions during the transport. Apparently, the mean transport distance not decreases with particle size, suggesting that under high hydraulic forcing the sediment entrainment was unaffected by size of the particle. The transition between size selective transport to equal mobility is particularly evident in the Estero Morales

results (Fig. 62). In order to further investigate the role of particle size on sediment transport, also the grain size distribution (i.e. D_{16p} , $D_{50p,}$ D_{84p} and D_{90p}) of the tracers mobilized was analyzed. Promising results were achieved by the relationship between GSD and Q_{peak}, especially in the Rio Cordon. In this study area, the percentiles of the GSD mobilized are positively correlated with Q_{peak}, In particular, the regression lines increase their slope with increasing of the percentile tested, behaviour particularly evident in the D_{84p}/Q_{peak} and D_{90p}/Q_{peak} relationships. This result seems to suggest that in the Rio Cordon, the finer material mobilized by bedload remains quite constant in terms of particle size, while the coarser bedload fraction strongly increases with increasing Q_{peak}. In turn, such result seems to confirm how a great attention should be paid to the transport of large particles, especially as regards the hazard assessment in mountain streams. Contrary to what observed in the Rio Cordon, in the Estero Morales a clear relationship between Q_{peak} and GSD was not observed, with a positive correlation exhibited only by the D_{16p}/Q_{peak} relationship. This distinction in the results seems to suggest that in the Rio Cordon the sediment entrainment is strongly affected by particle size, while in the Estero Morales the transport of coarse sediment seems to not be influenced by the grain size.

4.2.3. The sediment entrainment was affected by hydraulic forcing?

In order to investigate the influence of hydraulic forcing on sediment entrainment, the unit stream power (ω) is derived from discharge. Particularly, the role of the 25^{th} (ω_{25}), 50^{th} (ω_{50}) and 75^{th} (ω_{75}) significant percentiles as well as the peak of unit stream power (ω_{peak}), obtained by the flow duration curves, was analyzed. The analysis performed in the Rio Cordon highlighted that the Li/ω correlation enhances with increasing the percentile considered, while the displacement appears weakly related with the ratios between the significant percentiles. On the whole, the best correlation was observed among Li and ω_{peak}, suggesting that in the Rio Cordon the percentiles close to the peak are the most relevant descriptors as regards the sediment entrainment. In the Estero Morales the scaling relationships showed a slightly different behaviour. Overall, Li appears better related with the ratios between the significant percentile, especially with $\omega_{peak}/\omega_{25}$ (Fig. 66D) and $\omega_{peak}/\omega_{50}$ (Fig. 66E), while the correlations with ω_{25}, ω_{50} and ω_{75} are quite weak. Consistently with the scaling relationships observed in the Rio Cordon, also in the Estero Morales the correlation enhances with increasing ω, reaching the best correlation between Li and ω_{peak}.

In the light of the results achieved, in both study areas the ω_{peak} seems to be the most relevant descriptor as regards the sediment entrainment. This result, coupled with the use of a

dimensionless value (ω) to describe the hydraulic forcing conditions, has allowed to compare between them the dynamics observed in study areas investigated. In Fig. 70, the Li/ω_{peak} relationships obtained in the Rio Cordon and Estero Morales were plotted.

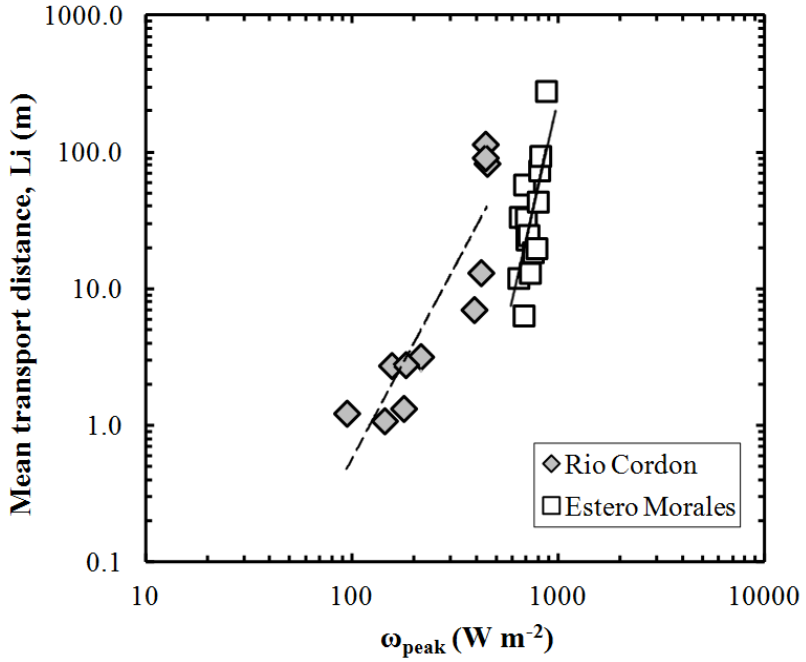

Figure 70: Relationship between Li and ω_{peak} observed in the Rio Cordon and in the Estero Morales.

The Estero Morales regression exhibits a very steep trend, showing as Li strongly increases with increasing peak of unit stream power. This behaviour suggests that during the study period, the Andean stream was characterized by high transport capacity with highly-effective sediment entrainment conditions. In the Rio Cordon, a wide range of ω_{peak} was investigated. In this sense, it is worth to noticing that several floods close to the threshold of incipient motion, equal to 140 W m^{-2} (Lenzi, 2004), were analyzed. In the Rio Cordon, the Li/ω_{peak} relationship appears more scatter. The regression here obtained shows a flatter trend, suggesting a lower transport capacity compared to the Estero Morales. In this sense, a dual trend can be appreciated in the results regarding the Alpine channel: the Li/ω_{peak} relationship scale roughly linearly under the lower hydraulic forcing (94-215 W m^{-2}) while abruptly increases the slope with increasing ω_{peak} (> 390 W m^{-2}). These results seem to suggest that in the Rio Cordon, over the threshold detected (i.e. 390 W m^{-2}), the sediment dynamic become comparable to that observed in the Estero Morales, with a very steep trend of the Li/ω_{peak} relationship. Specifically, when ω_{peak} > 390 W m^{-2} the Rio Cordon exhibits a transport capacity higher compared to the Andean channel, with the same magnitude of Li triggered by lower peaks of unit stream power. Notably, the threshold detected among low-high transport

capacity appears consistent with the results obtained analyzing the particle size influence, in which equal mobility conditions and larger displacements were triggered by $Q_{peak} > 2.0$ m^3 s^{-1} (i.e. 430 W m^{-2}). In this sense, in the Rio Cordon it would be very interesting to investigate the sediment entrainment caused by ω_{peak} between 200-400 W m^{-2} in order to better characterize the threshold for the start of high transport capacity condition. As regards the Estero Morales, a wider range of ω_{peak} might permit to verify the presence of an analogous threshold, currently not detected.

The different sediment dynamics observed can partly be explained by the features that characterize the study basins. The Rio Cordon is a typical nivo-pluvial basin, with a current low-moderate sediment supply (Mao et al. 2009; Rainato et al, under review), strongly degree of bed armouring and rough channel bed with a stable step-pool morphology and large boulders. Even in the Estero Morales creek the prevalent configuration is boulder-cascade/step-pool but the channel-bed is characterized by a lower degree of bed armouring, with the prevalence of loose coarse material. Such material is constantly delivered by the glacial tills, especially during the glacier-melt period when the basin is clearly characterized by high sediment supply conditions.

Such conditions affect the sediment dynamic in the two mountain channel. The Estero Morales constantly exhibited a high transport capacity, while the Rio Cordon shows comparable conditions only above a hydraulic threshold (~ 400 W m^{-2}). Over that threshold the Alpine stream exhibits higher transport efficiency compared to the Andean channel.

5. CHAPTER FIVE – FINAL REMARKS

5.1. Three decades of monitoring in the Rio Cordon instrumented basin

This study investigated 29 years of sediment fluxes recorded in the Rio Cordon instrumented Alpine basin. The data recorded by the monitoring station from 1986 to 2014 were used to analyze the short- and long-term sediment dynamics. A total sediment load of 14936.9 t was assessed in the period 1986-2014, corresponding to a mean sediment yield of 103.0 t km^{-2} y^{-1}. The sediment budget in the Rio Cordon appears to be dominated by the amounts mobilized by high magnitude/low frequency floods and particularly by the exceptional September 1994 event. This result confirms that exceptional floods, rarely assessed by short time series, can strongly influence the long-term budget, providing massive amounts of material. The lack of high magnitude events in the last 13 years can partially explain the relatively low sediment yield detected in the Rio Cordon compared to similar Alpine basins. The long-term partitioning highlighted the prevalence of SSL contribution over BL yield, with fractions equal to 0.79 and 0.21, respectively. The resulting partitioning differs with respect to the fractions predictable by the published equations, which clearly overestimate the BL contribution. Similarly to what was observed for the sediment yield, a large variability in the annual and floods fractions was detected in the partitioning.

The September 1994 flood caused a clear change in the sediment dynamics. The exceptional event altered the fluxes observed until then, intensifying the sediment availability and increasing the transport efficiency over the long term. The reactivation of several old source areas, triggering of new ones, removal of the armour layer and the increased transport capacity favored by step-pool removal have contributed to this alteration. The evidence appears be consistent with the hypothesis that the September 1994 flood caused a memory effect in the Rio Cordon basin, altering the sediment dynamics for roughly 10 years.

The bedload equations exhibit low performances in the Rio Cordon, failing to depict the different sediment availability conditions. Particularly attractive to fill the gap could be the possibility to formulate a parameter as a function of the different sediment availability conditions of the basin, thus enabling the predicted bedload to be adjusted and the observed fluxes better described.

In the Alpine range, long-term monitoring programs that enable time series of more than 10/15 years to be analyzed are rare. This study based on 29 years of data produced at the Rio Cordon monitoring station, emphasizes the importance of having long-term series to properly explore sediment dynamics. Particularly, in the light of the poor performances shown by the

predictive equations, the opportunity to investigate the short- and long-term dynamics using field data appears to be highly useful.

5.2. Tracing bedload using PIT tracers in high gradient streams: the Rio Cordon (Alps) and Estero Morales (Andes) study cases

The measurement campaigns performed using PIT tracers allowed to monitor and investigate the sediment entrainment in two different study areas. The passive integrated transponders are used in fluvial experiments since about a decade (Lamarre et al, 2005), but still few are the works aimed to the bedload tracing. In order to analyze the sediment motion, in the Rio Cordon and Estero Morales creeks were installed 250 and 429 PIT tracers, respectively. Since 2010, in the Alpine stream were performed 11 surveys to analyze the tracers displacement, while 14 PITs inventories were carried out during the austral summer 2014 in the Andean channel. In terms of peak of unit stream power (ω_{peak}), in the Rio Cordon the monitored floods range between 94.44 W m^{-2} to 451.78 W m^{-2}, while in the Estero Morales the ω_{peak} varies among 627.11 W m^{-2} and 872.86 W m^{-2}. The average recovery rates reached by the measurement campaigns, (i.e. 70% and 50%, respectively) are in line with the recoveries obtained by similar experiments in fluvial environment.

The analysis of the influence of particle size on the sediment entrainment highlighted that in both study areas the relative low-moderate magnitude floods exhibited a size-selective transport while equal mobility conditions were triggered by the higher magnitude events. Notwithstanding the similar dynamics, the relationship between the grain size distribution of tracers mobilized and Q_{peak} seems to suggest that in the Rio Cordon the sediment entrainment is strongly affected by particle size, while in the Estero Morales such relationship is poorly defined.

In both study areas, the mean transport distances are strongly correlated with the ω_{peak} of individual transport events, which appears the most relevant descriptor as regards the sediment entrainment. In this sense, the Estero Morales showed a persistent high transport capacity, while the Rio Cordon exhibited similar conditions only above a specific threshold, approximately equal to 400 W m^{-2}. Over such threshold the Alpine stream exhibits a higher transport efficiency compared to the Andean channel.

The results obtained tracing the bedload with PIT tracers demonstrated as this method is very fitting to monitoring the bedload without disturbing the channel bed and avoiding empirical assumptions regarding the sediment transport.

6. REFERENCES

Aich, V., Zimmermann, A., Elsenbeer, H., 2014. Quantification and interpretation of suspended-sediment discharge hysteresis patterns: How much data do we need? Catena 122, 120‐129.

Andrews, E.D., 1983. Entrainment of gravel from naturally sorted riverbed material. Geological Society of America Bulletin. 94 (10), 1225-1231.

Ashiq, M., Bathurst, J.C., 1999. Comparison of bed load sampler and tracer data on initiation of motion. Proceedings of the American Society of Civil Engineers, Journal of Hydraulic Engineering 125 (6), 661–664.

Ashworth, P.J., Ferguson, R.I., 1989. Size-selective entrainment of bed load in gravel bed streams. Water Resour.Res. 25 (4), 627-634.

Asselman, N.E.M., 2000. Fitting and interpretation of sediment rating curves. J. Hydrol. 234, 228-248.

Bagnold, R.A., 1966. An approach to the sediment transport problem from general physics. paper 422-I, United state department of interior, Washington, 37.

Banasik, K., Bley, D., 1994. An attempt at modelling suspended sediment concentration after storm events in an Alpine torrent. Lecture Notes in Earth Sci. 52, 161–170.

Barry, J.J., Buffington, J.M., King, J.G., 2004. A general power equation for predicting bedload transport rates in gravel bed rivers. Water Resour. Res. 40, 10401–10423.

Barsch, D., Gude, M., Mäusbacher, R., Schujraft, G., Sculte, A., 1994. Sediment transport and discharge in a high arctic catchment (Liefdefjorden, NW Spitsbergen). In: Ergenzinger, P., Schmidt, K.-H. (Eds.), Dynamics and Geomorphology of Mountain Rivers, 225 – 237, Springer, Berlin.

Bathurst, J.C., Graf, W.H., Cao, H.H., 1983. Initiation of sediment transport in steep channels with coarse bed material. Mechanics of sediment transport. Proc.Euromech 156, Istanbul, July 1982, 207-213.

Bathurst, J., Graf, W.H., Cao, H.H., 1987. Bed load discharge equations for steep mountain rivers. In: Thorne, C. R., Bathurst, J. C., Hey, R. D. (Eds.), Sediment Transport in Gravel-Bed Rivers, John Wiley & Sons Ltd., pp.453–477

Bathurst, J.C., 2013. Critical conditions for particle motion in coarse bed materials of nonuniform size distribution. Geomorphology 197, 170–184.

Beecroft, I., 1983. Sediment transport during an outburst from Glacier de Tsidjiore Nouve, Switzerland, 16–19 June 1981. J. Glaciol., 29, 185–190.

Bennett, G.L., Molnar, P., McArdell, B.W., Schlunegger, F., Burlando, P., 2013. Patterns and controls of sediment production, transfer and yield in the Illgraben, Switzerland. Geomorphology, 188, 68-82.

Billi, P., D'Agostino, V., Lenzi, M.A., Marchi, L., 1998. Bedload, slope and channel processes in a high-altitude alpine torrent. In: Klingeman, P. C. P., Beschta, R. L., Komar, P.D., Bradley, J. B. (Eds.), Gravel-Bed Rivers in the Environment. Water Resources Publications, LLC, Highlands Ranch, Colorado, 15-38.

Bogen, J., 1995. Sediment transport and deposition in mountain rivers. In: Foster, I.D.L., Gurnell, A.M., Webb, B.W. (Eds.), Sediment and water quality in river catchments. J. Wiley, Chichester, 437-451.

Buffington, J.M., Montgomery, D.R., Greenberg, H.M., 2004. Basin-scale availability of salmonid spawning gravel as influenced by channel type and hydraulic roughness in mountain catchments. Can.J.Fish.Aquat.Sci. 61 (11), 2085-2096.

Bunte, K., Abt, S.R., Potyondy, J.P., Swingle, K.W., 2008. A comparison of coarse bedload transport measured with bedload traps and Helley–Smith samplers. Geodinamica Acta 21 (1/2), 53–66.

Campbell, F.B., Bauder, H.A., 1940. A rating-curve method for determining silt-discharge of streams. Transactions, American Geophysical Union, 21, 603-607.

Cavalli, M., Trevisani, S., Comiti, F., Marchi, L., 2013. Geomorphometric assessment of spatial sediment connectivity in small Alpine catchments. Geomorphology 188, 31-41.

Chacho, E.F. Jr., Burrows, R.L., Emmett, W.W., 1994. Monitoring gravel movement using radio transmitters. In Hydraulic Engineering 94, Proceedings of the 1994 ASCE National Conference on Hydraulic Engineering, August 1994 Cotroneo GV, Rumer RR (eds), Buffalo, NY; 785 – 789.

Church, M., Hassan,M., 2002. Mobility of bed material in Harris Creek.Water Resour. Res. 38 (11), 1237–1249.

Collins, D.N., 1990. Seasonal and annual variations of suspended sediment transport in meltwaters draining from an Alpine glacier. In: Lang, H., Musy, A. (Eds.), Hydrology in Mountainous Regions. I-Hydrological Measurements: The Water Cycle. (Proc. Lausanne Symp, August 1900), IAHS Publ. 193, 439-446.

Comiti, F., Andreoli, A., Lenzi, M.A., 2005. Morphological effects of local scouring in step-pool streams. Earth Surf. Process. Landf. 30 (12), 1567-1581.

D'Agostino, V., Lenzi M.A., 1997. Origine e dinamica della morfologia a gradinata (step-pool) nei torrenti alpini ad elevata pendenza. Dendronatura 18 (2): 7-38.

D'Agostino, V., Lenzi, M.A., 1999. Bedload transport in the instrumented catchment of the Rio Cordon: Part II. Analysis of the bedload rate. Catena 36 (3), 191–204.

D'Agostino, V., Lenzi, M.A., Marchi, L., 1994. Sediment transport and water discharge during high flows in an instrumented watershed. In: Ergenzinger, P., Schmidt, K.H. (Eds.), Dynamics and Geomorphology of Mountain Rivers. Lecture Notes in Earth Sciences, 52, Springer Verlag, Berlin-Heidelberg, 67-81.

Dalla Fontana, G., Marchi, L., 2003. Slope-area relationships and sediment dynamics in two alpine streams. Hydrol.Process. 17 (1), 73-87.

DeBoer, D.H., Campbell, I.A., 1989. Spatial scale dependence of sediment dynamics in a semi-arid badland drainage basin. Catena 16, 277-290.

Durst, U., 1990. Schwebstofftransport in Wildbachen – Ein Vergleich von Vogelbach, Lumpenenbach und Erlenbach. Alptal, Internal Report, WSL Birmensdorf, Switzerland (in German).

Eder, A., Strauss, P., Krueger, T., Quinton, J.N., 2010. Comparative calculation of suspended sediment loads with respect to hysteresis effects (in the Petzenkirchen catchment, Austria). J. Hydrol. 389, 168-176.

Einstein, HA. 1937. Bedload transport as a probability problem. PhD thesis, Eidgenoess. Tech. Hoschch, Zurich. (In German.) (English translation by W. W. Sayre in Sedimentation, edited by H.W. Shen, Appendix C, H. W. Shen, Fort Collins, CO, 1972.).

Ergenzinger, P., Schmidt, K. H., Busskamp, R., 1989. The Pebble Transmitter System (PETS): first results of a technique for studying coarse material erosion, transport and deposition. Zeitschrift fur Geomorphologie. 33 (4), 503-508.

Fattorelli, S., Keller, H.M., Lenzi, M.A., Marchi, L., 1988. An experimental station for the automatic recording of water and sediment discharge in a small alpine watershed. Hydrol. Sciences Journal 33(6), 607–617.

Fenton, J.D., Abbott, J.E., 1977. Initial movement of grains on a stream bed: the effect of relative protrusion. Proceedings of the Royal Society of London A352, 523–537.

Ferguson, R.I., 2005. Estimating critical streampower for bedload transport calculations in gravel-bed rivers. Geomorfology. 70, 33–41.

Fonstad, M.A., 2003. Spatial variation in the power of mountain streams in the Sangre de Cristo Mountains, New Mexico. Geomorphology. 55 (1-4), 75-96.

Fraley, L., 2004. Methods of measuring fluvial sediment. Center for Urban Environment Research and Education. [Online Article].

Gao, P., Josefson, M., 2012. Event-based suspended sediment dynamics in a central New York watershed. Geomorphology 139, 425–437.

Grant, G.E., Swanson, F.J., Wolman, M.G., 1990. Pattern and origin of stepped-bed morphology in high-gradient streams, Western Cascades, Oregon. Bull.Geol.Soc.Am. 102 (3), 340-352.

Gurnell, A.M., Warburton, J., Clark, M.J., 1988. A comparison of the sediment transport and yield characteristics of two adjacent glacier basins, Val d'Hérens, Switzerland. Sediment Budgets (Proceedings of the Porto Alegre Symposium, Dec. 1988), IAHS Publ. no. 174, 247-259.

Hammond, F.D.C., Heathershaw, A.D., Langhorne, D.N., 1984. A comparison between Shields' threshold criterion and the movement of loosely packed gravel in a tidal channel. Sedimentology. 31 (1), 51-62.

Haschenburger, J.K., Church, M., 1998. Bed material transport estimated from the virtual velocity of sediment. Earth Surf. Process. Landf. 23, 791–808.

Hassan, M.A., Church, M., Schick, A.P., 1991. Distance of movement of coarse particles in gravel bed streams. Water Resour.Res. 27 (4), 503-511.

Hinderer, M., Kastowski, M., Kamelger, A., Bartolini, C., Schlunegger, C., 2013. River loads and modern denudation of the Alps – A review. Earth-Science Reviews 118, 11–44.

Houbrechts, G., Van Campenhout, J., Levecq, Y., Hallot, E., Peeters, A., Petit, F., 2012. Comparison of methods for quantifying active layer dynamics and bedload discharge in armoured gravel-bed rivers, Earth Surf. Processes Landforms.

Houbrechts, G., Levecq, Y., Peeters, A., Hallot, E., Van Campenhout, J., Denis, A., Petit, F., 2015. Evaluation of long-term bedload virtual velocity in gravel-bed rivers (Ardenne, Belgium). Geomorphology, in press.

Iida, T., Kajihara, A., Okubo, H., Okajima, K., 2012. Effect of seasonal snow cover on suspended sediment runoff in a mountainous catchment. J. Hydrol. 428–429, 116–128.

Infante Fabres, N.O., 2009. El Monumento natural El Morado (Andes Centrales Chilenos). Análisis del medio biofísico, paisaje y propuestas para su gestión. University of Barcelona, Spain.

Kirchner, J.W., Finkel, R.C., Riebe, C.S., Granger, D.E., Clayton, J.L., King, J.G., Megahan, W.F., 2001. Mountain erosion over 10 yr, 10 k.y., and 10 m.y. time scales. Geology, 29, 591–594.

Klein, M., 1984. Anti-clockwise hysteresis in suspended sediment concentration during individual storms. Catena 11, 251-257.

Lamarre, H., MacVicar, B., Roy, A. G., 2005. Using passive integrated transponder (PIT) tags to investigate sediment transport in gravel-bed rivers, J. Sediment. Res., 75, 736–741.

Lauffer, H., Sommer, N., 1982. Studies on sediment transport in mountain streams of the Eastern Alps. 14th International Congress on Dams, Rio de Janeiro, 431–453.

Lenzi, M.A., 2000. Variation in suspended sediment concentration during floods in the instrumented catchment of the Rio Cordon. In: Dynamics of Water and Sediments in Mountain Basins. Ed: Lenzi M.A., Quaderni di Idronomia Montana, 20, 53-67.

Lenzi, M.A., 2001. Step-pool evolution in the Rio Cordon, Northeastern Italy. Earth Surf. Process. Landf. 26 (9), 991-1008.

Lenzi, M.A., 2004. Displacement and transport of marked pebbles, cobbles and boulders during floods in a steep mountain stream. Hydrological Processes 18(10), 1899-1914.

Lenzi, M.A., Marchi, L., 2000. Suspended sediment load during floods in a small stream of the Dolomites (Northeastern Italy). Catena, 39, 267-282.

Lenzi, M.A., Mao, L., 2003. Analisi del contributo del trasporto solido in sospensione alla produzione di sedimento del bacino del Rio Cordon nel periodo 1986 – 2001. Quaderni di idronomia montana, 21(1), 361-379.

Lenzi, M.A., Marchi L., Scussel, G.R., 1990. Measurement of coarse sediment transport in a small Alpine stream. Hydrology in mountainous regions I, IAHS Publication 193, 283-290.

Lenzi, M.A., Billi, P., D'Agostino, V., 1997. Effects of an extremely large flood on the bed of a steep mountain stream. In: Wang, S.S.Y., Langendoen, E.J. & Shields, F.D.Jr. (Eds.), Management of landscapes disturbed by channel incision, stabilization, rehabilitation, restoration. 19-23 May 1997, Oxford, University of Mississippi, 1061-1066.

Lenzi, M.A., D'Agostino, V., Billi, P., 1999. Bedload transport in the instrumented catchment of the Rio Cordon: Part I: Analysis of bedload records, conditions and threshold of bedload entrainment. Catena 36 (3), 171-190.

Lenzi, M.A., Mao, L., Comiti, F. 2003. Interannual variation of suspended sediment load and sediment yield in an alpine catchment. Hydrological Sciences Journal, 48(6), 899-915.

Lenzi, M.A., Mao, L., Comiti, F., 2004. Magnitude-frequency analysis of bed load data in an Alpine boulder bed stream. Water Resour. Res. 40 (7), 1-12.

Lenzi, M.A., Mao, L., Comiti, F., 2006a. Effective discharge for sediment transport in a mountain river: Computational approaches and geomorphic effectiveness. J. Hydrol. 326 (1-4), 257-276.

Lenzi, M.A., Mao, L., Comiti, F., 2006b. When does bedload transport begin in steep boulder-bed streams? Hydrological Processes. 20, 3517-3533.

Liébault, F., Laronne, J. B., 2008. Evaluation of bedload yield in gravel-bed rivers using scour chains and painted tracers: The case of the Esconavette Torrent (Southern French Prealps), Geodinamica Acta, 21(1–2), 23–34, doi:10.3166/ga.21.23-34.

Liébault, F., Bellot, H., Chapuis, M., Klotz, S., Deschâtres, M., 2012. Bedload tracing in a high-sediment-load mountain stream. Earth Surf.Process.Landforms. 37 (4), 385-399.

MacFarlane, W.A., Wohl, E., 2003. Influence of step composition on step geometry and flow resistance in step-pool streams of the Washington Cascades. Water Resour.Res. 39 (2), ESG31-ESG313.

Mao, L. 2004. Analisi comparativa del trasporto solido di corsi torrentizi in diversi ambiti geografici. Ph.D thesis, University of Padua, TeSAF Department, pp. 307 (in Italian).

Mao, L., Lenzi, M.A., 2007. Sediment mobility and bedload transport conditions in an alpine stream. Hydrol. Process. 21, 1882–1891.

Mao, L., Cavalli, M., Comiti, F., Marchi, L., Arattano, M., 2006. Long-term monitoring of bedload and debris flows in two small catchments of the Eastern Italian Alps. WIT Transactions on Ecology and the Environment 90, 147-157.

Mao, L., Uyttendaele, G.P., Iroumé, A., Lenzi M.A., 2008. Field based analysis of sediment entrainment in two high gradient streams located in Alpine and Andine environments. Geomorphology 93, 368-383.

Mao, L., Cavalli, M., Comiti, F., Marchi, L., Lenzi, M.A., Arattano, M., 2009. Sediment transfer processes in two Alpine catchments of contrasting morphological settings. J. Hydrol. 364 (1-2), 88-98.

Mao, L., Comiti, F., Lenzi, M.A., 2010. Bedload Dynamics in Steep Mountain Rivers: Insights from the Rio Cordon Experimental Station (Italian Alps). In: Gray, J. R., Laronne, J. B., Marr, J. D. G. (Eds.), Bedload-surrogate monitoring technologies, U.S. Geological Survey Scientific Investigations Report 2010-5091, 253-265.

Mao, L., Carrillo, R., Escauriaza, C., Iroume A., 2015. Flume and filed-based calibration of surrogate sensors for monitoring bedload transport. Geomorphology 253, 10-21.

Meyer-Peter, E., Muller R., 1948. Formulas for bed-load transport, in Proceedings of the 2nd Meeting of the International Association for Hydraulic Structures Research, 39–64.

Montgomery, D.R., Buffington, J.M., 1997. Channel-reach morphology in mountain drainage basins. Bull.Geol.Soc.Am. 109(5), 596-611.

Moore, R.D., 2004. Introduction to salt dilution gauging for streamflow measurement: Part I. Streamline Watershed Management Bulletin, 7(4):20–23.

Morche, D., Bryk, A., 2010. Bed load transport in an Alpine river after a high magnitude flood: results from the 2008 field campaign. IAHS-AISH Publication 336, 157-163.

Nelson, P.A., Venditti, J.G., Dietrich, W.E., Kirchner, J.W., Ikeda, H., Iseya, F., Sklar, L.S., 2009. Response of bed surface patchiness to reductions in sediment supply. Journal of Geophysical Research F: Earth Surface. 114 (2).

Nitsche, M., Rickenmann, D., Turowski, J.M., Badoux, A., Kirchner, J.W., 2011. Evaluation of bedload transport predictions using flow resistance equations to account for macro-roughness in steep mountain streams. Water Resour.Res. 47. W08513.

Petit, F., Gob, F., Houbrechts, G., Assani, A.A., 2005. Critical specific stream power in gravel-bed rivers. Geomorphology. 69 (1-4), 92-101.

Picco, L., Mao, L., Rigon, E., Moretto, J., Ravazzolo, D., Delai, F., Lenzi, M.A., 2012. An update of the magnitude-frequency analysis of Rio Cordon (Italy) bedload data after 25 years of monitoring. IAHS-AISH Publication, 65-71.

Rainato, R., Picco, L., Lenzi, M.A., Mao, L., Delai, F., Rigon, E., Moretto, J., Cesca, M., Vianello, A., García-Rama, A., 2013. Monitoring and analysis of the sediment transport event of November 2012 in the Rio Cordon station. Quaderni di Idronomia Montana 31, 323-338.

Rainato, R., Mao, L., Garcia-Rama, A., Picco, L., Cesca, M., Vianello, A., Preciso, E., Scussel, G.R., Lenzi, M.A., (under rewiew). Three decades of monitoring in the Rio Cordon instrumented basin: sediment budget and temporal trend of sediment yield. Geomorphology.

Recking, A., 2012. Influence of sediment supply on mountain streams bedload transport. Geomorphology. 175-176, 139-150.

Recking, A., Liébault, F., Peteuil, C., Jolimet, T., 2012a. Testing bedload transport equations with consideration of time scales. Earth Surf. Process. Landf. 37 (7), 774-789.

Recking, A., Leduc, P., Liébault, F., Church, M., 2012b. A field investigation of the influence of sediment supply on step-pool morphology and stability. Geomorphology. 139-140, 53-66.

Rickenmann, D., 1991. Hyperconcentrated flow and sediment transport at steep slopes, J.Hydraul. Eng., 117(11), 1419–1439.

Rickenmann, D., 1999. Empirical relationships for debris flows. Nat.Hazards. 19 (1), 47-77.

Rickenmann, D., D'Agostino, V., Dalla Fontana, G., Lenzi, M.A., Marchi, L., 1998. New results from sediment transport measurements in two Alpine torrents. Hydrology, Water Resources and Ecology in Headwaters. IAHS-AISH Publication 248, 283-289.

Rickenmann, D., Turowski, J.M., Fritschi, B., Klaiber, A., Ludwig, A., 2012. Bedload transport measurements at the Erlenbach stream with geophones and automated basket samplers. Earth Surf.Process.Landforms. 37 (9), 1000-1011.

Sadler, P.M., 1981. Sediment accumulation and the completeness of stratigraphic sections. J. Geol., 89, 569–584.

Schlunegger, F., Hinderer, M. 2003. Pleistocene/Holocene climate change, re-establishment of fluvial drainage network and increase in relief in the Swiss Alps. Terra Nova, 15, 88–95.

Schmidt, K.H., Morche, D., 2006. Sediment output and effective discharge in two small high mountain catchments in the Bavarian Alps, Germany. Geomorphology 80, 131-145.

Schneider, J.M., Turowski, J.M., Rickenmann, D., Hegglin, R., Arrigo, S., Mao, L., Kirchner, J.W., 2014. Scaling relationships between bed load volumes, transport distances, and stream power in steep mountain channels. J. Geophys. Res. Earth. Surf., 119.

Schoklitsch, A., 1962. Handbuch des Wasserbaues, 3rd ed., Springer, Wien.

Seeger, M., Errea, M.P., Beguería, S., Arnáez, J., Martí, C., García-Ruiz, J. M., 2004. Catchment soil moisture and rainfall characteristics as determinant factors for discharge/suspended sediment hysteretic loops in a small headwater catchment in the Spanish Pyrenees. J. Hydrol. 288, 299-311.

Shields, A., 1936. Anwendung der Aehnlichkeitsmechanik und der Turbulenzforschung auf die Geschiebebewegung. Preuß. Versuchsanstalt f. Wasserbau u. Schiffbau, Berlin.

Soler, M., Latron, J., Gallart, F., 2008. Relationships between suspended sediment concentrations and discharge in two small research basis in a mountainous Mediterranean area (Vallcebre, Eastern Pyrenees). Geomorphology 98, 143-152.

Sterling, S.M., Church, M., 2002. Sediment trapping characteristics of a pit trap and the Helley–Smith sampler in a cobble gravel bed river. Water Resources Research 38 (8), W01144.

Tropeano, D., 1991. High flow events and sediment transport in small streams in the 'Tertiary Basin' area in Piedmont (Northwest Italy). Earth Surf. Process. Landf. 16, 323–339.

Turowski, J.M., Yager, E.M., Badoux, A., Rickenmann, D., Molnar, P., 2009. The impact of exceptional events on erosion, bedload transport and channel stability in a step pool channel. Earth Surf. Process. Landf. 34, 1661–1673.

Turowski, J.M., Rickenmann, D., Dadson, S.J., 2010. The partitioning of the total sediment load of a river into suspended load and bedload: a review of empirical data. Sedimentology 57(4):1126–1146.

Vazquez-Tarrio, D., Menendez-Duarte, R., 2014. Bedload transport rates for coarse-bed streams in an Atlantic region (Narcea River, NW Iberian Peninsula). Geomorphology 217, 1–14.

Vazquez-Tarrio, D., Menendez-Duarte, R., 2015. Assessment of bedload equations using data obtained with tracers in two coarse-bed mountain streams (Narcea river basin, NW spain). Geomorphology 238, 78-93.

Vezzoli, G., 2004. Erosion in the Western Alps (Dora Baltea Basin) 2. Quantifying sediment yield. Sed. Geol., 171, 247–259.

Whittaker, J., 1987. Sediment transport in step-pool streams. Sediment Transport in Gravel-Bed Rivers.John Wiley and Sons New York.1987.p 545-579, 20 fig, 40 ref.

Wilcock, P.R., 1997. Entrainment, displacement and transport of tracer gravels. Earth Surf.Process.Landforms. 22 (12), 1125-1138.

Wilcock, P.R., 1998. Two-fraction model of initial sediment motion in gravel-bed rivers. Science. 280 (5362), 410-412.

Wilcock, P.R., McArdell, B.W., 1997. Partial transport of a sand/gravel sediment. Water Resour.Res. 33 (1), 235-245.

Wilcox, A.C., Wohl, E.E., 2006. Flow resistance dynamics in step-pool stream channels: 1. Large woody debris and controls on total resistance. Water Resour.Res. 42. W05418.

Williams, G.P., 1989. Sediment concentration versus water discharge during single hydrologic events in rivers. J. Hydrol. 111, 89-106.

Wohl, E.E., 2000. Mountain Rivers. Water Resources Monograph 14, Washington DC, USA. pp 320.

Yager, E.M., Turowski, J.M., Rickenmann, D., McArdell, B.W., 2012. Sediment supply, grain protrusion, and bedload transport in mountain streams. Geophys. Res. Lett., 39, L10402.

Yager, E.M., Kenworthy, M., Monsalve, A., 2015. Taking the river inside: Fundamental advances from laboratory experiments in measuring and understanding bedload transport processes. Geomorphology 244, 21-32.

ACKNOWLEDGEMENTS

There are many people that I would like to thank, people that helped me, who supported me or influenced me along the way.

First, I would like to thank Prof. Mario Aristide Lenzi, supervisor of this thesis, who gave me the opportunity to realize this 3-year pathway, always offering invaluable tips and suggestions.

A huge "thank you" is due to Prof. Luca Mao, both for the wonderful possibility to carry out my research project even in Chile, but also for the constant and precious support to all my research activities.

This work is the result also of several other persons, scattered across two continents, that helped me both in field and in laboratory. Many thanks to the entire "Lenzi Team": Lorenzo Picco, Emanuel Rigon, Diego Ravazzolo, Fabio Delai, Johnny Moretto, Adriana Garcia Rama e Alessia Tonon. Also, Muchas Gracias to the entire "Equipo Italo-Chileno": Ricardo Carillo, Matteo Toro, Joaquin Lobato, Rodrigo Perez, Fernanda Gordo, Ernesto Cobo and Sergio Gaete Carrasco.

I would like to express my sincere gratitude to the Arpav agency, in particular to Matteo Cesca and Walter Testor, for all work done in the Rio Cordon and for the productive collaboration.

Last, but not least, a special acknowledgement goes to all my family, especially to my mom and my brother, that have been always present in these years. A special thanks to Laura, who has always rooted for my PhD and that has constantly supported me during these years, also during the dark moments.

Lastly, I thank my wise dad, because I had promised.

Thank you very much to all of you.

Riccardo